

A CASE STUDY OF THE ODENPLAN STATION IN THE STOCKHOLM CITY LINK PROJECT – ANALYSIS OF IN SITU STRESSES AND OBSERVED GROUND BEHAVIOUR

Diego Mas Ivars, Fredrik Johansson

Rima Ghazal, Abel Sánchez Juncal

Roció Batres Estrada

**A CASE STUDY OF THE ODENPLAN
STATION IN THE STOCKHOLM CITY LINK
PROJECT
- ANALYSIS OF IN SITU STRESSES AND
OBSERVED GROUND BEHAVIOUR**

**En fallstudie av station Odenplan, Citybanan
- Analys av in situ spänningar och bergmassans
observerade beteende**

Diego Mas Ivars, SKB
Fredrik Johansson, KTH
Rima Ghazal, Itasca Consultants
Abel Sánchez Juncal, Itasca Consultants
Roció Batres Estrada, AECOM (former at Sweco)

PREFACE

The construction of tunnels in urban environments constitutes an important part of the infrastructure necessary for society. At the same time are these tunnels often shallow and their influence on the environment and nearby structures could be considerable. In order to study these tunnels from a rock mechanics perspective, it is necessary to have knowledge about prevailing in-situ stresses. However, the prevailing in-situ stress situation is often associated with large uncertainties, especially at shallow depths where the stresses could be influenced by topography, potential lower rock mass quality and/or bedding planes. Therefore, it is important to complement performed stress measurements, which generates large variations in results, with back analyses in larger scales to increase our knowledge within this area.

In this project, a case study of the tunnels at the Odenplan Station in the Stockholm City Link has been performed. The case study shows how difficult and complex this is and has enabled a unique opportunity to numerically analyse the in-situ stresses and at the same time investigate our ability, by using state of the art rock mechanical knowledge, to numerically model the behaviour of the rock mass in accordance with measured deformations during construction.

The work was mainly performed by Diego Mas Ivars (SKB/former at Itasca Consultants), Fredrik Johansson (KTH), Rima Ghazal (Itasca Consultants), Abel Sánchez Juncal (Itasca Consultants) and Roció Batres Estrada (AECOM/former at Sweco). A reference group has followed the project and contributed with valuable suggestions and comments. The group consisted of Lars Rosengren (Rosengren Bergkonsult), Rolf Christiansson (SKB), Anders Fredriksson (Fredriksson Geokonsult), Erling Nordlund (LTU), Thomas Dalmalm (the Swedish Road Administration) and Per Tengborg (BeFo). The project was funded by the Rock Engineering Research Foundation – BeFo and in-kind support from Sweco and Itasca.

Stockholm 2017

Per Tengborg

FÖRORD

Byggande av tunnlar i urbana miljöer utgör en viktig del av den infrastruktur som är nödvändig för samhället. Samtidigt är dessa tunnlar ofta ytliga och deras inverkan på miljön och närliggande konstruktioner kan vara betydande. För att bergmekaniskt kunna studera dessa tunnlar är det nödvändigt att ha kunskap om rådande in situ spänningar. Kunskapen om rådande spänningsförhållanden är emellertid behäftade med stora osäkerheter, speciellt för ytliga tunnlar då spänningsbilden påverkas av exempelvis topografi, en potentiellt sämre bergkvalité och eventuella bankningsplan. Det är därför viktigt att komplettera utförda spänningsmätningar, som generellt även genererar en stor spridning i resultaten, med bakåtanalyser i större skala för att öka vår kunskap inom detta område.

I detta projekt har en fallstudie genomförts av tunnarlarna vid Odenplan station i Stockholm, vilka byggdes i samband med Citybanan. Fallet, som visar hur svårt detta kan vara, har utgjort en unik möjlighet att numeriskt analysera rådande in situ spänningar och samtidigt undersöka våra kunskaper att med dagens bergmekaniska kunskap numeriskt modellera bergmassans beteende i överensstämmelse med uppmätta deformationer.

Utvecklingsarbetet har huvudsakligen utförts av Diego Mas Ivars (SKB/fd Itasca Consultants), Fredrik Johansson (KTH), Rima Ghazal (Itasca Consultants), Abel Sánchez Juncal (Itasca Consultants) och Roció Batres Estrada (AECOM/fd Sweco). En referensgrupp har följt arbetet med projektet och bistått författarna. Gruppen bestod av Lars Rosengren (Rosengren Bergkonsult), Rolf Christiansson (SKB), Anders Fredriksson (Fredriksson Geokonsult), Erling Nordlund (LTU), Thomas Dalmalm (Trafikverket) och Per Tengborg (BeFo). Projektet finansierades av Stiftelsen Bergteknisk Forskning – BeFo samt in-kind från Sweco och Itaca.

Stockholm 2017

Per Tengborg

SUMMARY

The Odenplan Station in the Stockholm City Link project is located directly under the existing subway station with a minimum rock cover of approximately 7 m. The span of the Odenplan Station is 25 m. When the Odenplan station was excavated, deformations larger than anticipated in previous calculations were observed. The main reason for this discrepancy is believed to be high horizontal *in situ* and/or persistent fractures in the area parallel with the excavation.

The excavation of the Odenplan station constitutes a case study with well-documented rock mass characteristics, excavation sequences, support sequences and measured deformations. It therefore provides a unique project to analyse. Based on this case study, the main objectives of this study was to (1) suggest a general technique for numerical back analyses based on measured deformations under geological conditions as those present in the Stockholm area, and (2) analyse the range of possible *in situ* stresses at Odenplan Station in the City Link project.

The complex three-dimensional *3DEC* model lead to rather long computational times. A general technique for a real back analysis was therefore not possible to obtain in this study, since it would require unrealistically long computational time. Instead, a sensitivity study on the *in situ* stresses and different types of continuum and discontinuum approaches were performed. The results from the analyses gave valuable insight into which types of models that were able to properly recreate the observed ground behavior at Odenplan. The results from the study clearly showed that a continuum approach does not capture the true behavior of the blocky rock mass at Odenplan. It is therefore recommended that discontinuum approaches are used in the future when structurally controlled block movements could be expected. However, the exact cause behind the discrepancy between the continuum and the discontinuum model has not been determined in this report.

The performed sensitivity analysis suggests that the *in situ* stresses are high and in the range of those previously measured. Maximum horizontal *in situ* stresses are probably in the range of 5.7-7.2 MPa at a depth of 0-20 m, which agrees well with the results of previous rock stress measurements, which were, on average, 8.1 MPa at a depth of 30 m.

The encouraging results from this project indicate that further stress sensitivity analyses should be performed to have a better estimation of the range of *in situ* stresses in the Stockholm area by fitting displacements obtained from modeling to those measured *in situ*

in different projects. These analyses are important in order to understand our present ability to perform numerical simulations reflecting true rock mass behavior.

Keywords: in situ stresses, numerical modeling, back analyses, sensitivity analyses, case study

SAMMANFATTNING

Odenplan station i Citybanan är belägen direkt under existerande tunnelbanestation, med en minsta bergtäckning på 7 m. Spännvidden på stationsrummet är 25 m. När bergmassan för stationsrummet sprängdes ut uppstod deformationer som var större än de som förväntats och prognosticerats i tidigare beräkningar. Den huvudsakliga anledningen till denna avvikelse tros vara höga horisontella *in situ* spänningar och/eller sprickplan med stor utbredning parallella med stationsrummet.

Uttaget av stationsrummet vid Odenplan utgör en väldokumenterad fallstudie med data från tunnelkartering, uttagssekvenser, bergförstärkning och uppmätta deformationer. Baserad på denna fallstudie har syftena med detta arbete varit att (1) föreslå en generell metodik för bakåtanalys baserat på uppmätta deformationer under geologiska förhållanden vanligt förekommande i Stockholmsområdet och (2) analysera det troliga intervallet för rådande *in situ* spänningar vid Odenplan.

Den komplexa tredimensionella modellen i *3DEC* som togs fram inom projektet resulterade i relativt långa beräkningstider. En generell teknik för en fullständig bakåtanalys var därför inte möjlig att uppnå i denna studie, eftersom det skulle krävas orimligt långa beräkningstider. Istället genomfördes en känslighetstudie avseende rådande *in situ* spänningar samt olika typer av kontinuum- och diskontinuum-modelleringar. Resultaten från dessa analyser gav värdefull förståelse i hur olika typer av modeller klarar av att återskapa det observerade beteendet för bergmassan vid Odenplan. Resultaten visar tydligt att kontinuum-modellen i detta fall, med givna indata, inte klarade av att återskapa det korrekta beteendet av den blockiga bergmassan vid Odenplan. Det rekommenderas därför att beräkningar i framtiden genomförs med diskontinuum-modeller när den strukturella stabiliteten domineras av rörelser i en blockig bergmassa. Den exakta orsaken till avvikelsen mellan kontinuum- och diskontinuum modellen har emellertid inte fastställts i denna rapport.

Den genomförda känslighetsanalysen antyder att *in situ*-spänningarna är höga. Största horisontella huvudspänningen ligger sannolikt i intervallet 5.7-7.2 MPa vid ett djup på mellan 0-20 m, vilket stämmer bra överens med tidigare utförda bergspänningsmätningar som gav ett genomsnittligt värde på 8.1 MPa vid ett djup på 30 m.

De värdefulla och intressanta resultaten från detta projekt innebär att ytterligare känslighetsstudier av genomförda projekt rekommenderas. Dessa analyser är viktiga för att förstå vår kapacitet och utveckla vår förmåga att genomföra numeriska beräkningar som korrekt återskapar bergmassans verkliga beteende.

Nyckelord: in situ spänningar, numerisk modellering, bakåträkning, känslighetsanalys, fallstudie

TABLE OF CONTENTS

SUMMARY	V
SAMMANFATTNING.....	VII
TABLE OF CONTENTS	IX
1 INTRODUCTION.....	1
1.1 Background.....	1
1.2 Objectives	3
2 GENERAL METHODOLOGY.....	5
3 LITERATURE REVIEW.....	7
3.1 Stress measurements in the Stockholm area.....	7
3.2 Back analysis	9
4 DESCRIPTION OF THE ODENPLAN STATION	13
4.1 Geometry	13
4.2 Geology and mapped fractures.....	15
4.3 Excavation sequences	18
4.4 Rock support.....	18
4.5 Monitoring system	19
5 NUMERICAL MODELING.....	23
5.1 Overall model geometry and numerical mesh.....	25
5.2 Input data simplification and assumptions.....	28
5.2.1 Soil and rock surface topology.....	29
5.2.2 Fracture network.....	30
5.2.3 In situ and boundary conditions.....	32
5.2.4 Input properties.....	33
5.3 Simulation sequence.....	40
5.4 Monitoring points.....	46
5.5 Sensitivity study	47

5.6	Results	48
5.6.1	Simulated vertical displacement magnitude.....	49
5.6.2	Simulated extensometers response.....	66
5.6.3	Simulated Platform tunnel vertical displacement	73
6	DISCUSSION.....	81
7	CONCLUSIONS AND SUGGESTIONS FOR FUTURE RESEARCH	85
8	REFERENCES.....	87
	APPENDIX 1: Vertical displacement magnitude at vertical cross-sections parallel and perpendicular to the Platform tunnel centered on the Elevator shaft.....	91
	APPENDIX 2: vertical displacement Magnitude at top surface of model.....	101

1 INTRODUCTION

1.1 Background

Underground constructions in urban areas constitute an important part of the infrastructure needed for society. Being at shallow depth, their potential impact on the environment and surrounding structures can be significant. Particularly in Scandinavia, where horizontal stresses are high, performing excavations at shallow depth in brittle hard rock, combined with irregular surface topology and open fractures, can lead to large deformations and upheaving of the ground. The estimation of *in situ* stresses is required in order to study the behaviour of the rock mass around such excavations and limit its potential deformation. However, data concerning the *in situ* stress field is usually associated with high uncertainties, particularly at shallow depth where it is affected by the topography of the rock surface, near-surface weathering, exfoliation joints etc. Additionally, stress measurements are performed at specific points and are usually subjected to high scatter. It is therefore important to complement these measurements with back analysis at a larger scale (Kaiser et al. 2000), in order to gain insight into the *in situ* stress field in a specific area.

A 6 km long railway tunnel, the Stockholm City Link, has in the recent years been constructed in Stockholm by Trafikverket, see Figure 1. In the tunnel, two new stations are included, the City Station and the Odenplan Station. The Odenplan Station is located directly under the existing subway station with a minimum rock cover of approximately 7 m, see Figure 2. The span of the Odenplan Station is 25 m.

When the Odenplan station was excavated, deformations larger than anticipated in previous calculations were observed. In the previous calculations, three dimensional numerical analyses with a continuum material model showed that up to 3 mm large deformations could be anticipated. However, measured observations at the time of construction were up to 10 mm. These deformations were measured with several extensometers in the rock mass where the City Link is crossing the existing subway and the heave of the rock surface is measured with a hydrostatic levelling system.

The main reason for this discrepancy is believed to be that high horizontal *in situ* stresses exist in the rock mass. Due to this discrepancy, analyses which could specify the range of these *in situ* stresses at Odenplan are of specific interest. Another main source of uncertainty is that there existed open fractures in the area parallel with the excavation

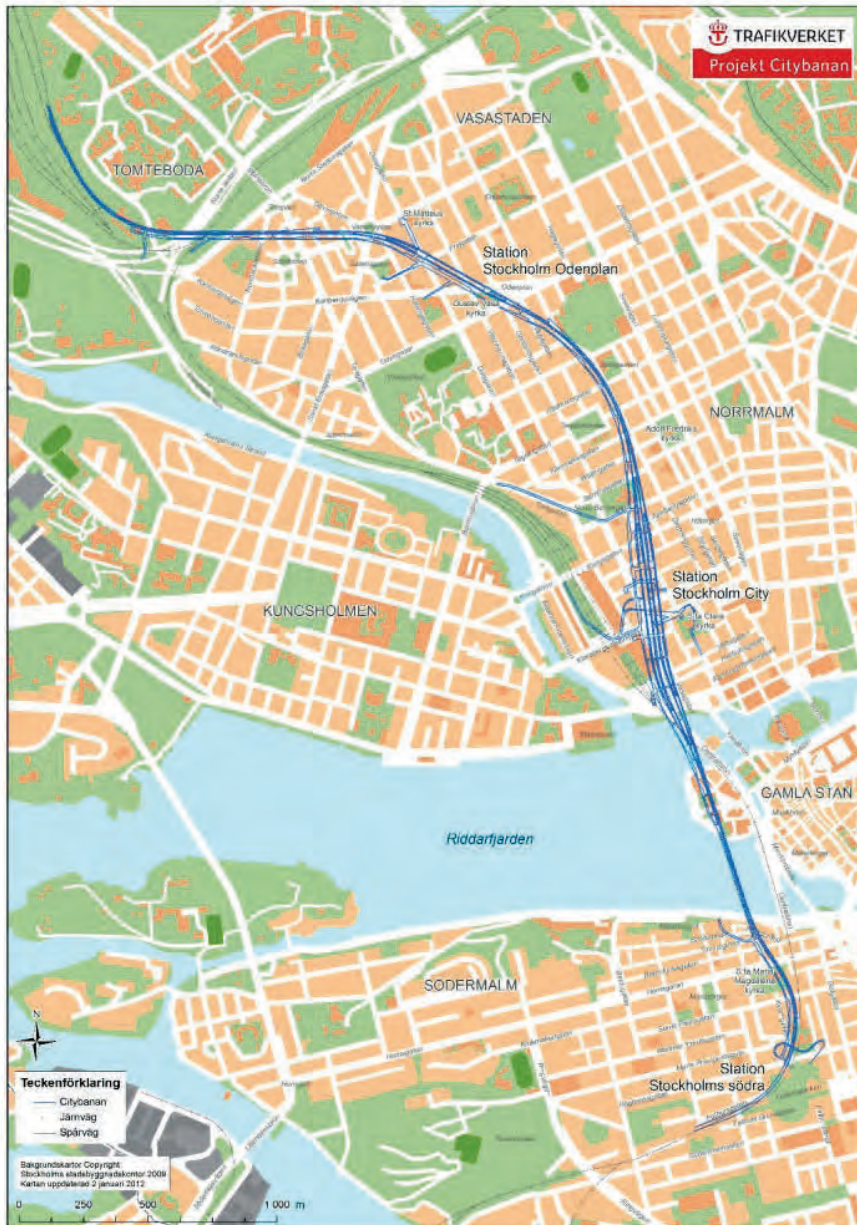


Figure 1 Overview of the Stockholm City Link (Source: Trafikverket).

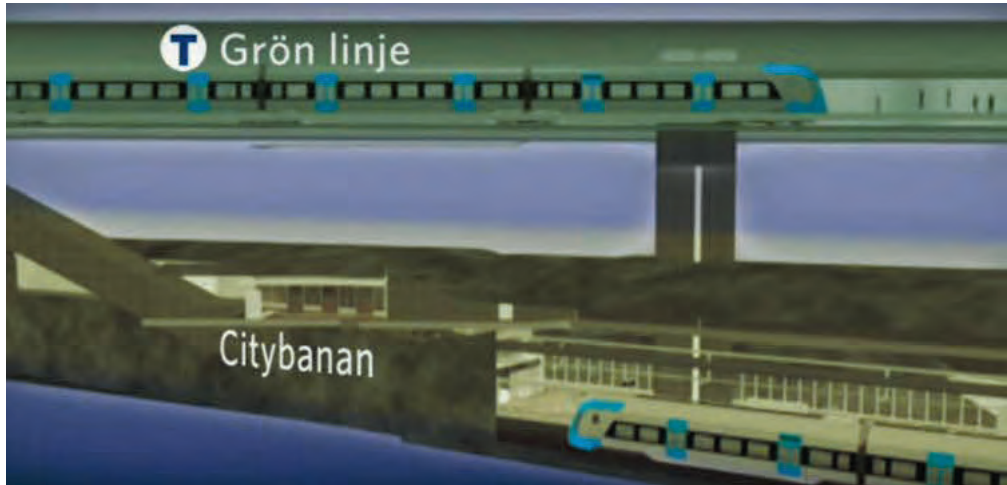


Figure 2 Illustration of the new Odenplan station with the new City Link located under the existing subway (Source:Trafikverket).

which were unusually persistent, especially those with a dip angle of 50° to 70° . This could imply that even if the rock mass quality was judged to be good, the rock mass behaviour could be controlled by these fractures. Therefore, it is probably necessary to explicitly consider these structures in the analysis to understand the deformations caused by this excavation.

The access to *in situ* measurements, comprehensive data of deformations, both at the ground surface and in the tunnels, together with information about rock mass quality and characteristics from mapping of the surfaces, means that the construction of Odenplan Station provides a unique opportunity to analyse the range of possible *in situ* stresses in the rock mass in the Stockholm area. This analysis also enables us to control our present ability to perform numerical calculations capable of describing the magnitude of possible settlements or heaves for shallow tunnels in urban areas and the global behaviour of the rock mass.

1.2 Objectives

There are two objectives with this report. The first objective of this report are to summarize available information on performed *in situ* stress measurements in the Stockholm area and to

suggest a general technique for numerical back analyses based on measured deformations under geological conditions as those present in the Stockholm area.

The second objective is to analyse the range of possible *in situ* stresses at Odenplan Station in the Stockholm City Link project using actual measurements. By doing so, our understanding of *in situ* stresses at shallow depths in the Stockholm area will increase and the capability to predict the magnitude of deformations of the ground surface will be investigated.

2 GENERAL METHODOLOGY

The aim of this study is to suggest a suitable technique for numerical back analyses under geological conditions as those present in the Stockholm area, and analyse the range of possible *in situ* stresses at Odenplan Station in the City Link project. In order to obtain these aims, a methodology involving the following five steps has been used:

Literature review of *in situ* stresses and available techniques for back analyses. The review of the *in situ* stress measurements covers those performed in the Stockholm area with the aim of identifying possible ranges of the stresses. The results from the *in situ* stress measurement performed at Odenplan are covered in more detail. The review for common techniques for back analyses aims to identify if some of those techniques are suitable to use within this project to narrow down the range of possible *in situ* stresses.

Compilation of existing data concerning the Odenplan station. In this step, existing data of the station are compiled. This includes geometry, geological conditions and mapped fractures in the tunnels, excavations sequences and sequences for installing the support. Finally, the measurement system at Odenplan is covered and measured deformations are presented.

Building the numerical model in 3DEC. This step includes how the numerical was built and includes the layout of it and how the fracture network was set up based on the mapped fractures in the tunnels. It also contains a description of how the excavation sequences and rock support was modelled, and how history points was included in the model to obtain deformations in the model comparable to those from the measurements used at the station.

Performing numerical calculations with different numerical modelling approaches at different *in situ* stresses. This includes both continuum and discontinuum modelling approaches. In the continuum approach two different constitutive models will be used; the linear elastic model and the elasto-plastic Hoek Brown constitutive model. In the discontinuum approach the peak shear strength of the joints will be modelled with the Mohr Coulomb criterion. To study the influence from a possible overestimation of the shear strength of the fractures at low normal stresses two cases will be analysed; one with an existing cohesion in the fractures and one with no cohesion existing in the fractures. All the cases above will be performed at different *in situ* stresses.

Compare and discuss the results from the numerical calculations against the measured deformations of the rock mass.

These steps are described in more detail in the following chapters.

3 LITERATURE REVIEW

3.1 Stress measurements in the Stockholm area

Performed *in situ* stress measurements in the Stockholm area have been summarized in a report by Perman & Sjöberg (2007). In the report, measurements performed at the following locations/projects in Stockholm were summarized: Huvudsta subway station, the Royal Library, SOS rescue central, the Southern Link, the Northern Link, the Eastern Link, the Arlanda airport rail link, Björkö Energy project and the Stockholm City Link. The methods used for the in-situ stress measurements were overcoring with the Borre cell, hydraulic fracturing (HF-tests) and hydraulic fracturing on pre-existing fractures (HFPPF-tests).

The Stockholm area contains a number of faults and larger weakness zones. One example is the fault with an E-W strike that limits the northern part of Södermalm. This fault is persistent and the topography is different on both sides of it. According to Perman and Sjöberg (2007), this fault could therefore be considered to constitute a natural limit between different domains with respect to *in situ* stresses. In the northern part of Stockholm, the relative tectonic movement, which is often considered to be an indication of the regional *in situ* stress direction, is NW-SE. In the area between these two regions, where Riddarholmen is located, Perman and Sjöberg (2007) write that structures within the rock mass are more difficult to identify. As a result, they suggest dividing the Stockholm area into three domains: Södermalm, Riddarholmen and Norrmalm. This division into three domains also resulted in more narrow ranges of the confidence intervals of the *in situ* stresses obtained from the measurements, which otherwise were relatively large due to the combinations of measurements error and spatial variations in the stresses. The analyses of the measurements in each domain resulted in two suggested *in situ* stress profiles; one for Norrmalm and Riddarholmen and one for Södermalm. The suggested *in situ* stress profiles according to Perman and Sjöberg (2007) are presented in Table 1 and Table 2.

The overcoring *in situ* stress measurements at Odenplan are described in the report by Berg and Sjöberg (2007). The measurements were performed in the investigation core hole denoted KB_OD3 at two different levels. The first level consisted of four measurements at a depth of 17-21 m. The second level consisted of three measurements at a depth of 31-36 m. According to Berg and Sjöberg (2007), calculated confidence intervals were relatively large, which indicated a certain uncertainty in the measurements. The confidence interval of the upper level was larger than the lower level, which might be explained by the close location to the rock surface for these measurements. The average value of σ_H was equal to 11.2 MPa for the first level and 8.3 MPa for the second level. The average value of σ_h for the

first and second level was equal to 7.2 MPa and 4 MPa respectively. It can be observed that the measured values at the second level are close to those which corresponds to the maximum value in the stress domain at Norrmalm and Riddarholmen as suggested by Perman and Sjöberg (2007), where $\sigma_H=8.1$ MPa and $\sigma_h=4.3$ MPa at a depth of 30 m.

Table 1 Suggested *in situ* stress profiles by Perman and Sjöberg (2007).

Stress Domain		Vertical Depth (m)	σ_H (MPa)	σ_h (MPa)	σ_v (MPa)
Norrmalm & Riddarholmen	Min	0-80	$3.0+0.075z$	$0.5+0.0275z$	$0.021z$
	Typ	0-80	$4.7+0.075z$	$2.3+0.0275z$	$0.0265z$
	Max	0-80	$5.8+0.075z$	$3.5+0.0275z$	$0.032z$
Södermalm	Min	0-80	$2.0+0.075z$	$0.0265z$	$0.021z$
	Typ	0-80	$2.0+0.125z$	$1.0+0.100z$	$0.0265z$
	Max	0-80	$5.8+0.125z$	$2.0+0.100z$	$0.032z$

Table 2 Suggested orientation for in situ stress profiles given by Perman & Sjöberg (2007). Orientation is given relative to geographic North.

Stress Domain		Orientation σ_H (°)
Norrmalm & Riddarholmen	Min	110
	Typ	143
	Max	170
Södermalm	Min	90
	Typ	110
	Max	160

In addition to the measurements summarized by Perman and Sjöberg (2007), only two other measurements have been performed in the Stockholm region according to the knowledge of the authors; at Lovön for the Stockholm Bypass Project and at the Henriksdal Wastewater Treatment Plant. The measurements at Lovön are described in the report by Ask (2013). However, due to a problem during the hydraulic measurements, building the necessary pressure for hydraulic fracturing was problematic and the results could not be properly verified. Therefore, the results from these measurements are equipped with significant uncertainties and are considered to not give any additional information to the summary performed by Perman and Sjöberg (2007). The measurements at the Henriksdal Wastewater Treatment Plant were recently performed and have not yet been released for public use.

3.2 Back analysis

Back analysis problems may in principle be solved in two different ways, with the inverse and the direct approaches (Cividini et al. 1981). In the inverse method, a formulation opposite to that adopted for the stress analysis is used to calculate the unknown parameters. Such a method was e.g. presented by Sakurai and Takeuchi (1983). In this method, Poisson's ratio and the vertical initial stress were assumed to be known and the initial state of stress and the Young's modulus were back-calculated through an inverse method based on measured displacements.

The direct approach, on the other hand, uses the same numerical model used for the stress analysis together with an iterative search procedure in order for the trial values of the unknown parameters to minimise the discrepancy between the calculated and measured data. According to Cividini et al. (1981), the direct approach has a more general validity and is suitable to use for a range of different back analysis (or characterization) problems.

In order to carry out a back analysis, it is necessary to have (Oreste 2005):

- A representative calculation model that can determine the stress/strain field in the rock mass
- An error function
- An efficient algorithm that reduces the error (difference) between the calculation results of the numerical model and the observed *in situ* measurements.

According to Miranda et al. (2013) the most commonly used error function is the least square defined as:

$$\epsilon = \frac{1}{m} \sum_{j=1}^m \left[\frac{u_j - f_j(\hat{x})}{u_j} \right]^2$$

Where ϵ is the mean squared error, \hat{x} is the vector of n components of the parameter to be estimated, n_j is the j obtained measurement, f_j is the computed value corresponding to the j measurement and m is the *in situ* measurement number.

Miranda et al. (2011) performed a state of the art review of optimisation algorithms. A common optimization algorithm used in the displacement back analysis is the Simplex method, which was used by Calvadini et al (1981) to back analyse some different types of the geotechnical problems. Another common optimisation technique is the univariate optimization algorithm. It was used by e.g. Yazdani et al. (2012) for the back analysis of rock mechanical parameters and *in situ* stresses at the Siah Biseh powerhouse cavern for both continuum and discontinuum modelling. In the univariate method, only one variable is changed at a time and the values of the other $n-1$ variables are fixed. After optimization of one variable in the first step while the others are fixed; the value of another variable is changed in the next step, while the remaining ones are fixed. This procedure continues until the values all variables have been optimized and fulfil a predefined acceptance criterion.

A limitation with the above technique is that it usually requires relatively large number of computations which is time-consuming, especially for three-dimensional discrete element elasto-plastic calculations (Yazdani et al. 2012). For example, in the work by Jeon and Yang (2004), at least 6-8 iterations steps were required to reach the optimal values for two unknown parameters. In these analyses, it was unclear how many runs with the numerical model that was required to reach the optimum value for the varied parameter in each iteration step.

Another limitation according to Miranda et al. (2011) is that a maximum of two to three parameters are possible to back analyse with the commonly used optimisation algorithms, which means that it is usually advisable to perform sensitivity analyses before the back analysis process are performed. They also point out that in geotechnical problems with several unknown parameters to optimise, highly non-linear optimisation functions are common in geotechnical problems, which means that several local minima might exist, which could lead to different solutions depending on the start value. A possible strategy to

validate the results is to carry out several runs of the optimisation process with different initial start values and analyse the results.

Other examples of a displacement based back analysis using a direct approach are the work by Yang et al. (2000) and Zhang et al. (2006).

Another type of approach was suggested by McKinnon (2001), which minimizes the error between measured stresses and stresses computed with numerical models, to obtain the *in situ* stress field. The technique is mainly used if the stresses in the measurement points are influenced from nearby complex structures such as caverns or tunnels. With the technique it is possible to estimate the far field stress or boundary conditions that best reproduce the stress measurements. According to McKinnon (2001), the stress field at any point is assumed to consist of gravitational and tectonic components, where the tectonic component is assumed to act in the horizontal plane and the gravitational component is assumed to act in the vertical direction. At the model boundary, unit normal and shear tractions are applied and the response is computed at the measurement point in the model. The error between measured and computed errors are minimised through a least square approach and used to compute the proportions of each unit response tensor to reproduce the measured stress in the measurement point.

A similar methodology was used by Chang (2007) to calculate the *in situ* stresses in the rock mass around the platform cavern for the subway station T-Centralen (blue line). In this case, three stress measurements had been performed below the platform room (not influenced by the cavern) and ten measurements in the two pillars in the platform room. To use all measured stresses to estimate the *in situ* stress state, the sum of the squares of the components of the error tensor were minimized by derivation of the error function and setting it equal to zero. After that, the constant representing the proportions of each elementary stress field required to reproduce the stress field in the measurement points was calculated.

At the Odenplan station measured deformations from three extensometers located in the tunnel roof exist. These measured deformations are suitable to use in order to perform a direct back analysis. The relatively large deformations that occur in the rock mass indicate plastic behaviour with slip occurring along existing fractures. A proper back analysis should therefore include an optimisation of horizontal *in situ* stresses, the Young's modulus of the intact rock (including the intact rock and minor fractures not included in the *3DEC* model) and the cohesion and friction angle of the fractures. However, the *3DEC* model of Odenplan used in this study, under elasto-plastic conditions, requires approximately two-three weeks for one single run. Even if only two parameters were optimised in the back analysis, it will

most likely result in a computational time of at least 6 months. In addition to this, it would be advisable performing a parametric sensitivity study to identify the most important parameters before the back analysis started.

Due to these long computational times, a parametric study on the *in situ* stresses will be performed in this work instead of a complete back analysis. Vardakos et al. (2007) used this methodology when back analysing the Shimizu research tunnel No. 3 to determine the effects of model parameters on the predicted tunnel response, which were compared against field measurements.

4 DESCRIPTION OF THE ODENPLAN STATION

4.1 Geometry

The Odenplan City Link Station consist of a 250 m long platform room with exists to Vanadisvägen and Odenplan. Parallel and south to the platform room, a service tunnel is located. The analyzed part of Station Odenplan in this project is where the new station crosses the existing subway station at chainage 32+600, where the elevator shaft up to the subway is located. A plan of the eastern part of the station at the exit to Odenplan can be seen in Figure 3.

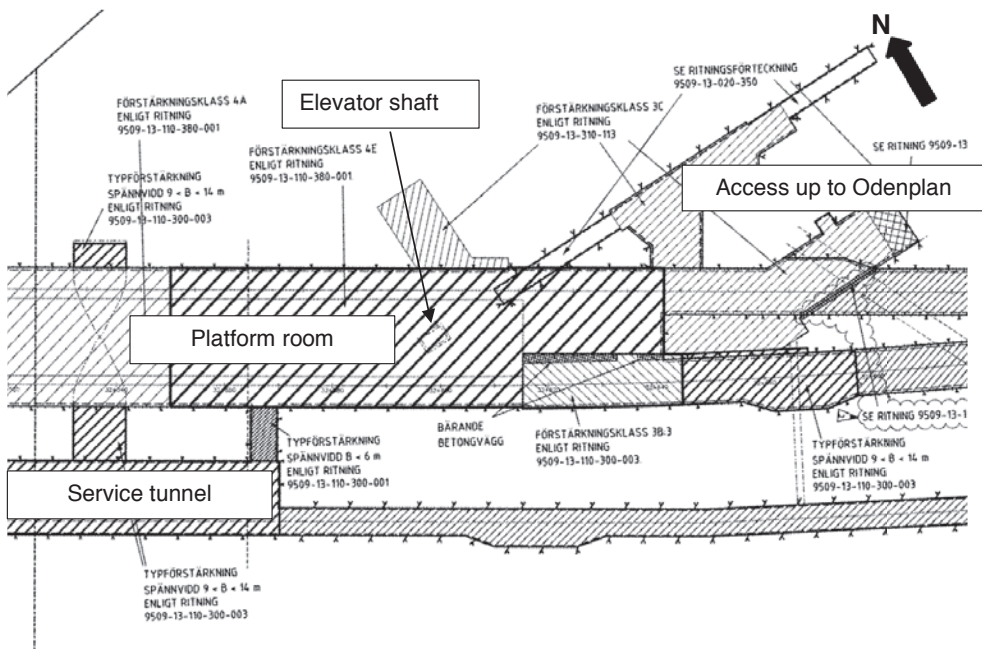


Figure 3 Plan over the eastern part of the station with the exit up to Odenplan (From drawing 9509-13-110-136-002).

The width of the station cavern is 25 m with a height of approximately 14 m in connection to the exit up to Odenplan, see Figure 4. However, in this project only the first upper part of the excavation is considered in this project, which has a height of 6.4 m. The rock cover between the existing subway and the platform cavern is approximately 7 m. At chainage

32+615 the platform room is divided into two separate tunnels, the southern track tunnel U2 with a width of 8.5 m and the exit tunnel up to Odenplan with a width of 14 m. The exit tunnel up to Odenplan from chainage 32+615 is not included in this study. Since tunnel U2 is being located at a lower level than the upper part of the platform cavern, a ramp down to tunnel U2 is included in this work, which can be seen in Figure 5.

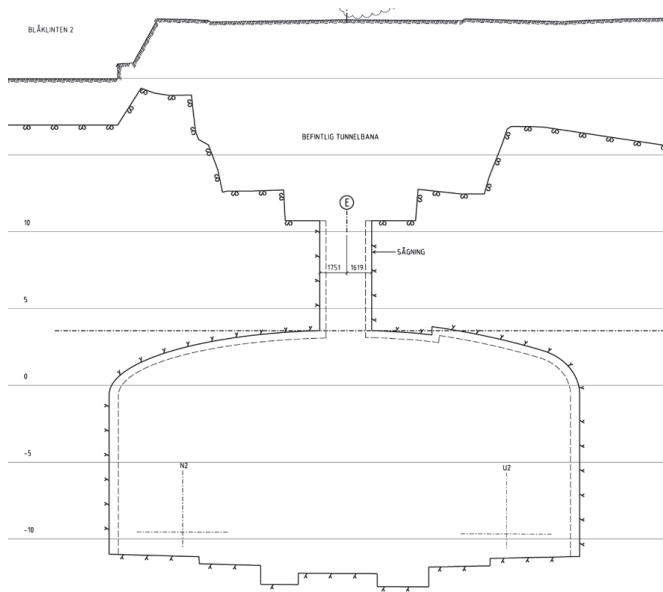


Figure 4 Section through the platform room at chainage 32+600 through the elevator shaft (From drawing 9509-13-110-370-009).



Figure 5 Photo of the upper part of the platform room taken towards future exit up to Odenplan (left) and ramp down to tunnel U2 (right) (Photo: Jonas Paulsson, SWECO).

4.2 Geology and mapped fractures

The eastern part of the Odenplan station with the exit up to Odenplan, which is of interest in this study, is located in a geological domain denoted SO in the engineering geology prognosis (Fjelberg et al. 2009). This domain, estimated in the prognosis to be located between chainage 32+550 and 32+665 mainly consist of granite with smaller intrusion of pegmatite. The rock mass quality was in the prognosis estimated to be of slightly lower quality than the rest of the rock mass around Odenplan, mainly due to a higher content of smooth planar rock joints with infillings of chlorite. Also, the average fracture distance in the domain is 3 fractures/m compared to about 2 fractures/m in the other domain. Data of estimated rock mass quality from the engineering geology prognosis at domain SO is presented in Table 3.

Table 3 Data from estimated rock mass quality of domain SO (Fjelberg et al. 2009).

	Domain SO		
Statistical data	RMR_{base}	GSI	Q_{base}
Min	55	60	4
Typ	70	65	20
Max	80	75	60

Performed mapping of the rock mass in the elevator shaft gave an RMR_{base} of 67 with three dominant joint sets with a strike and dip of 100/40, 240/50 and 040/10 (Johansson et al. 2013). The platform room has a direction of 120°. The mapping of rock mass quality between the access to the subway and the platform room (approximately at chainage 32+640) gave an RMR_{base} of 76. These values agreed well with the prognosis in Table 2.

Performed mapping of the joints in the platform room can be seen in Figure 6 and Figure 7 (Johansson et al. 2009). In these figures, those fractures with the most dominant persistence, of importance for the global stability, are illustrated. In the figures, it can be seen that there exists a large number of persistent fractures with lengths over 20 m at the location around the elevator shaft. In Figure 8, a photo of the tunnel face clearly illustrates a joint system with a dip of approximately 70°, which dominates the joint pattern. The strike of this joint system is parallel with the platform room and the average joint distance is 1,5-2 m. The joint roughness could be described as planar and relatively smooth with a JRC=2-4.

Mechanical properties of the rock mass, fracture network and *in situ* stresses used in the numerical calculations are presented in detail in chapter 5.

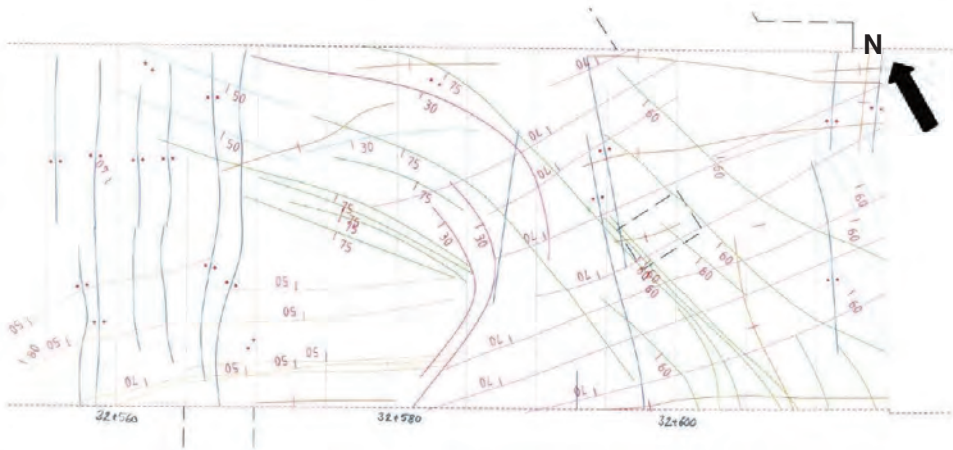


Figure 6 Mapping of platform room between chainage 32+560 to 32+615 (From Johansson et al. 2013).

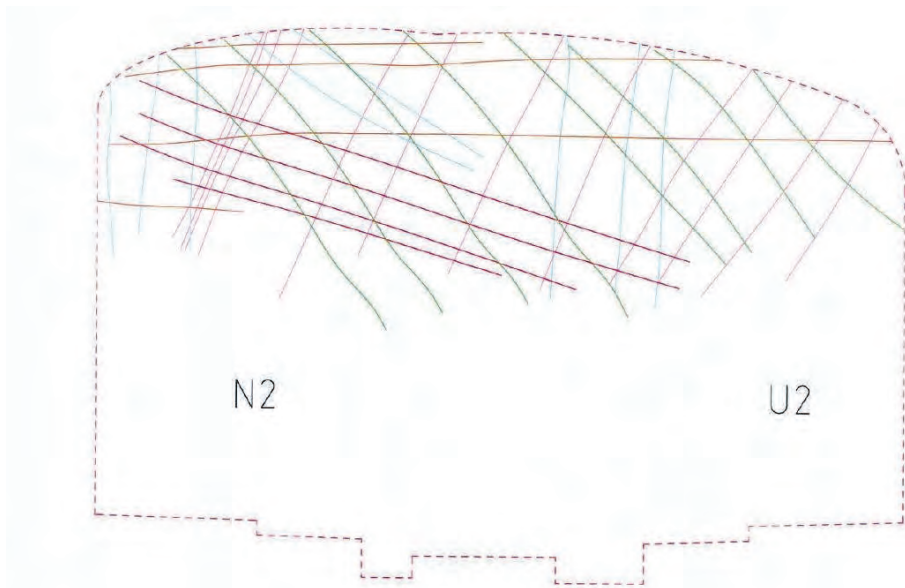


Figure 7 Mapping of tunnel face at chainage 32+615 (From Johansson et al. 2013).



Figure 8 Photo of tunnel face, approximately at chainage 32+600 (From Johansson et al. 2013, Photo: Jonas Paulsson, SWECO).

4.3 Excavation sequences

The service tunnel and the access tunnel were excavated before the platform room. The upper part of the platform room, from chainage 32+580 to 32+615, was excavated from 2012-07-03 to 2012-09-12. All the excavation sequences were 4 m long, except for the last one from chainage 32+612 to 32+615, which was 3 m long.

4.4 Rock support

In the platform room after each excavation, 100 mm shotcrete was applied up to 2 m from the tunnel face. 100 mm of additional shotcrete was applied up to 4 m from the tunnel face. Once a total of 200 mm of shotcrete had been applied in the roof and 50 mm on the walls had been applied, systematic bolting diameter 25 mm, with s-distance of 1.7 m and a length of 6 m was installed.

The service tunnel and the connection tunnel to the platform room had a support of 50 mm of shotcrete in the roof and walls and systematic bolting, diameter 25 mm, with a s-distance of 2 m and a length of 2.4 m installed.

In tunnel U2, a support of 75 mm of shotcrete in the roof and 50 mm in the walls was applied combined with systematic bolting, diameter 25 mm, with s-distance 1.7 m and a bolt length of 4 m.

Around the elevator shaft, bolts with a diameter of 25 mm parallel with it was installed at a distance of 0.5 m from the walls of the shaft. The bolt length was 3 m and the distance between the bolts was 1 m.

Support properties used in the calculations are presented in chapter 5.

4.5 Monitoring system

In January 2012, measurements started in a shelter under the existing Odenplan subway station with a liquid levelling system, and in July 2012 measurements started with extensometers. Water levelling gauges MC51-526 and MC-530 were placed in the walls of the shelter under the platform for the existing subway station. Extensometers E04, E05 and E06 were installed in the shelter at chainage 32+590. Water levelling gauges LLS 536, LLS537 and LLS 538 were installed at the head of the extensometers E04, E05 and E06 respectively. There were three more extensometers installed, E01, E02 and E03, but measurement data was not available. The location of the water levelling gauges and extensometers is illustrated in Figure 9 and Figure 10.

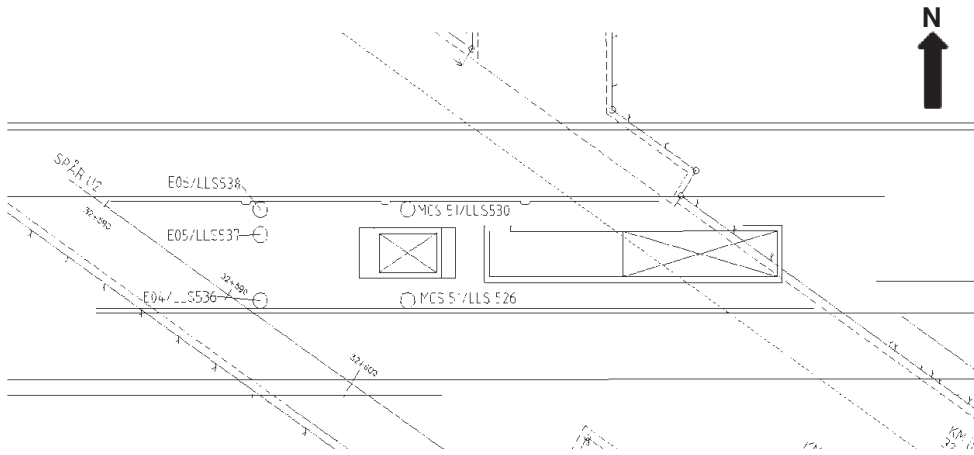


Figure 9 Plan over crossing between the new platform room and the existing subway at Odenplan with location of water levelling gauges and extensometers (From Johansson et al. 2013).

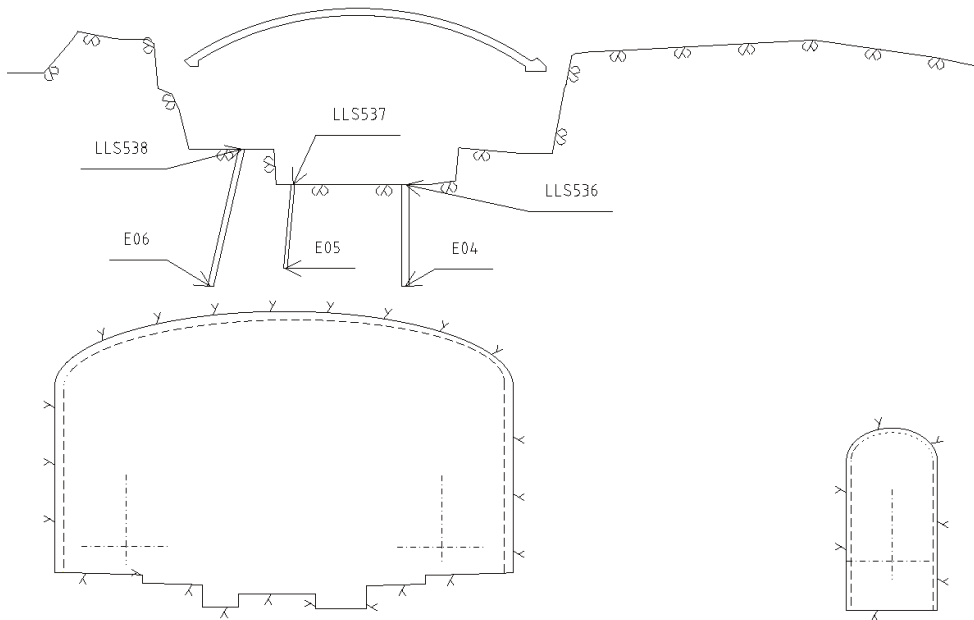


Figure 10 Section at chainage 32+590 showing the location of extensometers and liquid levelling gauges (From Johansson et al. 2013).

The observed deformations in the extensometers and the liquid levelling system are associated with two different events, the excavation of the platform room and the sawing of the elevator shaft at chainage 32+600. Results from the water levelling gauges LLS526 and LLS530 are presented in Figure 11.



Figure 11 Results from measurements with liquid levelling gauges LLS 526 and LLS530 (From Johansson et al. 2013).

As the results in Figure 11 shows, a heave of 4 and 6 mm of LLS526 and LLS530 respectively were observed from July to October. From November to January, no larger excavations were performed in the platform room under the shelter, and subsequently no deformations were observed during this period. When the elevator shaft was sawed in January, an additional heave of approximately 3 mm was observed in LLS 526 and LLS530. The final heave was stabilized at 6-7 mm for LLS 526 while the final heave for LLS 530 was 8-9 mm. The heave for the liquid levelling gauges installed at the top of the extensometers was stabilized at 6-7 mm for LLS536, LLS537 and LLS 538, behaving similar to that of LLS526.

The observed deformations in the extensometers E04, E05 and E06 are presented in Figure 12. After the excavation of the platform room (July to October) an extension of the extensometers between 2 to 7 mm was observed. A tendency for small creep deformations could be observed from October 2012 to January 2013 before the elevator shaft was excavated. In connection with the sawing of the elevator shaft, the deformations in the extensometers increased approximately 2 mm. The final extensions of the extensometers were between 5 to 10 mm. Since the liquid levelling system observed a heave of the top of the extensometers with approximately 6 mm, it means that the bottom anchor of E05 has moved upwards with 1 mm while the bottom anchor of E04 and E06 has moved downwards with 1 and 4 mm respectively.

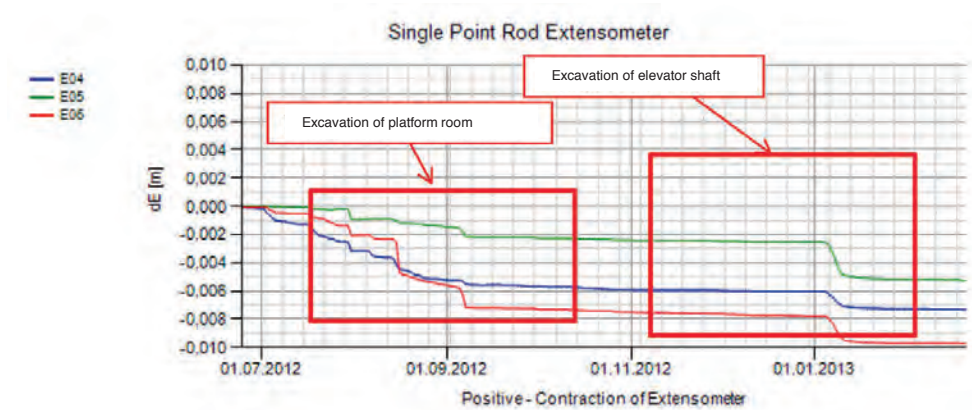


Figure 12 Results from measurements with extensometers E04, E05 and E06 (From Johansson et al. 2013).

In addition to the measurements with the liquid levelling system and the extensometers, convergence measurements were performed in the platform room. Each measurement section contained 5 prisms every 10 m. No significant movements were observed with the convergence measurements except in section 32+590. In this section, two measurement points located in the northern part of the roof observed relatively high deformations. The deformations were directed downwards into the center of the platform room and measured 10-15 mm.

5 NUMERICAL MODELING

As mentioned in Section 1.1, previous continuum modeling had not been able to predict the measured rock mass behavior during the construction of the Odenplan station. Taking into account the large amount of rock mass characterization data, including good quality mapping of the tunnel surface, it was decided to investigate if, in cases like this (i.e., shallow tunnel with visible blocky rock structure) discontinuum modeling including a representation of the fracture network can capture the measured heterogeneous rock mass response in a better way than continuum modeling. Even though researchers, consultants and other practitioners are hesitant to adopt discontinuum modeling including a dense fracture network representation, there are cases in which it cannot be avoided, if a proper representation of the rock mass behavior and therefore a reliable prediction is desired. As stated by Hoek & Brown (1997): “Where the block size is of the same order as that of the structure being analyzed, the Hoek-Brown criterion should not be used”. In the present report this refers to the inability of the continuum approach to properly capture the heterogeneous dilational behavior of blocky rock, which is dominated by the local block geometry.

Following the recommendations from Palmström and Stille (2010), taking into account that the average fracture spacing of the dominant joint system from the mapping data (Söder and Johansson, 2007) is in the order of 1-2 m and the Platform tunnel has a span of around 25 m, this yields a continuity factor $CF = \text{tunnel diameter} / \text{block diameter} = 12.5 - 25$. This range of CF falls in what Palmström and Stille call discontinuous (blocky) systems, and they advise a discontinuum approach to study its behavior.

Furthermore, according to Martin, Kaiser and Christiansson (2003), and based on the available data by Söder and Johansson (2007) and the recommended *in situ* stress by Perman and Sjöberg (2007), the expected instability mode would be gravity-induced structurally controlled block movement, which is also illustrated in Figure 13.

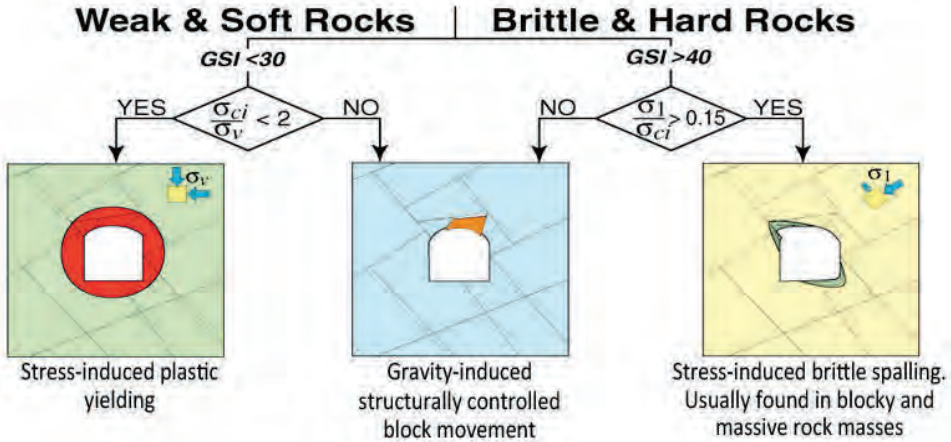


Figure 13 Instability mode based on rock quality (GSI), intact rock strength and stress level (Martin et al., 2003).

The discontinuum numerical software used in this project is *3DEC* (Itasca, 2013). *3DEC* is based on DEM (distinct element method). The formulation and development of the distinct element method embodied in *3DEC* has progressed for a period of over 40 years, beginning with the initial presentation by Cundall (1971). The main features that make *3DEC* an optimal option for this project are:

- *3DEC* represents an assembly of discrete blocks in 3D separated by joints, fractures or faults.
- *3DEC* provides a realistic representation of problems at different scales in rock where discontinuities (e.g., joints, fractures or faults) control the behavior.
- The model is generated by
 - defining geometry of the blocks in space, and
 - cutting existing blocks by specified discontinuity planes.
- Discontinuities between blocks can shear, slip and/or open.
- Blocks and discontinuities can be assigned different constitutive models (e.g. Linear Elastic, Mohr-Coulomb, Hoek-Brown, Coulomb slip law, Barton-Bandis law, etc).

5.1 Overall model geometry and numerical mesh

Odenplan station consists of two parallel sets of tunnels located at a depth of around 20 m (measured from the roof of the tunnels) and oriented 118.8°N: Platform tunnel, tunnel U2 and Service tunnel connected by the Connection tunnel (Figure 14,

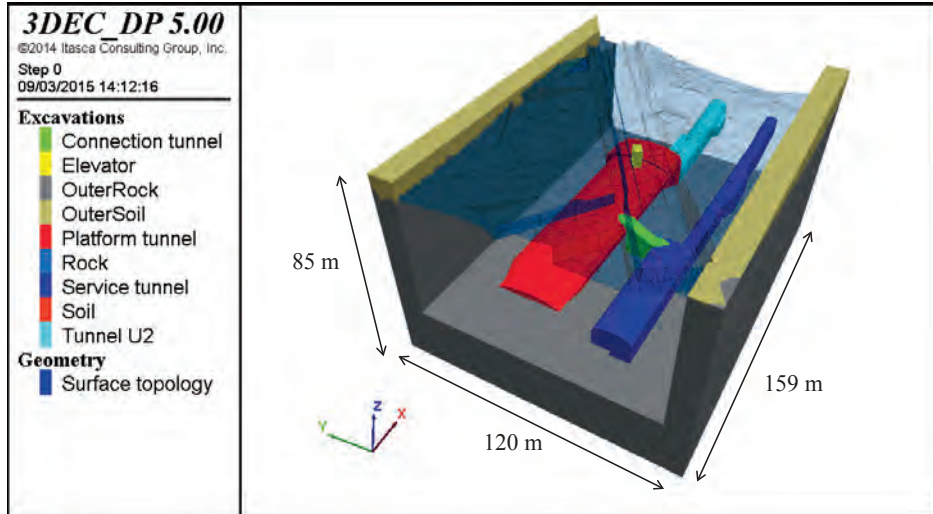


Figure 15 and Figure 16). The Platform tunnel (or railway tunnel) has a span of around 25 m. Only its upper part (of 6.4 m height) is excavated before the end of the phasing considered in this study. The rock surface topology is irregular. It separates the rock mass from the soil layer. Furthermore, a subway track (section 19 m x 13 m) is excavated on the ground surface; it crosses over the railway tunnel in the area where the elevator shaft is present, limiting the rock cover to around 7 m. It is in this area where, during the final step, excavation of the elevator shaft, large values of displacement were recorded at some monitoring points installed at the roof of the railway tunnel (up to 10 mm) and large values of rock dilatancy (from 5 to 10 mm) were recorded in extensometers installed between the roof of the railway tunnel and the ground surface.

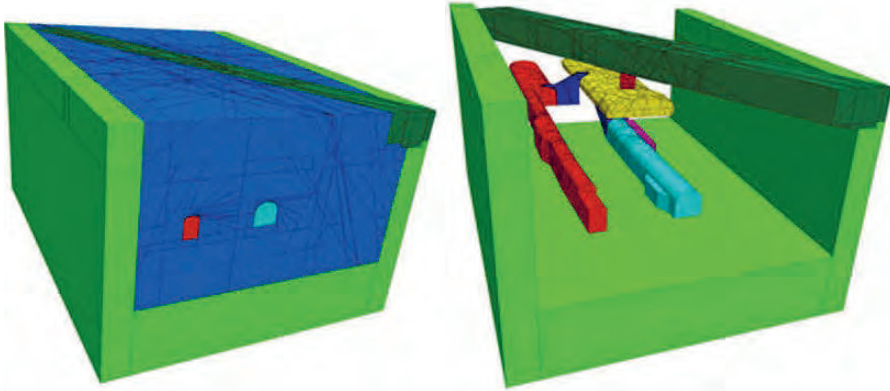


Figure 14 Modeled tunnels inside the finer model region (blue region in left figure) with respect to the lateral coarser boundary region (clear green region). The region in dark green is the part of the soil that represents the subway track volume and it is excavated in the first stages of the modeling sequence.

There are both an outer soil and outer rock regions which act as buffer boundary regions on the lateral sides and at the bottom of the model. Their role is the representation of the far field rock and soil.

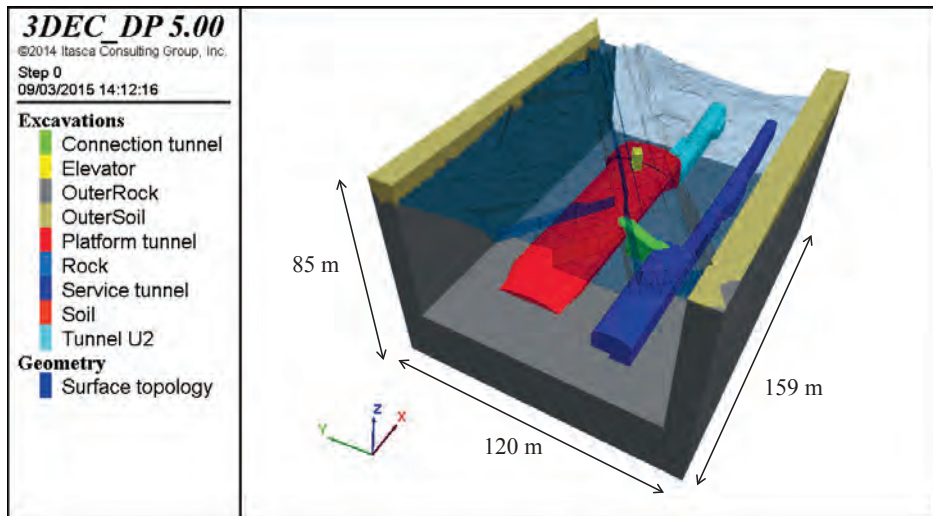


Figure 15 View of the model with its dimensions. Surface topology refers to the rock surface under the soil layer.

Figure 16 shows the parts of the tunnels as well as the traces of the fractures included in the model. Only the upper part of the platform tunnel was modeled because the excavation sequence selected for the modeling exercise didn't include the excavation of the lower part.

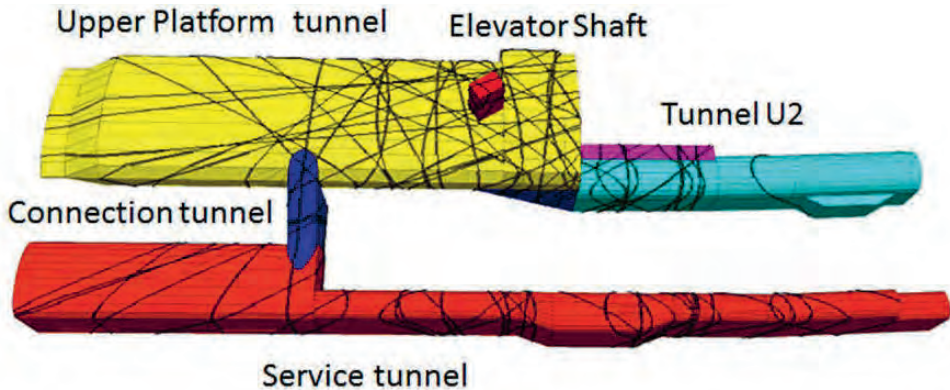


Figure 16 Simplified shape of the part of the tunnels included in the model (Upper Platform tunnel – yellow, Elevator Shaft – red, Tunnel U2 – cyan and pink, Connection tunnel – dark blue, and Service tunnel - orange). Traces of the included fractures are shown on the tunnels as well.

The model mesh consisted of 1515986 tetrahedral zones. The regions surrounding the tunnels and, in particular the central volume where large displacements occurred, have finer mesh than the farther boundary regions in the model (see Figure 17).

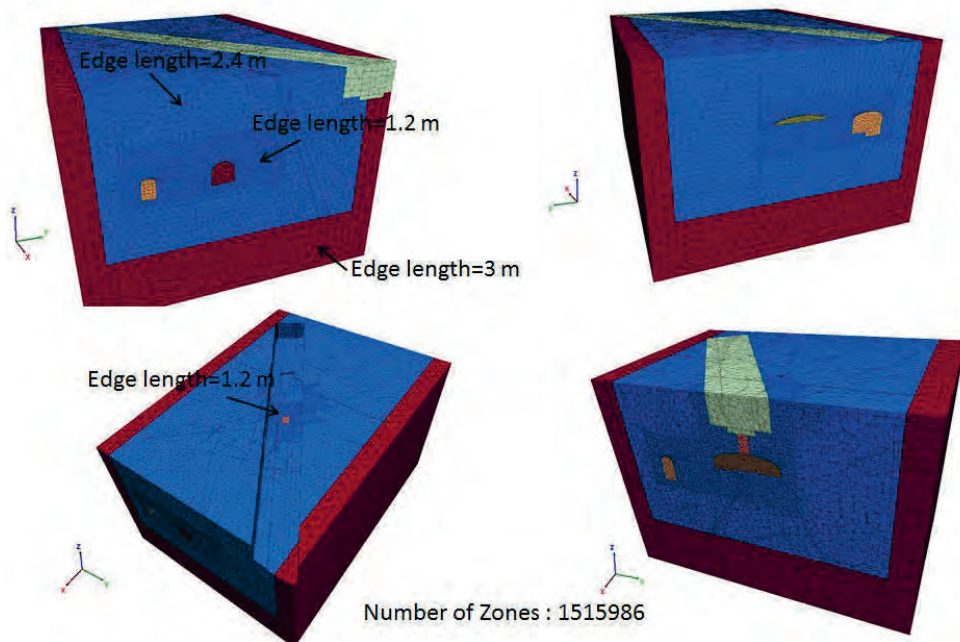


Figure 17 View of the model showing the numerical mesh size used in each region.

5.2 Input data simplification and assumptions

Models are useful because we cannot represent reality. In this sense, a model is a simplification of reality. We do simplifications and assumptions because:

- We never have enough information to know the whole rock-soil system we are working on.
- It would be impractical and overly complicated to include all the data collected with the current technology available. However, most often, there is no need to include all the data in order to capture the expected dominant behavior.

The following subsections present the simplifications and assumptions made in this modeling exercise.

5.2.1 Soil and rock surface topology

Both the surface topology and the tunnel shape were simplified in the model generation. Figure 18 shows the outer boundary model geometry and the different model regions. In the area represented by the model there is a soil layer on top with rather planar surface. In the model the soil upper surface was simplified and considered planar. The contact between the soil layer (red and cyan in Figure 18) and rock underneath (dark blue and green in Figure 18) was modeled in a rather coarse manner (boundary between cyan and dark blue and boundary between red and green in Figure 18). The only purpose of the soil layer is to include in the model the effect of the load of the soil that is transmitted to the rock underneath so even if the contact is coarse it is sufficient for this purpose. The purpose of the outer soil and outer rock regions is to have a coarser boundary region on the lateral sides and the bottom of the model. These coarser regions are sub-parallel to the main tunnels in the model, which are within the finer inner regions.

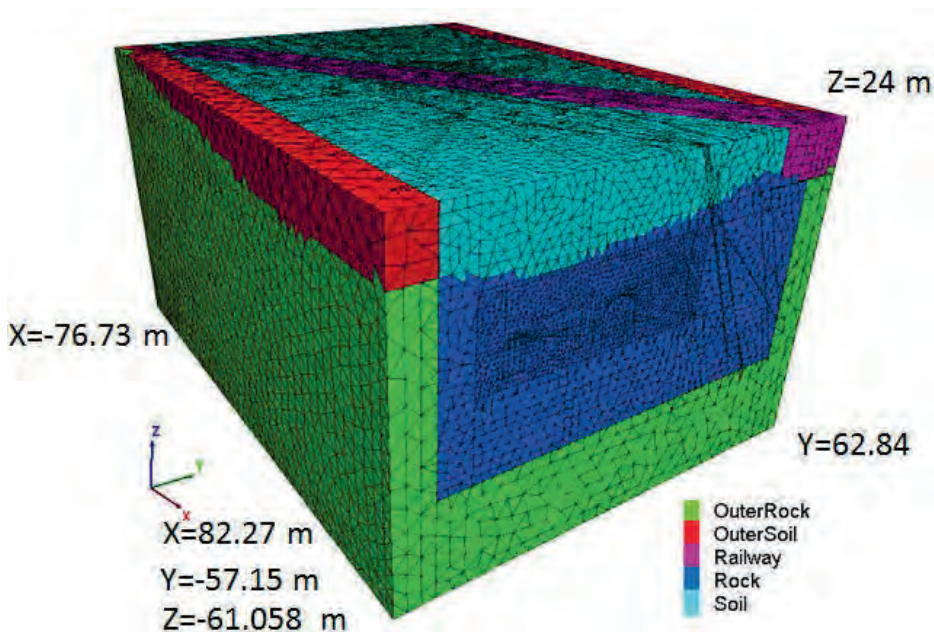


Figure 18 Outer boundary model geometry showing the different regions.

5.2.2 Fracture network

The available mapping data was first imported and visualized (see Figure 19). All the fractures were assumed to be fully persistent within the discontinuum volume of the model (see blue region in Figure 14) as there was no data available in this sense. Then, the fractures that did not intersect the central model volume were removed. The model volume of interest is centered at the elevator shaft and delimited by the green lines in Figure 20.

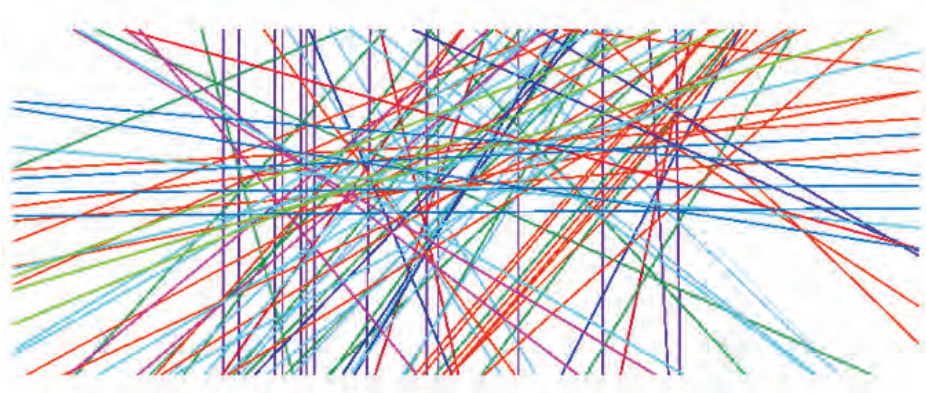


Figure 19 Vertical cut along the axis of the Platform tunnel (at $Y=0$, center of the elevator shaft) with all the fracture traces previous to any simplification.

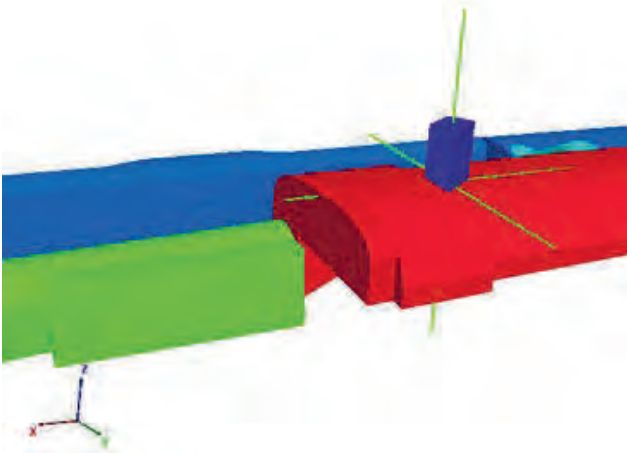


Figure 20 View of the tunnels with the central volume of interest centered at the center of the elevator shaft and delimited by the green lines.

The next step consisted in removing all joints with a dip angle inferior to 50° (see Figure 21). In fact, given that their traces were mainly in the lateral walls, their influence on the blocks structure at the roof is negligible.

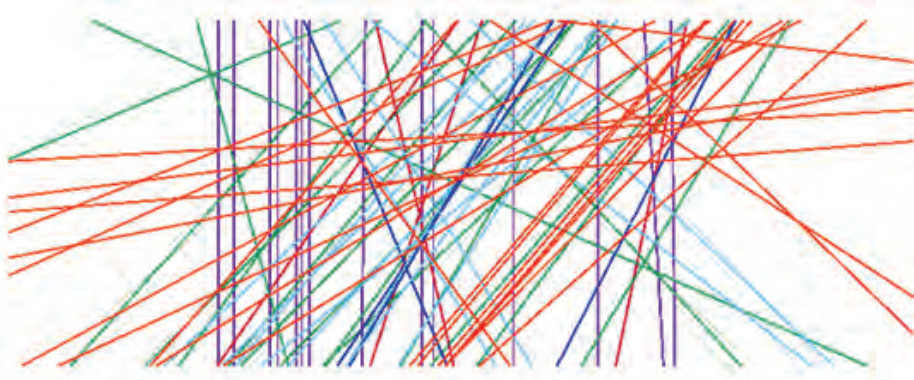


Figure 21 Vertical cut along the axis of the Platform tunnel (at $Y=0$, center of the elevator shaft) after removing all fractures with dip $< 50^\circ$.

Finally, from all the remaining fractures, when two fractures had an angle between them inferior to 15° , one was removed (see Figure 22).

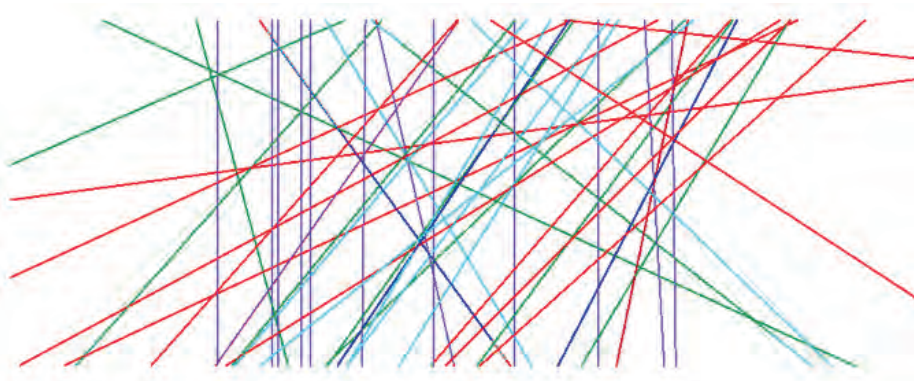


Figure 22 Vertical cut along the axis of the Platform tunnel (at $Y=0$, center of the elevator shaft) after the process by which from all the remaining fractures with an angle between them inferior to 15° one was removed.

These simplifications were mandatory as including all the discontinuities would have required a high refinement of meshing and very large computational time. After the

simplification adopted, the fracture network is still dense. Measurements of P10 (i.e., number of fracture intersections with a transect per unit length) were taken along the three green lines delimiting the central volume of interest (see Figure 20) giving the following values: $P10_x = 0.525$, $P10_y = 0.525$ and $P10_z = 0.45$. This means that around the shaft where the major deformations were monitored, the average distance between fractures in the model is around 2 m in the three coordinate directions. This is in agreement with the mean fracture spacing observed during mapping of the tunnels and observations in the available cores (Söder & Johansson, 2007).

5.2.3 In situ and boundary conditions

Factors such as topography and material heterogeneity (e.g. different rock types, faults, fractures, soil, etc.) can affect the *in situ* stress in an area. Unfortunately, in natural systems, there is never enough information to represent reality with perfect certainty, therefore, four stress states within the range of estimated *in situ* stress according to the available measurements in the Stockholm area (Perman & Sjöberg 2007) have been considered in this study. For each state, the initial minimum and maximum horizontal stresses σ_h and σ_H are given in equation (1) with z the vertical depth (considering equivalent rock cover) and parameters a and b stated in Table 4. Although there is also scatter in the horizontal stress orientation, it was decided in this study to use only the mean orientation (σ_H oriented $143^\circ N$) and to concentrate on the effect of stress magnitude as a first step. Vertical stresses in the soil and rock are calculated from gravitational loads with mass densities ρ given in Table 4. In the soil, the horizontal stresses are isotropic and calculated as a fraction K_0 of vertical stresses.

$$\sigma_H = \sigma_{0H} + a \cdot z \quad ; \quad \sigma_h = \sigma_{0h} + b \cdot z \quad (1)$$

Table 4 Parameters of the different stress cases.

		Case 0	Case 1	Case 2	Case 3
Rock	ρ [t/m ³]	2.1	2.65	3.2	2.65
	σ_{0H} [MPa]	3	4.7	5.7	5.7
	σ_{0h} [MPa]	0.5	2.3	3.5	2.3
	a [MN/m ³]	0.075			
	b [MN/m ³]	0.0275			
Soil	ρ [t/m ³]	2			
	K_0	0.33			

No pore pressure was simulated as fully drained conditions were assumed.

Fixed velocity boundary conditions have been used in this model (see Figure 23). All the lateral vertical boundaries have fixed null velocity both in x and y directions. The bottom horizontal boundary has fixed null velocity in x, y and z directions. The surface is considered as a free boundary.

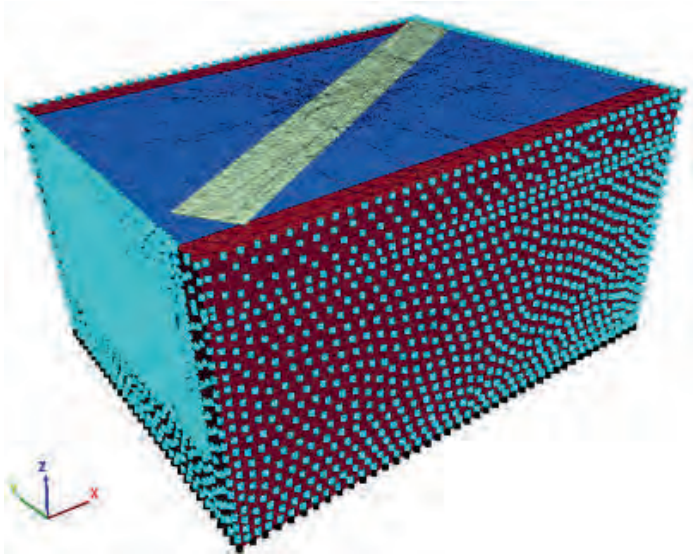


Figure 23 Boundary conditions in the model. Lateral vertical and bottom horizontal boundaries have fixed velocity conditions while the surface is a free boundary.

5.2.4 Input properties

The following subsections present the input properties used in the simulations.

5.2.4.1 Soil, intact rock and rock mass properties

The soil was considered as homogenous linear elastic material in all the different cases simulated.

The outer rock was considered as an equivalent continuous, homogenous and linear elastic material with rock mass Young's modulus derived according to Hoek & Diederichs (2006) based on the mapped GSI mean value. Based on the data compiled and analyzed by Söder &

Johansson (2007), the estimated GSI value for the rock domain SE is 65. This yields a rock mass Young's modulus of 47.3 GPa.

Using the value of the rock mass Young's modulus estimated based on the mapped GSI (Hoek & Diederichs, 2006), the intact rock Young's modulus and the mean fracture spacing, the fracture stiffness, k_n , can be estimated using the following Eq (2):

$$k_n = \frac{E_i * E_{rm}}{s * (E_i + E_{rm})} \quad (2)$$

where

k_n = fracture normal stiffness

E_i = intact rock Young's modulus.

E_{rm} = rock mass Young's modulus.

s = mean fracture spacing.

In the model there is an outer lateral and bottom buffer region where there are no fractures. This region is called outer rock and will always be given an equivalent rock mass Young's modulus of 47.3 GPa. The same Young's modulus will be used in the inner rock region around the tunnels when it is considered as an equivalent continuum. However, when the fractures are active the inner rock will have a Young's modulus of 75 GPa (that of the intact rock). In order for the inner rock mass to behave elastically in the same manner as the outer rock, and assuming a mean fracture spacing of around 2m, k_n needs to be approximately 75 GPa/m. Using Eq(1) this yields an equivalent Young's modulus of 50 GPa which is very close to that of the outer rock. The elastic soil and rock parameters used in the simulations are compiled in Table 5.

Table 5 Elastic rock and soil properties used in the model.

	Elastic properties		Density ρ (kg/m ³)			
	E (MPa)	ν	Case 0	Case 1	Case 2	Case 3
Outer Rock	47300	0.25	2100	2650	3200	2650
Rock	75000	0.24	2100	2650	3200	2650
Soil & Outer Soil	27	0.2	2000			

A continuum elasto-plastic model following the modified Hoek-Brown constitutive model (Itasca, 2013) with case 3 *in situ* stress was also simulated, to investigate if considering plasticity would improve the continuum simulations. In this case the soil was also elastic and had the same parameters as in all the other runs. The outer rock was elastic and had the parameters shown in Table 5. Based on the information in Söder & Johansson (2007),

$$GSI = 65$$

$$m_i = 27$$

$$E_i = 75 \text{ GPa}$$

$$\sigma_{ci} = 220 \text{ MPa}$$

the parameters used for the inner continuum rock mass that were estimated using RocLab (Rocscience, 2013) are summarized below:

$$a = 0.502$$

$$m_b = 7.736$$

$$s = 0.0205$$

$$E_m = 47.3 \text{ GPa}$$

$$\nu = 0.25$$

$$\text{tension cutoff} = 0.6 \text{ MPa}$$

5.2.4.2 Fracture properties

The fracture properties used in the simulations were derived based on the data available in Söder & Johansson (2007). Based on this report the estimated mean values of JRC and JCS at *in situ* scale are 7 and 50 MPa respectively. Additionally, the estimated mean residual friction angle is 30°.

Barton's shear strength criterion for joints (Barton, 1976; Barton & Choubey, 1977) states:

$$\tau_s = \sigma_n * \tan \left(JRC \log_{10} \left(\frac{JCS}{\sigma_n} \right) + \phi_r \right) \quad (3)$$

where

τ_s = shear strength (MPa)

σ_n = normal stress (MPa)

JRC = Joint Roughness Coefficient

JCS = Joint Wall Compressive Strength (MPa), and

ϕ_r = residual friction angle (°)

For dry, unweathered joint surfaces, the residual friction angle is equal to the basic friction angle, (i.e., the basic friction angle, ϕ_b is the shear resistance of flat, unweathered rock surfaces) whereas it can be significantly lower for weathered and/or wet surfaces.

Even though k_s is a parameter that varies slightly for different levels of shear stress, it is usual practice to estimate it as the mean value of the slope of the shear stress-shear displacement curve when it reaches the peak shear stress τ_{peak} . This means:

$$k_s = \frac{\tau_{peak}}{\delta_{n,peak}} \quad (4)$$

Most frequently, τ_{peak} is reached for values of the shear displacement, δ_n , of approximately 1% of the fracture length, this is when $\delta_{n,peak} = L_n/100$. Taking this into account, Barton & Choubey (1977) suggested that the peak shear stiffness could be adjusted to the scale by introducing a factor $100/L$. According to this and inserting Barton's formula (Eq. (3)) in Eq. (4) we have the following Eq. (7):

$$k_s = \frac{100}{L} * \sigma_n * \tan \left(JRC * \log_{10} \left(\frac{JCS}{\sigma_n} \right) + \phi_r \right) \quad (5)$$

where

σ_n = effective normal stress acting on the fracture (MPa)

L = fracture length (m). If the scale effect does die out when a certain critical length of joint (L_c) is exceeded then the value of L used in Eq. (4) should not exceed L_c

Based on this and estimating a $\sigma_n = 10$ MPa around the tunnel, we have an estimated value of $k_s = 7$ GPa /m.

Additionally, the magnitude of k_n necessary for the rock mass Young's modulus calculated with Eq. (5) to be approximately the same as that based on the GSI approach (Hoek & Diederichs, 2006) is 75 GP/m. If we assume k_n to be 10 times larger than k_s , which is in agreement with the commonly accepted range (e.g. Glamheden et al., 2007; Hakami et al., 2008; Itasca, 2013), then $k_s = 7.5$ GPa/m, which agrees quite well with the k_s value estimated using Eq (5).

The Coulomb slip friction angle and cohesion were estimated using the approach proposed by Hoek et al., (1995) and presented in the following paragraphs.

These equivalent parameters are called instantaneous cohesion c_i and instantaneous friction angle ϕ_i for a given normal stress, σ_n (see Figure 24). Provided that the normal stress, σ_n , is

reasonably close to the value used to define the tangent point, these are the two parameters that may be used for stability analyses if the Mohr Coulomb failure criterion is applied.

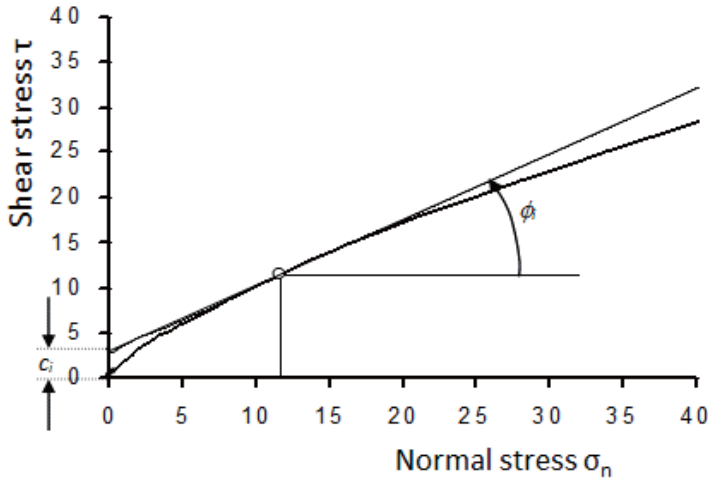


Figure 24 Definition of the instantaneous cohesion and friction angle for a non-linear failure criteria (Based on Hoek et al., 1995).

It is important to point that Eq. (3) is not valid for $\sigma_n = 0$ and it ceases to have any practical meaning for $\phi_b + JRC \log(JCS/\sigma_n) > 70^\circ$. This limit can be used to determine a minimum value for σ_n , while an upper limit for σ_n is given by $\sigma_n = JCS$.

In order to estimate the instantaneous friction angle, the following formula can be used:

$$\phi_i = \arctan\left(\frac{\partial\tau}{\partial\sigma_n}\right) \quad (6)$$

where

$$\frac{\partial\tau}{\partial\sigma_n} = \tan\left(JRC \log\left(\frac{JCS}{\sigma_n}\right) + \phi_b\right) - \frac{\pi JRC}{\ln 10} \left(\tan^2\left(JRC \log\frac{JCS}{\sigma_n} + \phi_b\right) + 1\right) \quad (7)$$

The instantaneous cohesion is calculated from:

$$c_i = \tau - \sigma_n \tan\phi_i \quad (8)$$

After applying this methodology and assuming a $\sigma_n = 10$ MPa, an instantaneous friction angle of approximately 32° and an instantaneous cohesion of approximately 0.8 MPa are obtained.

When the normal stress acting on the fracture is sufficiently lower than the rock strength or the strength of the fracture walls, the peak dilation angle is equal to the difference between the peak friction angle and the residual friction angle. This means that it can be estimated based on the following expression (Barton and Choubey, 1977):

$$d_{n-peak} = JRC \log_{10} \left(\frac{JCS}{\sigma_n} \right) \quad (9)$$

In this case the asperities will suffer almost no damage during shear. If, on the other hand, the normal stress is higher than the strength of the asperities, these will be damaged during the shear process and, according to Barton and Bandis (1990), the dilation angle will be reduced to approximately half of the value obtained using Eq. (9).

Using $\sigma_n = 5-10$ MPa in Eq (9) an estimated dilation angle of approximately $5-7^\circ$ is obtained. These values are also in range with those in recently published data for these levels of normal stress (Glamheden et al., 2007; Hakami et al., 2008).

Thus the fracture properties used in this project are as follows:

Normal stiffness: $K_n = 75$ GPa/m
 Shear stiffness: $K_s = 7.5$ GPa/m
 Cohesion: $c = 0.8$ MPa (or $c=0$ MPa*)
 Friction: $\phi = 32^\circ$
 Residual friction: $\phi_{res} = 30^\circ$
 Dilation: $\Psi = 7^\circ$

* $c = 0$ MPa may also be appropriate for very shallow environments with 0-5 MPa normal stress on the fractures.

Fractures in the soil zone group should not exist. Therefore they are assigned the following properties:

$c = 100$ MPa,
 T(tensile strength) = 100 MPa,
 $K_n = K_s = 75000$ MPa/m*

*calculation time increases dramatically if higher.

5.2.4.3 Support properties

Only the systematic support was modeled. Thus, specific local support measure were not included.

The systematic rock bolting strategy is as follows:

Table 6 Geometry of the systematic rock bolting.

	S_b (m)	L_b (m)
Service and connection tunnel	2	2.4
Platform tunnel	1.7	6
Tunnel U2	1.7	4
Elevator *	1	3

Where S_b = distance between two bolts, and L_b = bolt length.

* Bolts are parallel to the elevator's surface and 0.5 m distant from this surface.

The properties of the rock bolts are:

Rock bolt properties:

Diameter $D = 25$ mm

Young modulus $E = 200$ GPa

Tensile yield strength $F_y = 246$ kN

Compressive yield strength $F_c = 246$ kN

Interface properties:

Bond shear stiffness $K_{\text{bond}} = 9.62$ GN/m/m

Grout shear strength $G_{\text{bond}} = 707$ kN/m

The thickness of the shotcrete is presented in Table 7.

Table 7 Shotcrete thickness.

	t (mm) roof	t (mm) walls
Service and connection tunnel	50	50
Platform tunnel	200	50
Tunnel U2	75	50

No shotcrete was applied in the elevator shaft.

The properties of the shotcrete were as follows:

Shotcrete properties:

Density $\rho = 2300 \text{ kg/m}^3$

Youngs modulus $E = 16 \text{ GPa}$

Poisson ratio $\nu = 0.25$

Interface properties (representing good adhesion):

Cohesion $c = 0.5 \text{ MPa}$

Friction $\phi = 35^\circ$

Tensile strength $T = 0.5 \text{ MPa}$

Normal stiffness $K_n = 100 \text{ GPa}$

Shear stiffness $K_s = 100 \text{ GPa}$

5.3 Simulation sequence

The first modeling step is the initialization to equilibrium with *in situ* and boundary conditions installed.

The sequence of excavation is as follows:

1. (step 0) Subway track excavation at once and installation of subway track loads (Figure 25),
2. (Step 1) Connection and Service tunnels excavation at once + support,
3. (Steps 2 to 20) Platform tunnel excavation sequence + support,

4. (Steps 21 to 31) Tunnel U2 excavation sequence + support, and
5. (Step 32) Elevator shaft excavation at once + support. Step 32 consists of several sub-steps:
 - Removing the shotcrete and rock bolts inside the elevator region,
 - adding extra rock bolts around the elevator region, and
 - excavating the elevator and running to final equilibrium.

Around the area where large displacements were observed, the numerical model reproduces the sequential advancement of the face by steps of 3.5 m to 5 m (Figure 26). After each excavation stage the model is run to equilibrium allowing for 100% deconfinement to occur. After that the rock bolts and shotcrete are installed, the next excavation step is excavated and the system is again run to equilibrium.

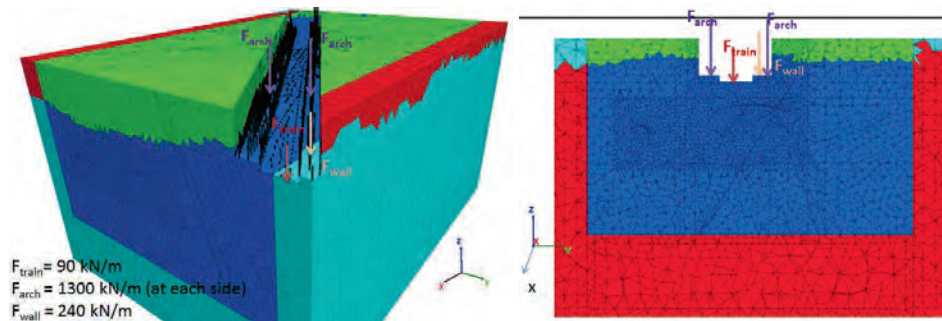


Figure 25 Subway track excavation plus application of surface loads (step 0).

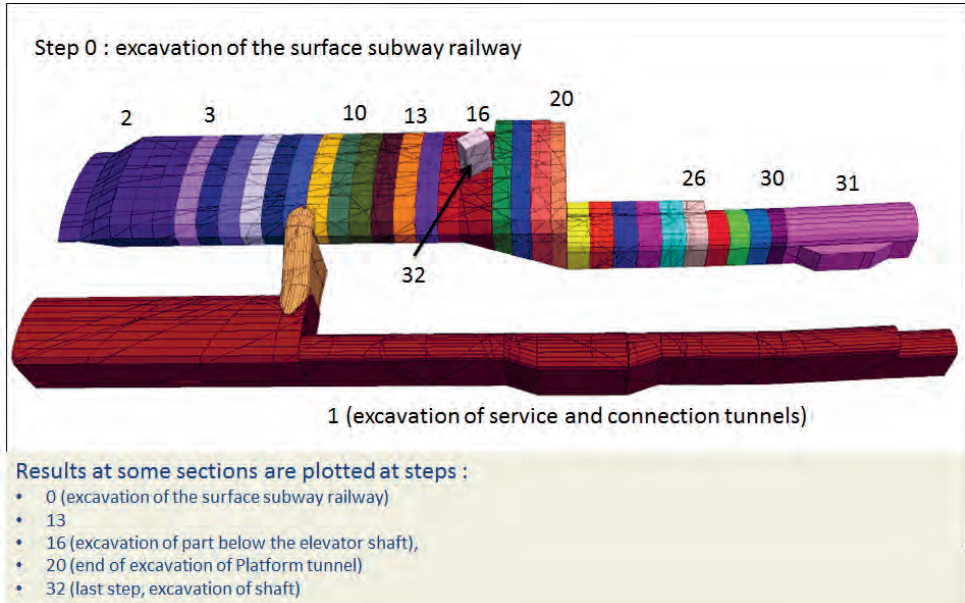


Figure 26 Sequence of tunnel and shaft excavation followed in the model and steps at which results have been plotted at certain model sections.

The following figures (Figure 27 to Figure 33) show the evolution of the excavation + support sequence for every simulation case considered.

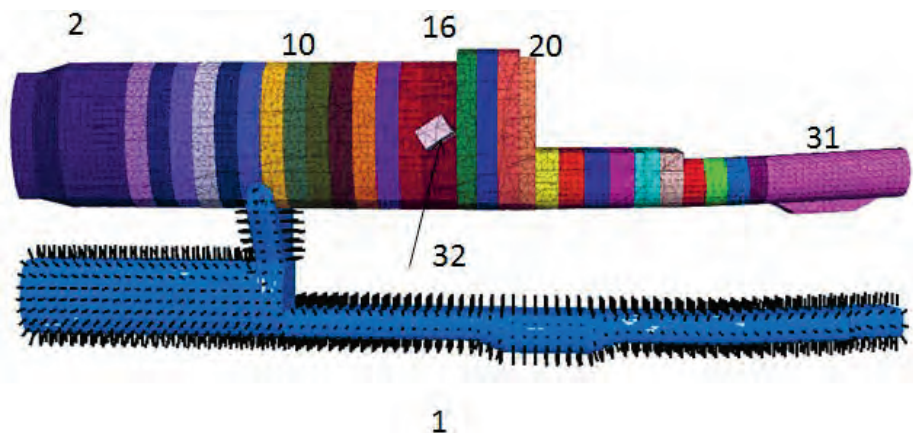


Figure 27 Excavation of the Service tunnel and Connection tunnel at once. Run to equilibrium and install support.

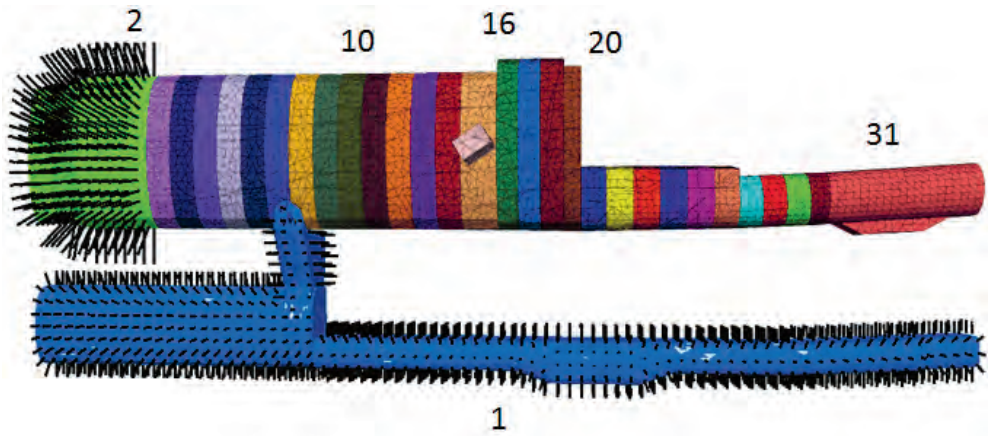


Figure 28 Progressive excavation of the Platform tunnel and progressive installation of support.

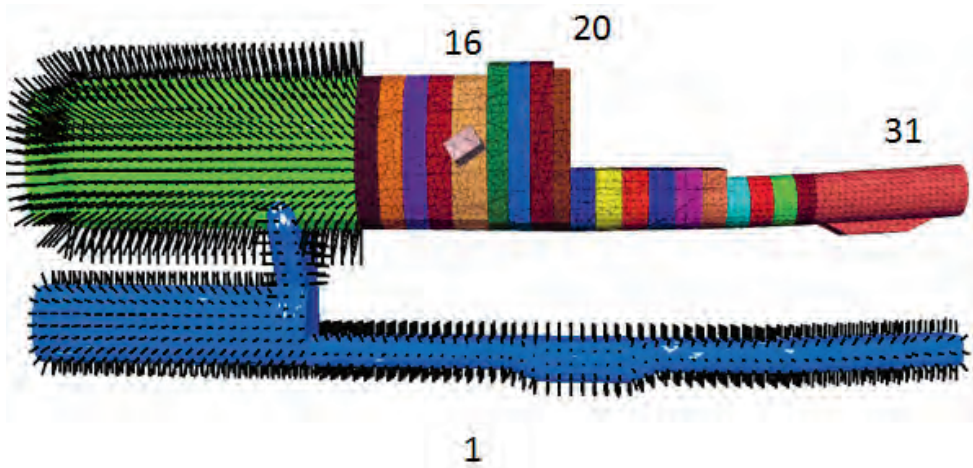


Figure 29 Progressive excavation of the Platform tunnel and progressive installation of support.

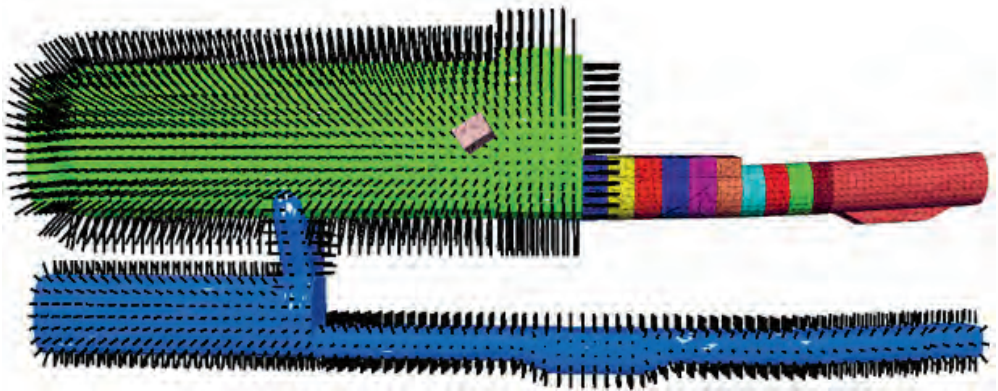


Figure 30 Progressive excavation of the Platform tunnel and progressive installation of support.

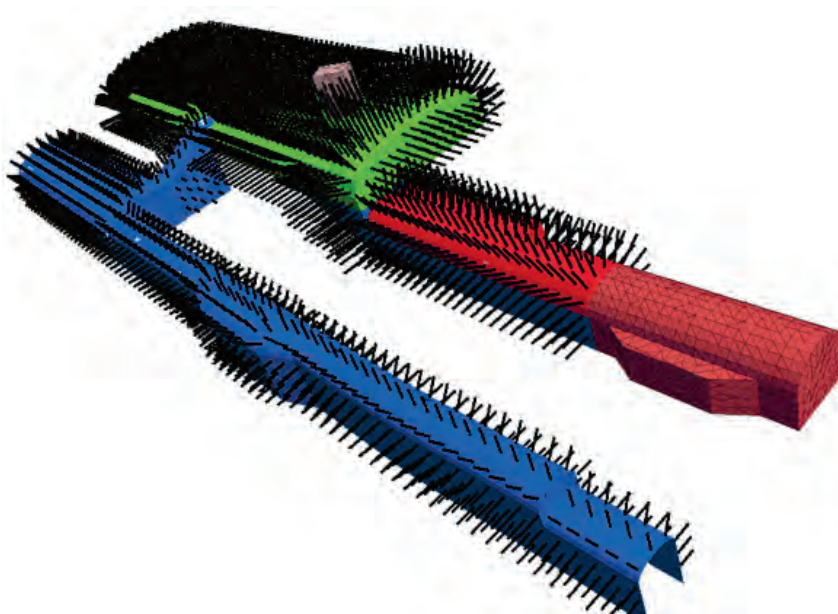


Figure 31 Progressive excavation of the tunnel U2 and progressive installation of support.



Figure 32 Excavation of last part of the tunnel U2 and installation of support.

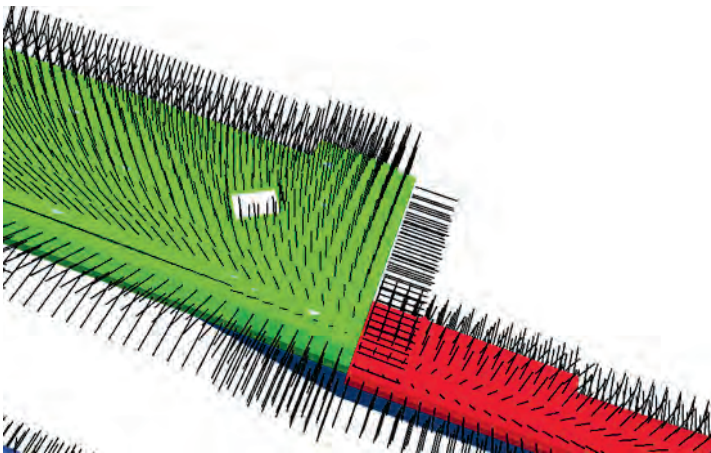


Figure 33 Last simulation step. Removing the shotcrete and rock bolts inside the elevator shaft region. Adding extra rock bolts around the elevator shaft region and excavating the elevator.

5.4 Monitoring points

Convergence measurements have been carried out during tunnel construction at a number of points. History points have been installed at exactly the same locations in the model and displacements in x, y and z-directions as well as displacement magnitude have been recorded during the whole simulation (see Figure 34). This allows for calculation of the convergence during the simulation.

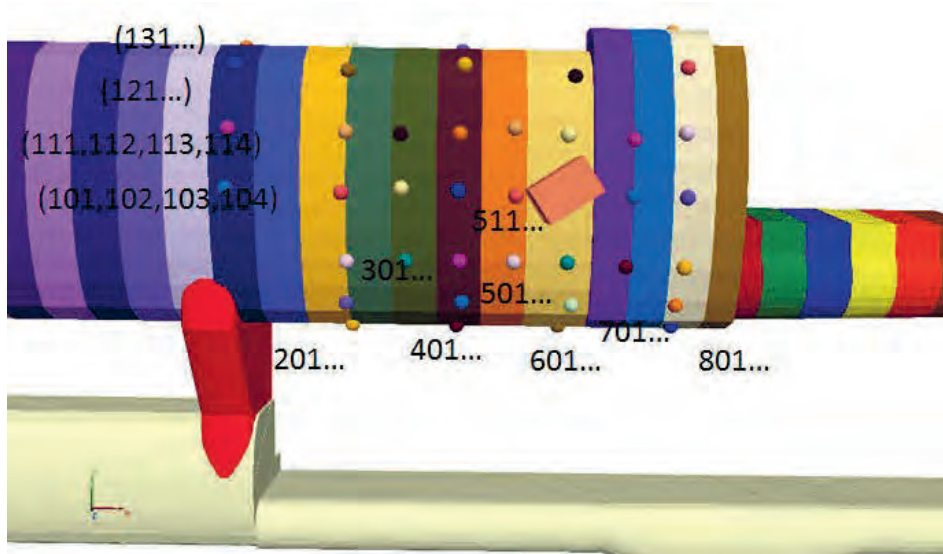


Figure 34 Location of the history points at the top of the Platform tunnel. Displacements in X, Y and Z-directions as well as displacement magnitudes are monitored during the whole simulation sequence at this locations.

Additionally, six extensometers were installed extending from the subway railway surface down to close to the Platform tunnel roof. History points have been installed in the model in the location of both extremes of each one of the extensometers (see Figure 35)

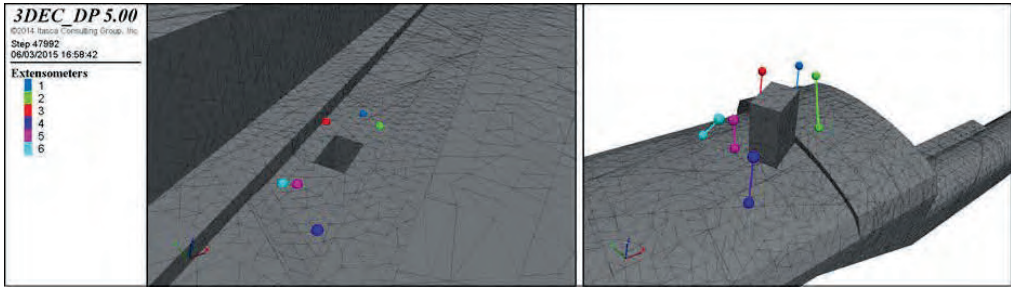


Figure 35 History points installed at the location of both extremes of the extensometers over the Platform tunnel (figure above). The same history points seen from the surface of the subway railway (figure below). The elevator shaft can be seen in yellow. Displacements in X, Y and Z-directions as well as displacement magnitudes are monitored during the whole simulation sequence at this locations.

5.5 Sensitivity study

In order to address as best as possible the objectives of the project a number of sensitivity analysis were conducted.

Four *in situ* stress states were selected within the range that represents the most likely *in situ* stress state within the Stockholm region according to Perman & Sjöberg (2007) (see Table 4). These stress states stand for the minimum, average and maximum in terms of stress magnitude. Besides, case 3 used the maximum horizontal stress in combination with the minimum horizontal stress and the average vertical stress. Only the mean orientation of the horizontal stress was used in all the modeled cases.

In addition, both continuum and discontinuum models were used. Both models had exactly the same geometry and mesh, however, in the discontinuum model the fractures were active (i.e., they could shear, slip and open/close) whereas in the continuum model the fractures were completely glued.

Furthermore, two different fracture cohesion magnitudes were used: 0.8 MPa and 0 MPa.

Therefore, the list of simulations carried out in this project is as follows:

- Discontinuum simulations:
 - With fracture cohesion ($c=0.8$ MPa)

- Stress case 0
- Stress case 1
- Stress case 2
- Reduction of the fracture cohesion ($c=0$ MPa) (probable for relatively low *in situ* stresses (i.e., shallow excavation))
 - Stress case 1
 - Stress case 2
 - Stress case 3
- Continuum simulations:
 - Elastic simulation
 - Stress case 1
 - Stress case 2
 - Elasto-plastic simulation (modified Hoek-Brown constitutive model)
 - Stress case 3

5.6 Results

Figure 36 shows the principal stress in the rock after initial equilibrium is reached (negative sign means compressive stress). At this stage no excavation has been performed, not even the subway railway in the top surface.

Simulations with discontinuous rock mass were performed considering the four *in situ* stress cases presented in Table 4 and two values of fracture cohesion ($c=0.8$ MPa and $c=0$ MPa) in order to evaluate the importance of including the fractures in the rock mass response to the tunnel excavation and support. Simulations with continuum elastic and continuum elasto-plastic rock mass were also run to evaluate the ability of continuum modeling to reproduce the observed behavior. The results are presented in terms of vertical displacement (z-displacement) around the Platform tunnel and at the ground surface in the zone where the subway track crosses the Platform tunnel in Section 5.6.1. The simulated extensometers displacement and the simulated Platform tunnel displacements are shown in Section 5.6.2 and Section 5.6.3 respectively.

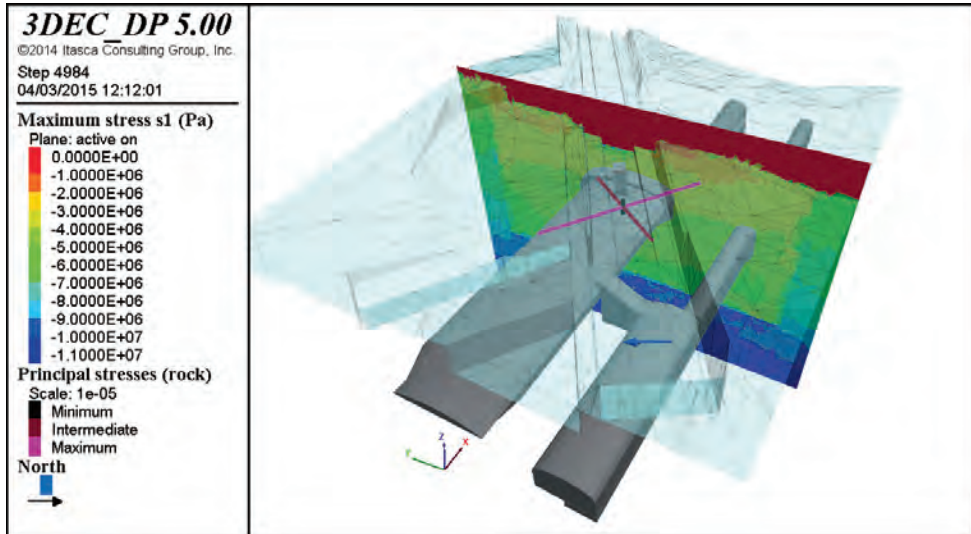


Figure 36 Vertical cross section perpendicular to the Platform tunnel axis showing the contours of the maximum principal stress magnitude for stress case 1 (negative sign means compressive stress). The orientation and relative magnitude of the principal stresses in the rock are also shown by the pink, brown and black lines. No excavation has been performed at this stage.

5.6.1 Simulated vertical displacement magnitude

The following figures (Figure 38 to Figure 42) present the simulated z-displacement (vertical) magnitude at two cross sections passing by the middle of the Platform tunnel at chosen excavation steps for the different sensitivity cases. The location and orientation of the cross-sections with respect to the Platform tunnel is shown in Figure 37 together with a view of the fractures intersecting those two chosen vertical cross-sections.

The complete series of these plots for all the studied cases at four different simulation steps (13, 16, 20 and 32) is presented in Appendix 1.

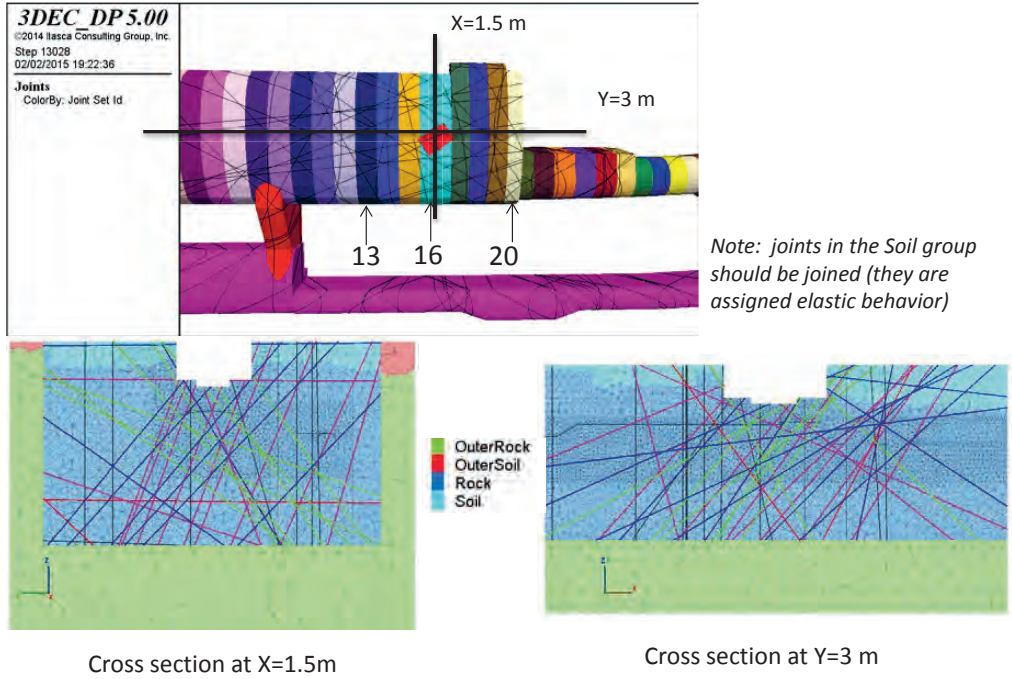


Figure 37 Above: Location of the two vertical cross-sections chosen for visualization of displacement and stress at different simulation steps. Below: View of the fractures intersecting the two chosen cross-sections once the subway railroad has been excavated.

The results in Figure 38 to Figure 42 suggest that continuum models are not able to reproduce the observed heterogeneous rock block movement and consequent rock mass dilatancy. The contours of displacement in the discontinuous models suggest that the block movements occur with a maximum magnitude for *in situ* stress case 2 and case 3 and fracture cohesion = 0 MPa.

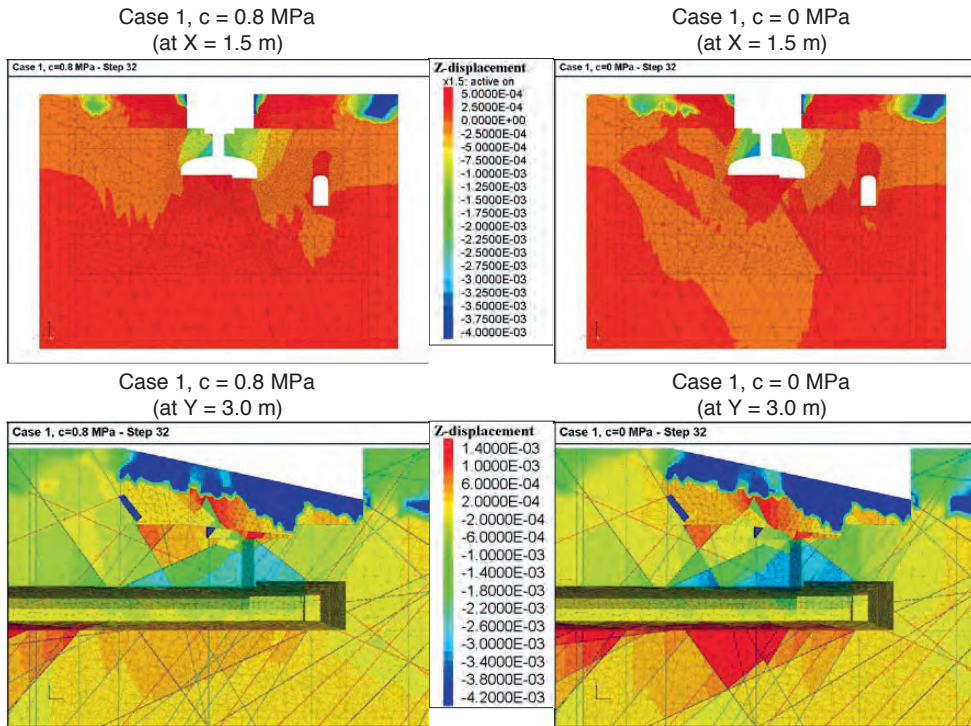


Figure 38 Vertical cross-section of the simulated z-displacement (vertical) perpendicular to the Platform tunnel at $X = 1.5$ m (above) and parallel to the Platform tunnel at $Y = 3$ m (below) at excavation step 32 for stress case 1, discontinuum with fracture cohesion = 0.8 MPa (left) and 0 MPa (right).

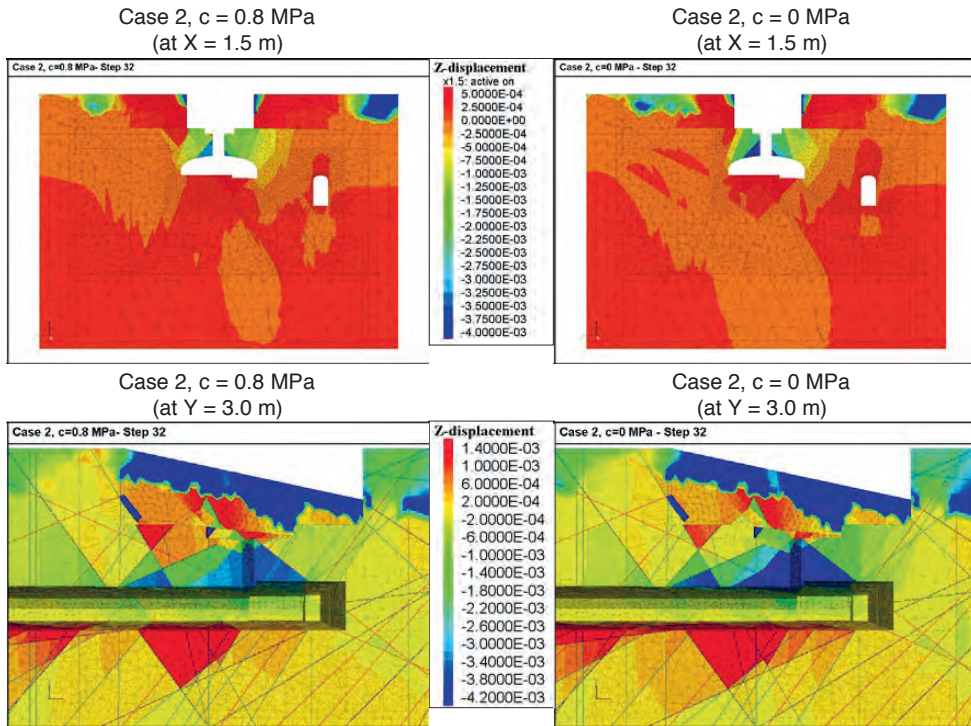


Figure 39 Vertical cross-section of the simulated z-displacement (vertical) perpendicular to the Platform tunnel at $X = 1.5$ m (above) and parallel to the Platform tunnel at $Y = 3$ m (below) at excavation step 32 for stress case 2, discontinuum with fracture cohesion = 0.8 MPa (left) and 0 MPa (right).

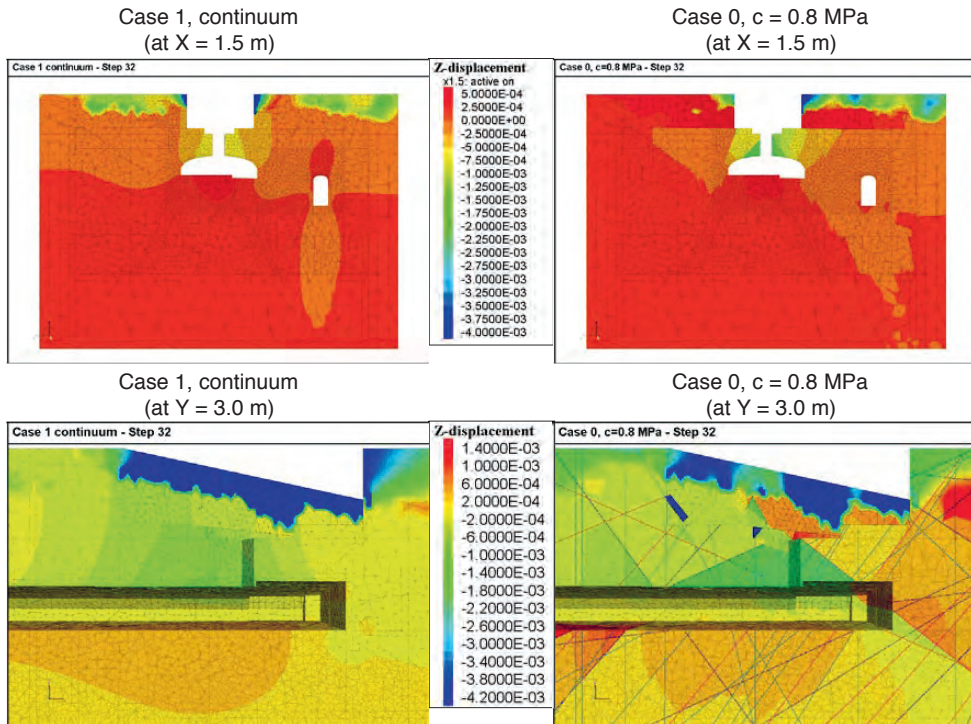


Figure 40 Vertical cross-section of the simulated z-displacement (vertical) perpendicular to the Platform tunnel at X = 1.5 m (above) and parallel to the Platform tunnel at Y = 3 m (below) at excavation step 32 for stress case 1, continuum elastic (left) and stress case 0, discontinuum with fracture cohesion = 0.8 MPa (right).

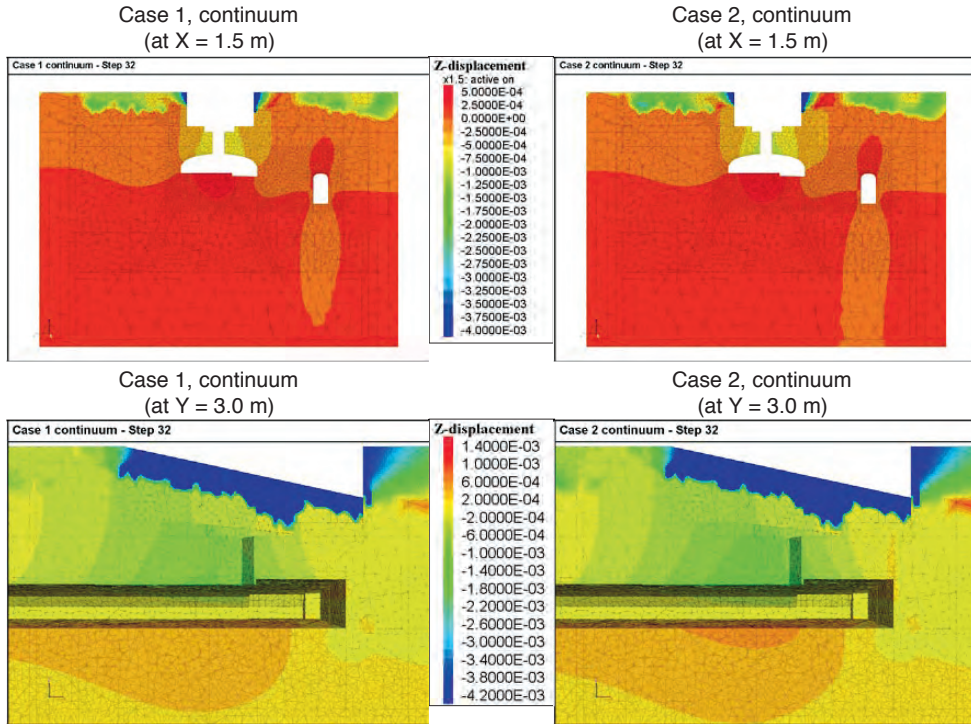


Figure 41 Vertical cross-section of the simulated z-displacement (vertical) perpendicular to the Platform tunnel at X = 1.5 m (above) and parallel to the Platform tunnel at Y = 3 m (below) at excavation step 32 for stress case 1 (left) and stress case 2 (right), continuum elastic model.

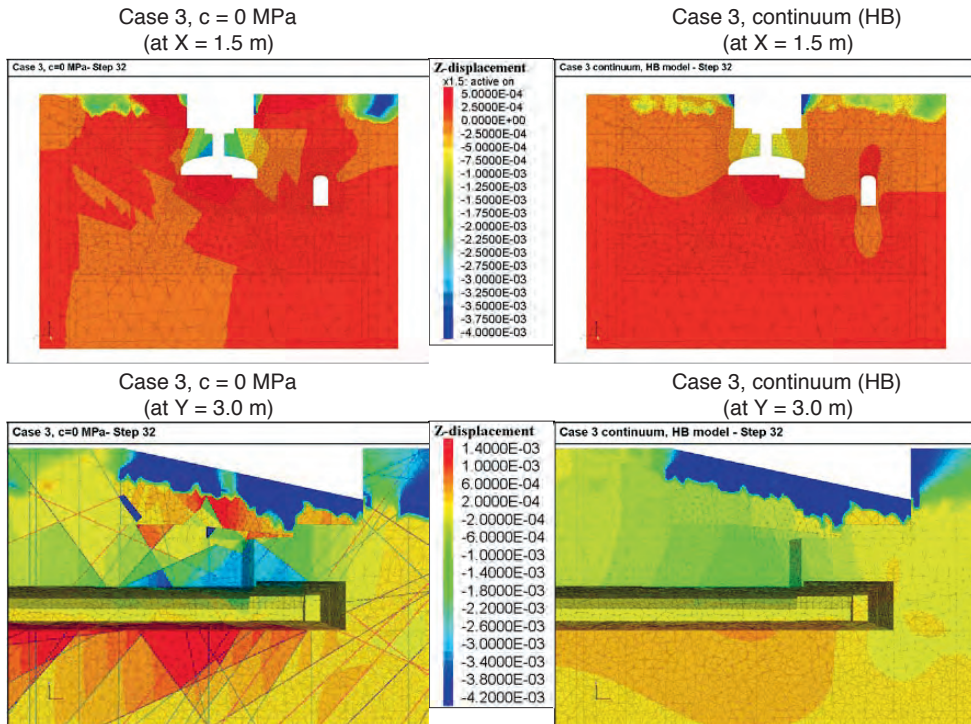


Figure 42 Vertical cross-section of the simulated z-displacement (vertical) perpendicular to the Platform tunnel at $X = 1.5$ m (above) and parallel to the Platform tunnel at $Y = 3$ m (below) at excavation step 32 for stress case 3, discontinuum with fracture cohesion = 0 MPa (left) and continuum elasto-plastic (modified H-B) model (right).

The following figures (Figure 43 to Figure 48) present contour plots of the magnitude of the vertical displacement at the top surface of the model.

The complete series of these plots for all the studied cases at four different simulation steps (13, 16, 20 and 32) is presented in Appendix 2.

The excavation of the surface subway track (step 0) induces upheaving of the rock in both the continuum and the discontinuum models, as can be seen in Figure 43 and Appendix 2. The excavation of the underground railway tunnel induces naturally the convergence of the tunnel roof. For the continuum model, this affects the top of the model that has a final downward settlement in the area where the subway intersects the tunnel. This is not true for

the discontinuum model, where upheave is still observed in this area, even at the end of excavation. Given that the two models have the same *in situ* stress case, this difference can be attributed to fracture shear/opening and rock mass dilatancy.

Figure 44 to Figure 48 confirm the observation made based on the previous figures that the continuum cases are not able to reproduce the large and heterogeneous displacements measured *in situ*.

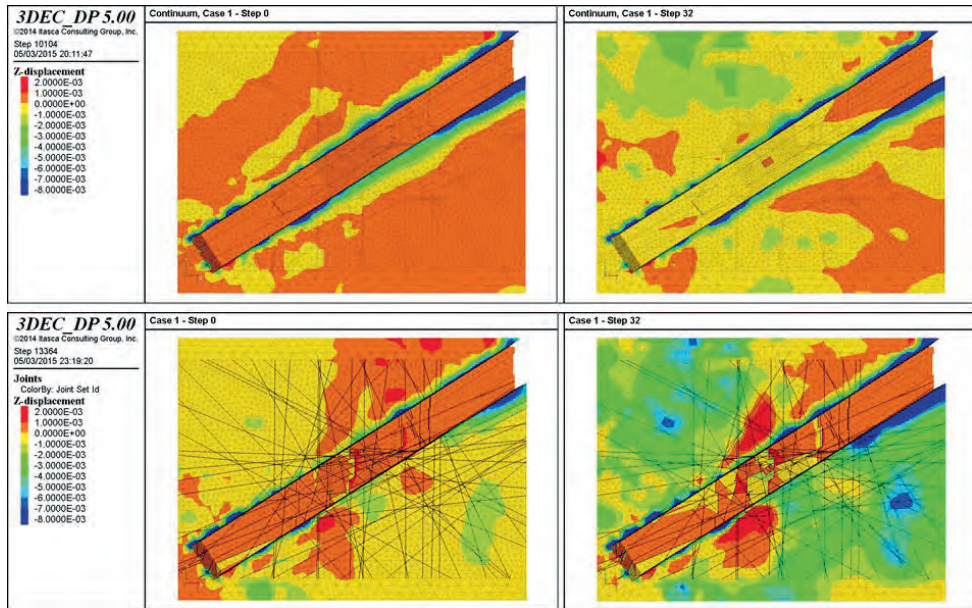
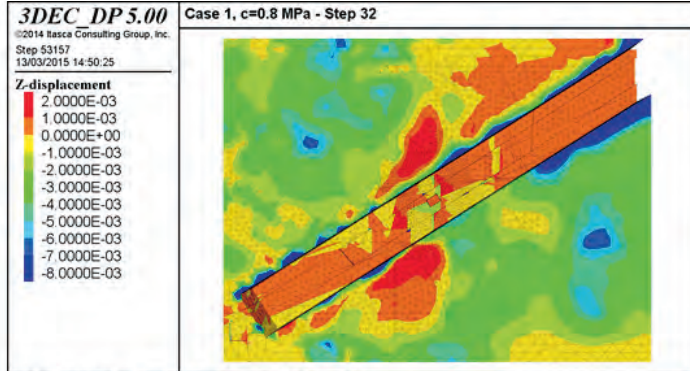


Figure 43 Simulated vertical displacement at the top of the model after excavation of the subway track (step 0, left) and after the excavation of the elevator shaft (step 32, right) for the discontinuum model with $c = 0.8$ MPa (below) and continuum elastic (above) model for stress case 1.

Case 1, $c = 0.8 \text{ MPa}$



Case 1, $c = 0 \text{ MPa}$

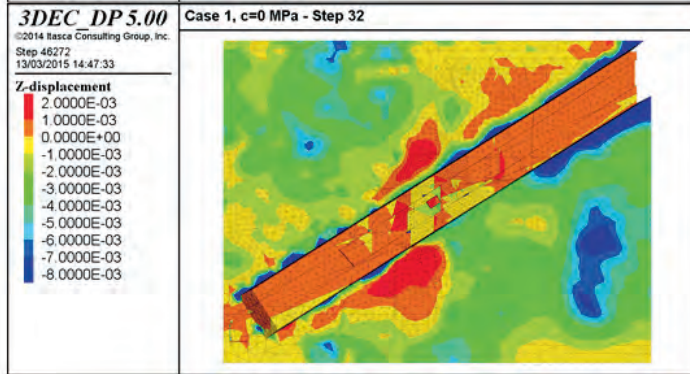
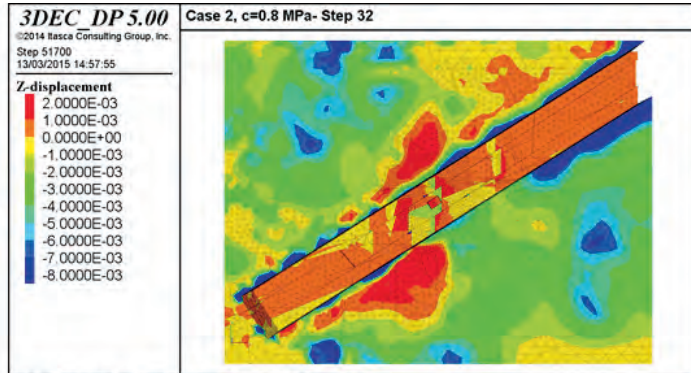


Figure 44 Simulated vertical displacement at the top of the model after the excavation of the Elevator shaft (step 32) for the discontinuum models (stress case 1).

Case 2, $c = 0.8 \text{ MPa}$



Case 2, $c = 0 \text{ MPa}$

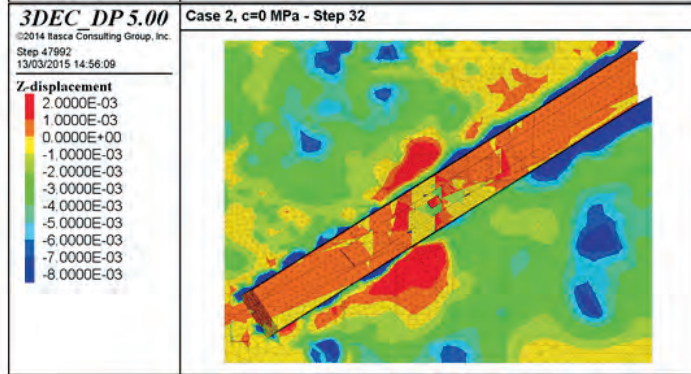
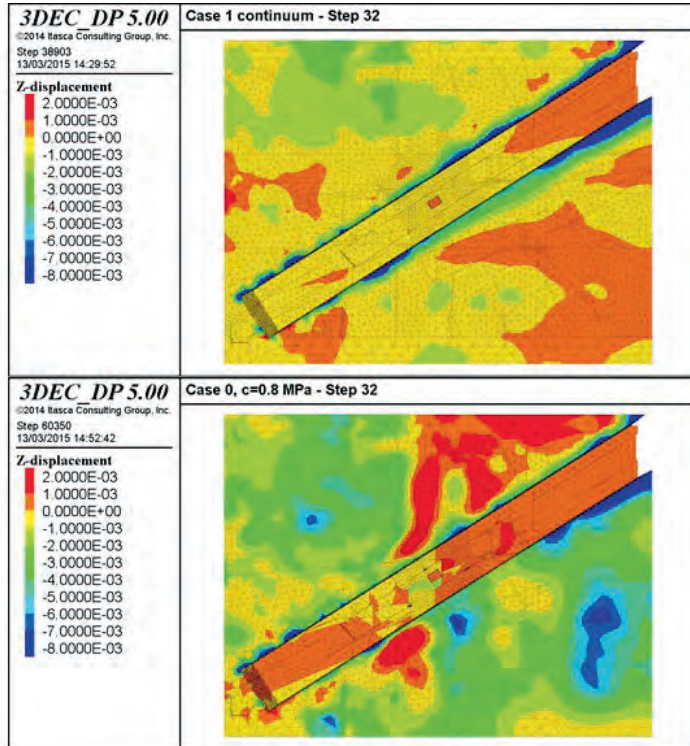


Figure 45 Simulated vertical displacement at the top of the model after the excavation of the Elevator shaft (step 32) for the discontinuum models (stress case 2).

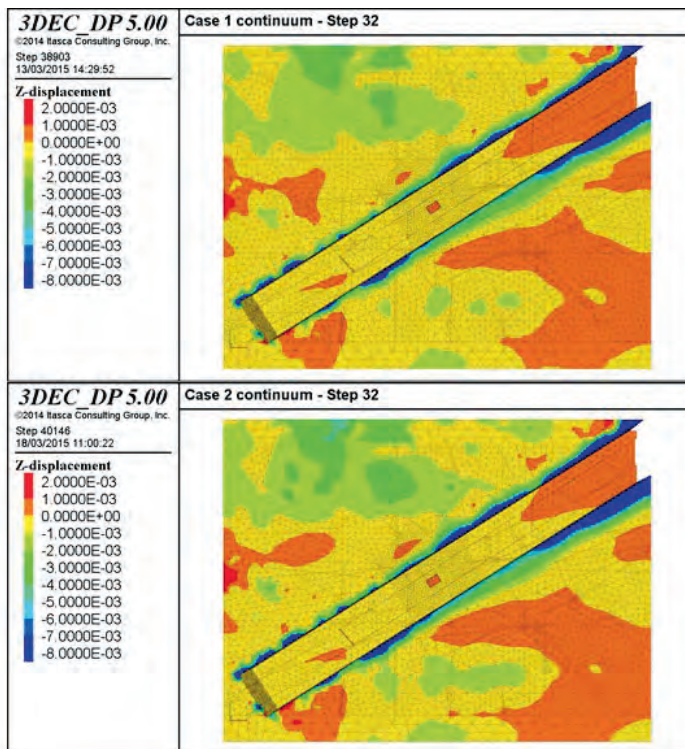
Case 1, continuum



Case 0, c = 0.8 MPa

Figure 46 Simulated vertical displacement at the top of the model after the excavation of the Elevator shaft (step 32) for the continuum elastic (stress case 1) and the discontinuum models with $c = 0.8$ MPa (stress case 0).

Case 1, continuum



Case 2, continuum

Figure 47 Simulated vertical displacement at the top of the model after the excavation of the Elevator shaft (step 32) for the continuum elastic models (stress case 1 and case 2).

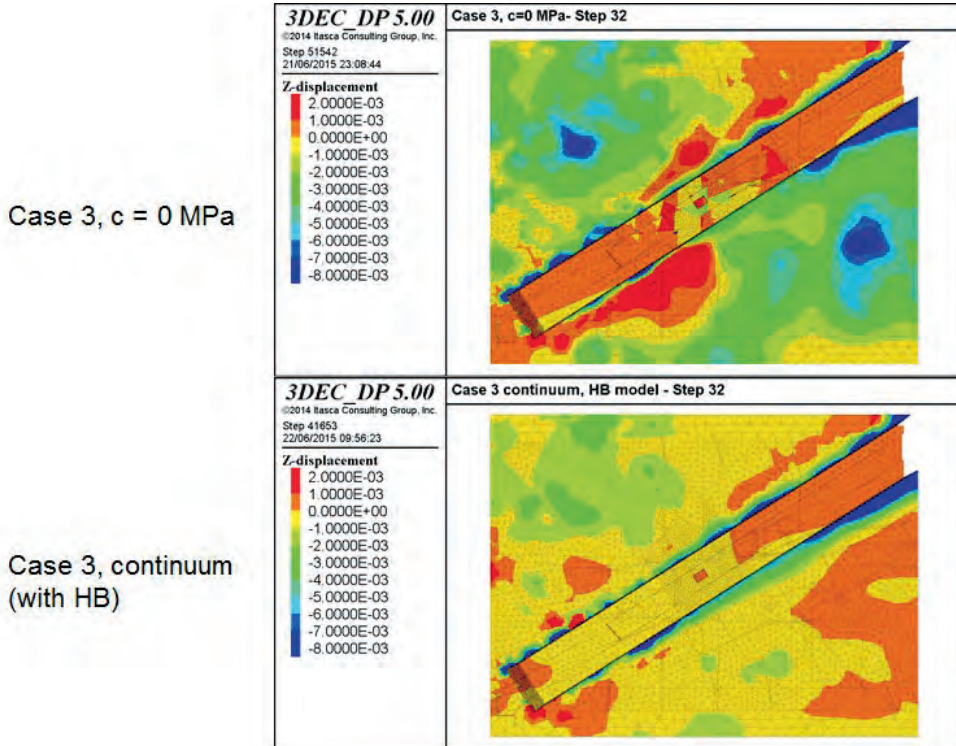


Figure 48 Simulated vertical displacement at the top of the model after the excavation of the Elevator shaft (step 32) for the continuum elasto plastic H-B model and the discontinuous model with $c = 0.8$ MPa (stress case 3).

The following figures (Figure 49 to Figure 53) show the simulated vertical displacement magnitude in a 3D-cut along the subway railway axis at the last step of the simulation (step 32). They also show the location of the simulated extensometers. These plots confirm the conclusions reached from the previous figures and also show that the extensometers 4, 5 and 6 were not located where the differential displacement is maximal in the models. In fact, the extensometers 4, 5 and 6 are located in the model in areas of small dilatancy, however, close to those areas there are blocks that are displacing 4 mm downwards while other blocks are displacing 2 mm upwards (see Figure 50 and Figure 53).

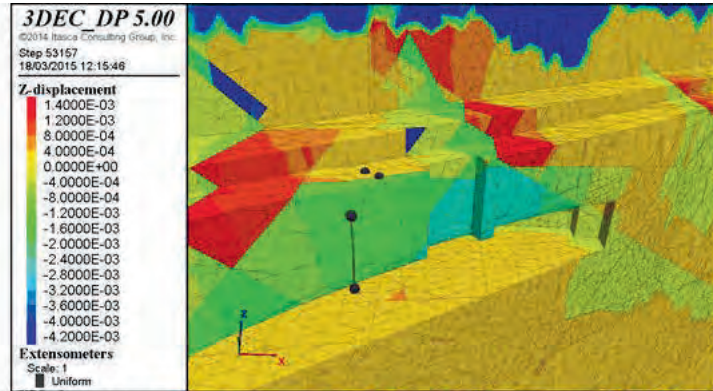
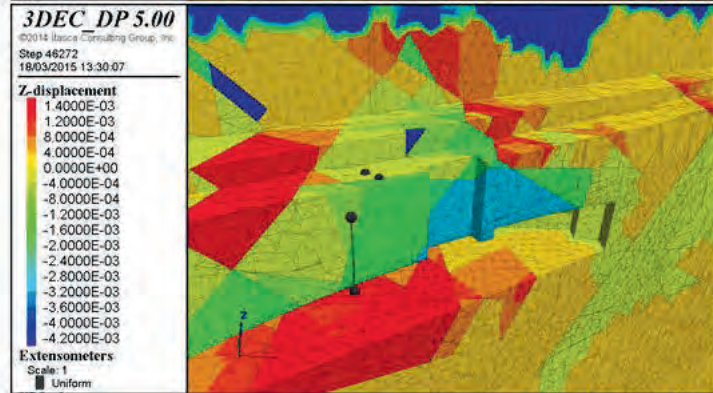
Case 1, $c=0.8$ MPaCase 1, $c=0$ MPa

Figure 49 3D-cut along the subway railway axis of the simulated vertical displacement at the top surface of the model at the last step of the simulation (step 32) for stress case 1, discontinuum with fracture cohesion = 0.8 MPa and with cohesion = 0 MPa.

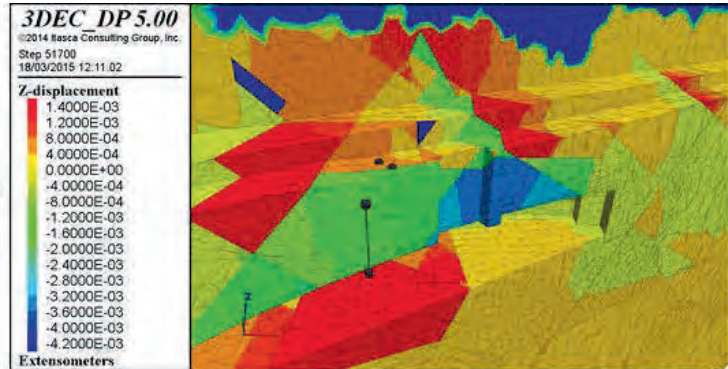
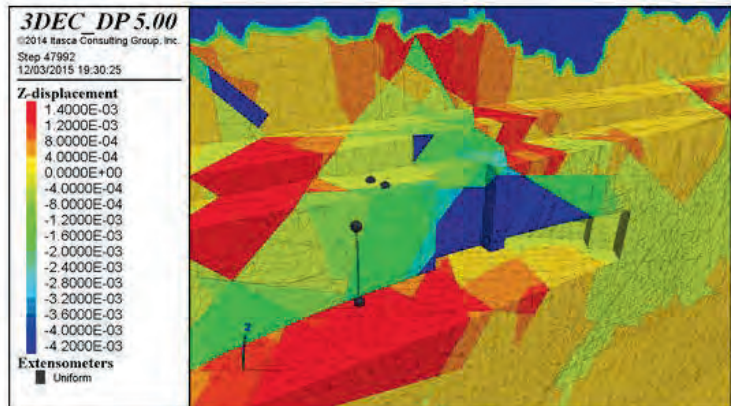
Case 2, $c=0.8$ MPaCase 2, $c=0$ MPa

Figure 50 3D-cut along the subway railway axis of the simulated vertical displacement at the top surface of the model at the last step of the simulation (step 32) for stress case 2, discontinuum with fracture cohesion = 0.8 MPa and with cohesion = 0 MPa.

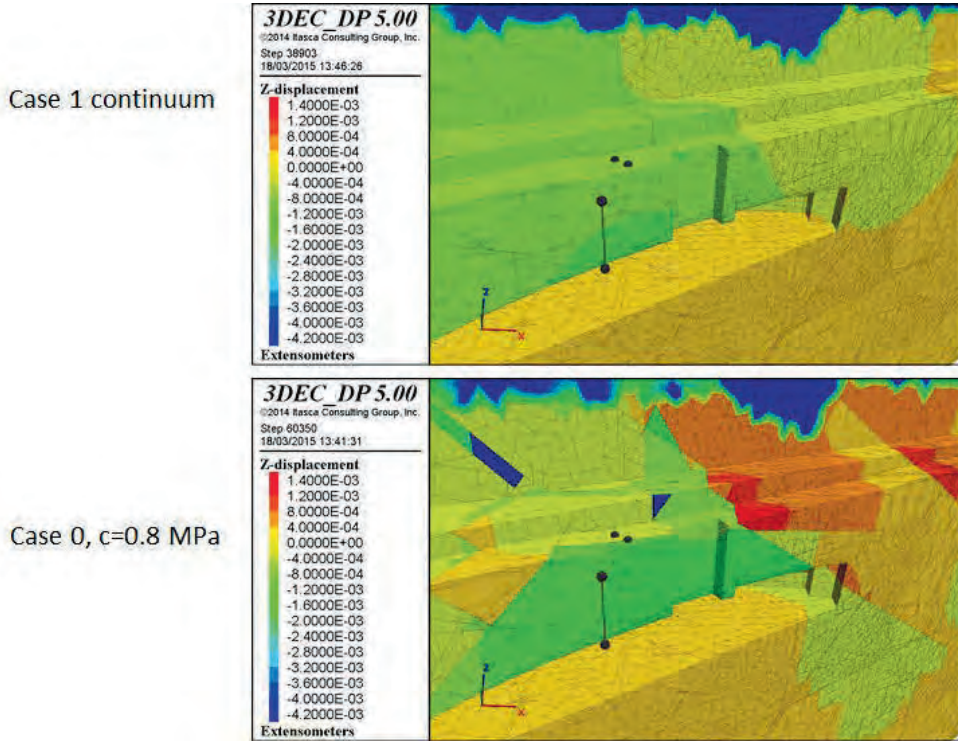


Figure 51 3D-cut along the subway railway axis of the simulated vertical displacement at the top surface of the model at the last step of the simulation (step 32) for stress case 1, continuum elastic and stress case 0, discontinuum with fracture cohesion = 0.8 MPa.

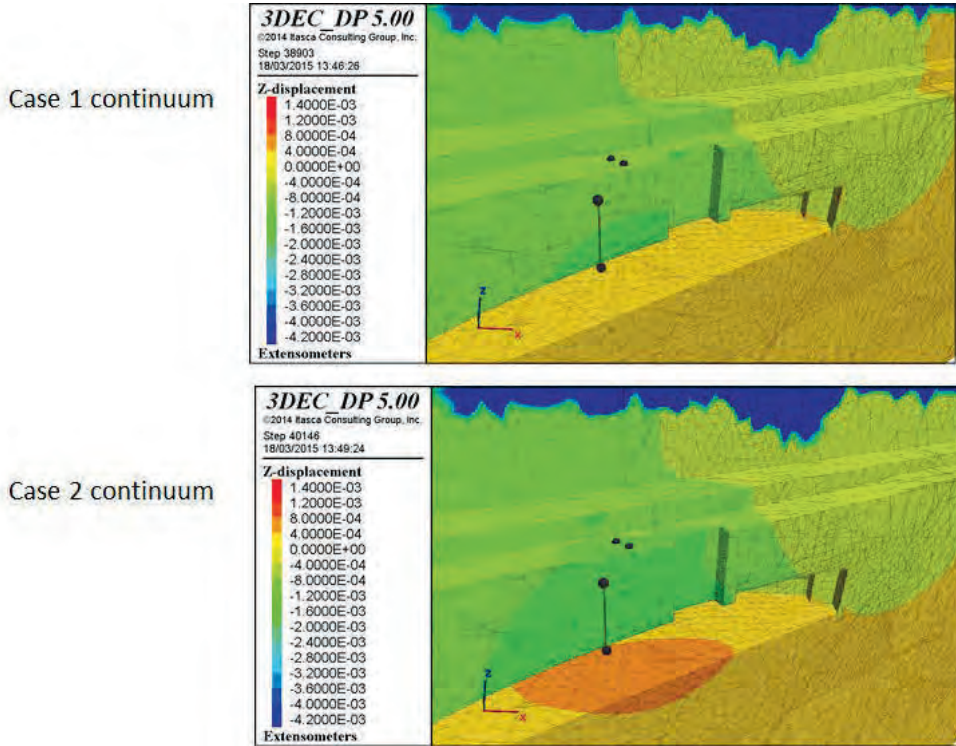


Figure 52 3D-cut along the subway railway axis of the simulated vertical displacement at the top surface of the model at the last step of the simulation (step 32) for stress case 1 and stress case 2, continuum elastic.

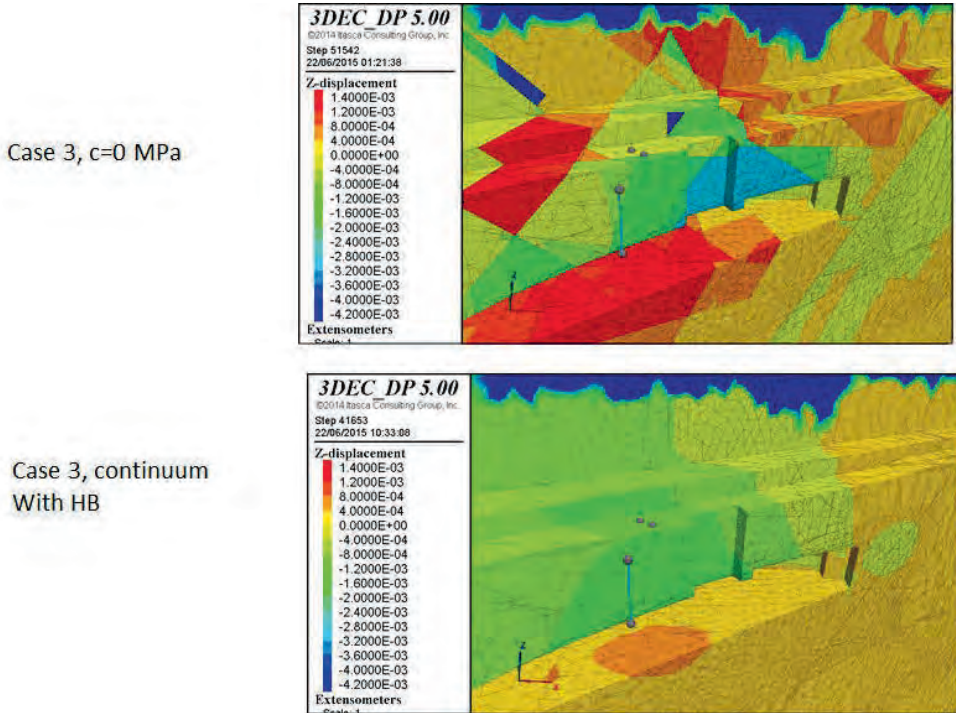


Figure 53 3D-cut along the subway railway axis of the simulated vertical displacement at the top surface of the model at the last step of the simulation (step 32) for stress case 3, discontinuum with fracture cohesion = 0 MPa, and continuum elasto-plastic (modified H-B).

5.6.2 Simulated extensometers response

The following figures (Figure 56 to Figure 64) present the convergence/extension in the simulated extensometers. A positive value means convergence and a negative value means extension.

The relative location of the simulated extensometers with respect to the top surface, the Platform tunnel and the Elevator shaft as well as the *in situ* measurements at the extensometers until after the excavation of the shaft are given in Figure 54. The values recorded in the field at the last excavation step (date around 03-2013, excavation of the shaft, step 32) vary between 5 and 10 mm of extension. Note that there was no measurement data available from extensometers E01, E02 and E03.

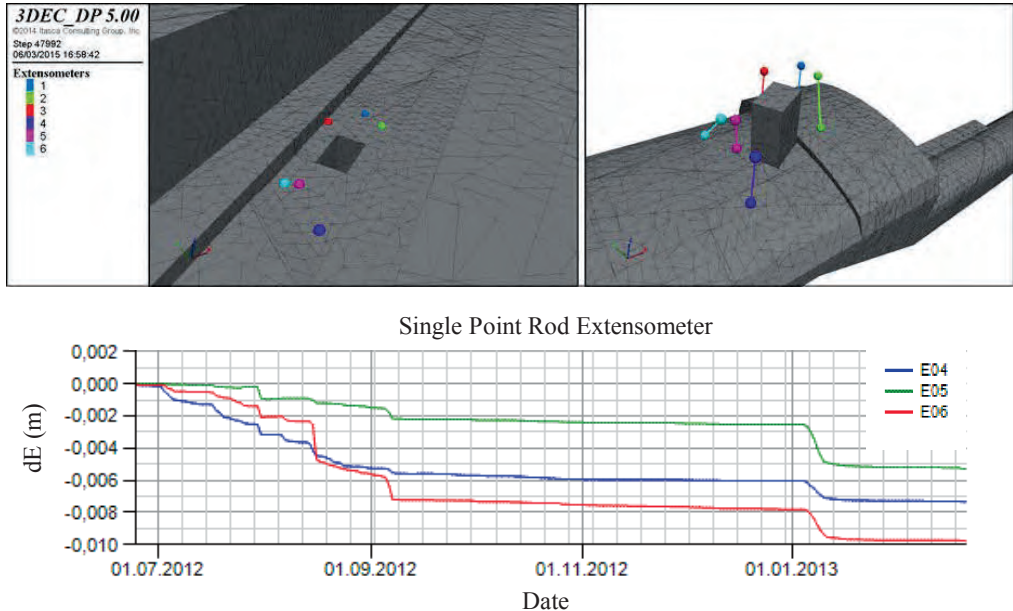


Figure 54 Above: Position of extensometers around the shaft. Below: Available *in situ* measurements at extensometers 4, 5 and 6 until after the date of the shaft excavation (around 03-2013) (Johansson & Batres-Estrada, 2014). Note that there was no measurement data available from extensometers E01, E02 and E03.

In the discontinuous model, the maximum value of extension simulated in the extensometers with available field measurements to compare to (i.e. E04, E05 and E06) reaches around 0.8 mm for stress case 2 and stress case 3 with fracture cohesion $c=0$ MPa (Figure 61 and Figure 64) at extensometer 6. Extensometer 4 shows the second largest deformation while extensometer 5 shows the least deformation. This is in qualitative agreement with the measurements *in situ*, although the simulated values are roughly one order of magnitude lower than the values recorded in the extensometer in the field. The difference in magnitude can be attributed to the fact that the numerical modeling does not reproduce exactly the position of discontinuities due to measuring errors and the fracture simplification adopted (see Section 5.2.2). This causes that, unfortunately, the extensometers E04, E05 and E06 in the models are located in areas with small dilatancy (see Figure 50 and Figure 53). However, extensometers E01, E02 and E03 were also included in the simulations (see Figure 54). The extension response modelled in those extensometers is of the same order of magnitude of the extension recorded in the field at extensometers E04, E05 and E06, even for stress case 1

with fracture cohesion = 0 MPa (see Figure 55 left). The simulated extensometer E01 response for stress case 2 with fracture cohesion = 0 MPa reaches close to 5 mm dilation (see Figure 55 right). Furthermore, Figure 50 and Figure 53 show that close to the location of the extensometers in the simulations some blocks are displacing downwards 4 mm and some other blocks are displacing upwards 2 mm. Therefore, the phenomenon of localized upheaving and heterogeneous displacements in the area around the shaft is quite well reproduced by the discontinuum models with stress case 2 and 3 and with fracture cohesion $c=0$ MPa.

The discontinuum model case 1 simulation with fracture cohesion = 0 MPa shows a similar behavior with a maximum extension of around 0.6 mm at extensometer 6 (Figure 58). The rest of the simulations whether continuum or discontinuum are not capable of reproducing the observed behavior.

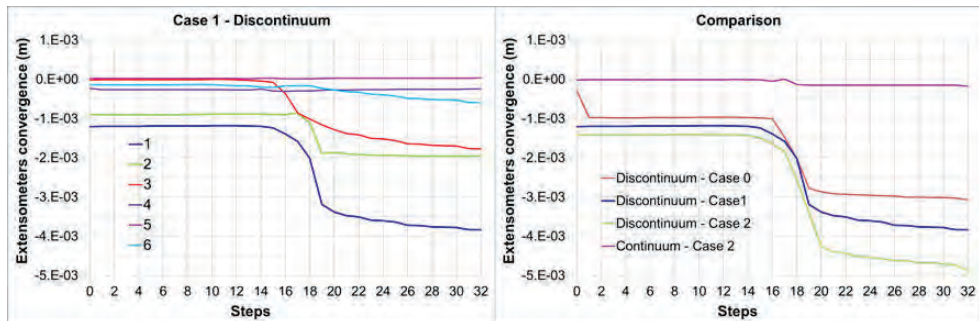


Figure 55 Left: simulated extensometers response for discontinuum stress case 1 with fracture cohesion = 0 MPa. Right: simulated extensometer E01 response for discontinuum stress case 0, 1 and 2 with fracture cohesion = 0 MPa, and for continuum stress case 2.

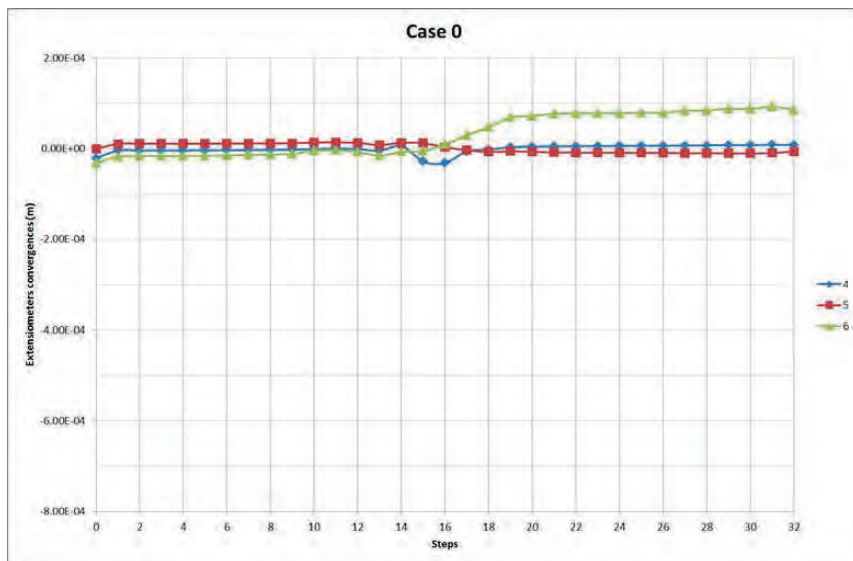


Figure 56 Simulated extensometer response in meters vs. simulation step for stress case 0, discontinuum with fracture cohesion = 0.8 MPa.

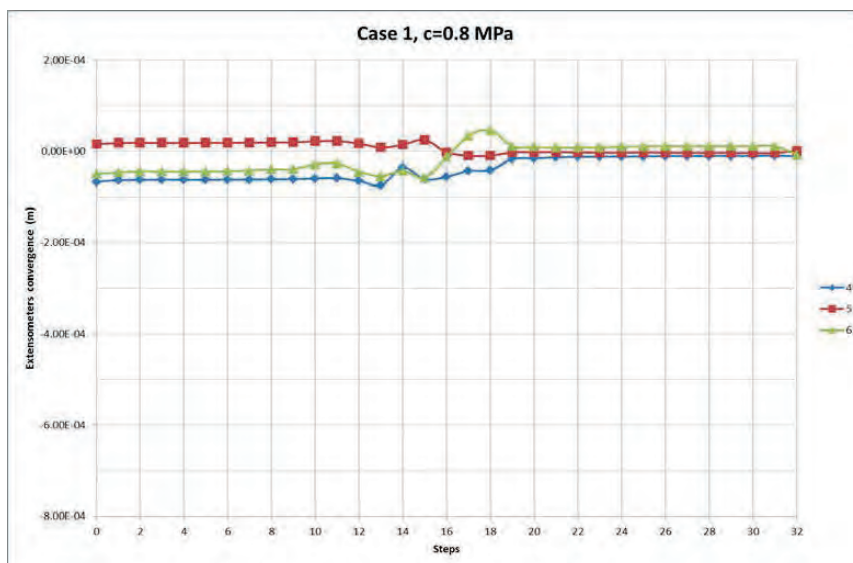


Figure 57 Simulated extensometer response in meters vs. simulation step for stress case 1, discontinuum with fracture cohesion = 0.8 MPa.

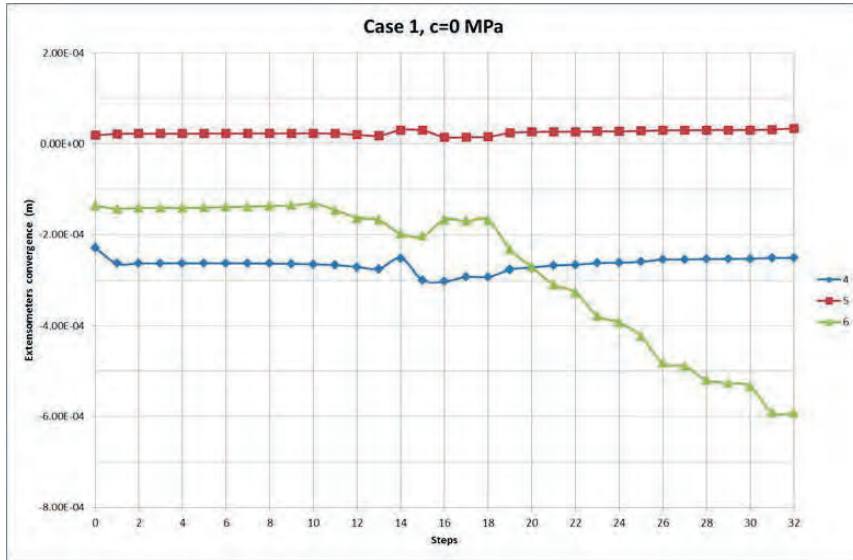


Figure 58 Simulated extensometer response in meters vs. simulation step for stress case 1, discontinuum with fracture cohesion = 0 MPa.

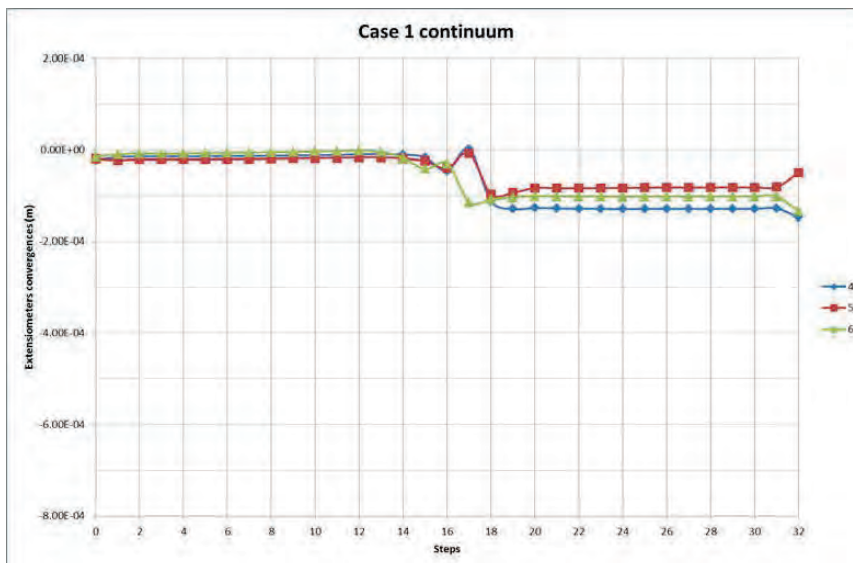


Figure 59 Simulated extensometer response in meters vs. simulation step for stress case 1, continuum elastic.

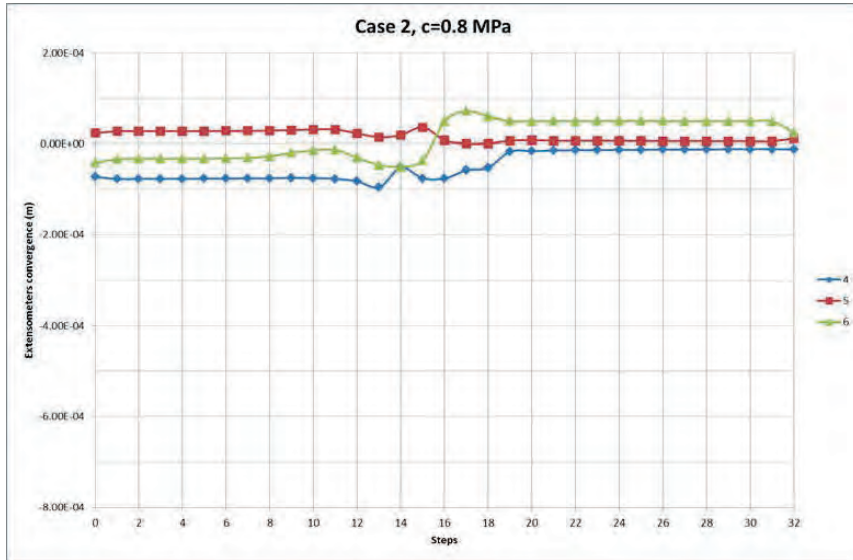


Figure 60 Simulated extensometer response in meters vs. simulation step for stress case 2, discontinuum with fracture cohesion = 0.8 MPa.

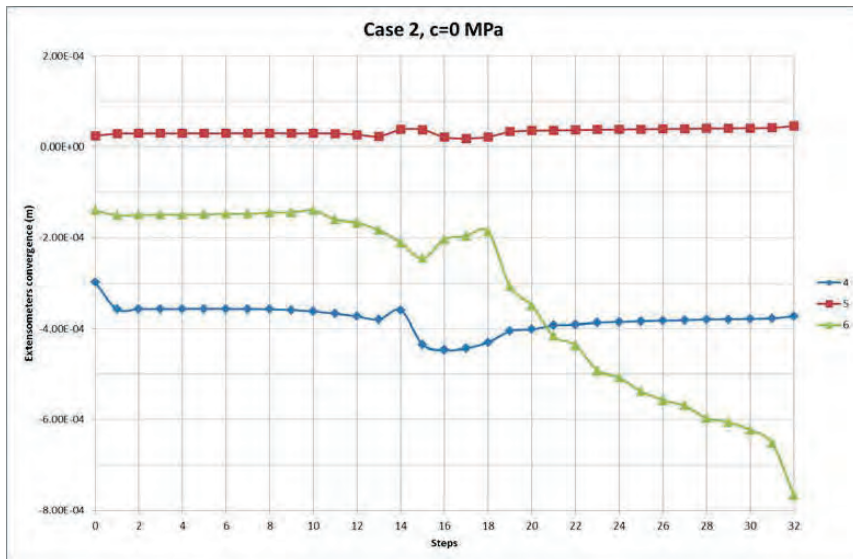


Figure 61 Simulated extensometer response in meters vs. simulation step for stress case 2, discontinuum with fracture cohesion = 0 MPa.

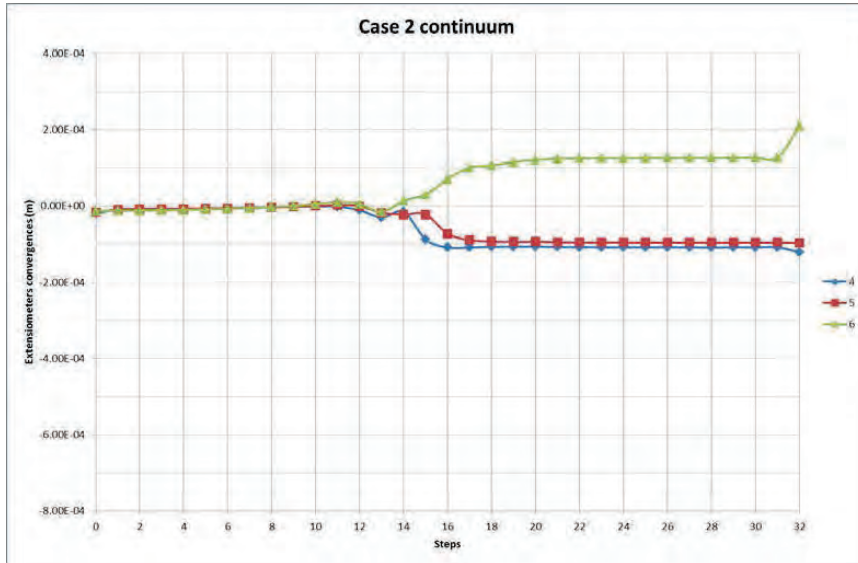


Figure 62 Simulated extensometer response in meters vs. simulation step for stress case 2, continuum elastic.

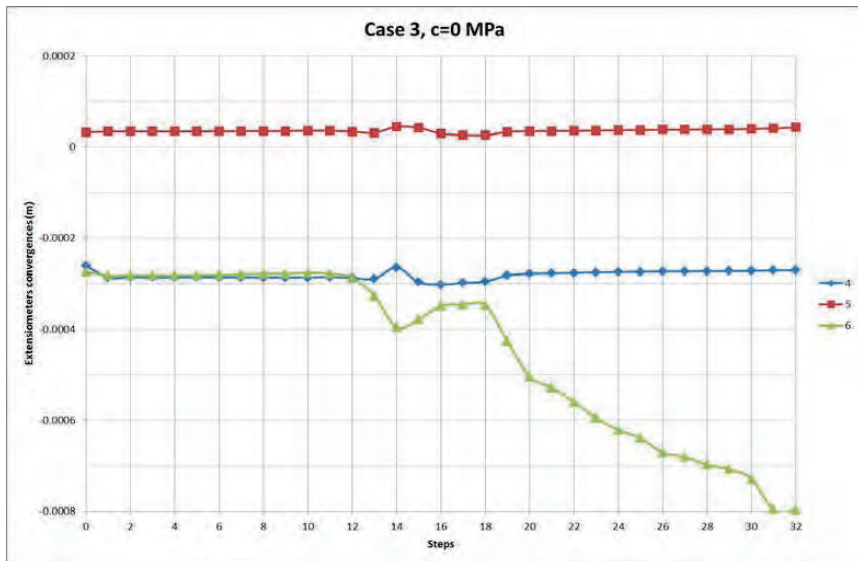


Figure 63 Simulated extensometer response in meters vs. simulation step for stress case 3, discontinuum with fracture cohesion = 0 MPa.



Figure 64 Simulated extensometer response in meters vs. simulation step for stress case 3, continuum elasto-plastic (modified H-B).

5.6.3 Simulated Platform tunnel vertical displacement

The following figures (Figure 66 to Figure 74) present the simulated vertical displacement (z-displacement) at several monitoring points at the roof of the Platform tunnel vs. the simulation step. The location of the monitoring points is shown in Figure 65.

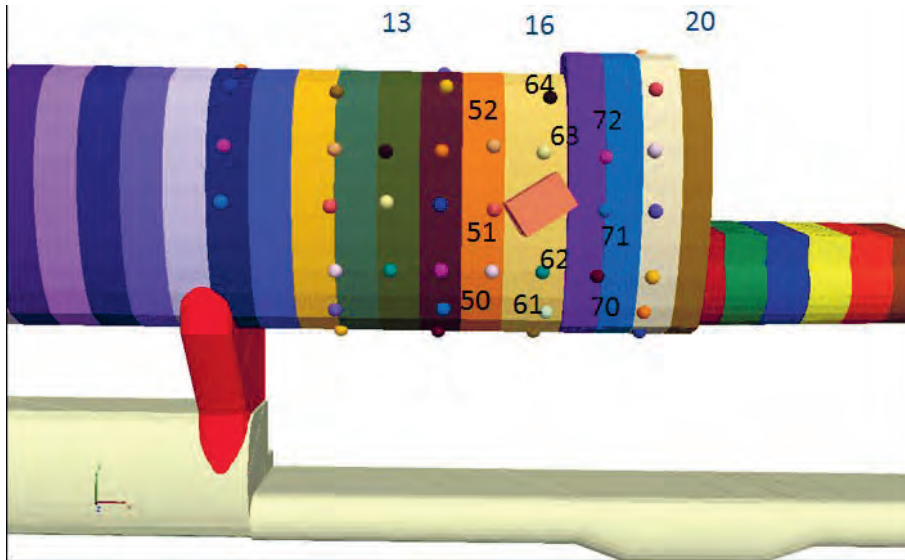


Figure 65 Location of the displacement monitoring points chosen for plotting at the roof of the Platform tunnel (in black). Excavation simulation step in blue.

For the discontinuous case 1, the maximum displacement at the roof of the Platform tunnel reaches 2.7 mm (with fracture cohesion 0.8 MPa) (Figure 67) while in the continuous elastic model it is less than 0.8 mm (Figure 69). Even with stress case 2 the displacement in the continuous elastic model is still limited to 1 mm (Figure 72). The continuum model only reaches up to 1 mm displacement in the roof even with the elasto-plastic modified H-B constitutive model and stress case 3 (Figure 74). Given that during the excavation, the maximum displacement reached 5 to 10 mm, the continuous models do not represent the proper behavior of the rock mass. It is also shown in these set of figures that the vertical displacement at the roof of the excavation is higher when fracture cohesion is set to 0 MPa. The models that better reproduce the observed *in situ* displacements are the discontinuous ones with stress case 1 with fracture cohesion set to 0 MPa (maximum displacement of 3 mm), stress case 2 (maximum displacement of 3.5 mm for $c=0.8$ MPa and 4.2 mm for $c=0$ MPa) and stress case 3 (maximum displacement of 3.2 mm for $c=0$ MPa).

It is worth noting that even if the simulated tunnel displacement magnitudes in the discontinuum models do not reach the large measured values *in situ*, they do capture the qualitative heterogeneous behavior and quite large displacement magnitudes when stress case

2 and 3 are used in combination with fracture cohesion = 0 MPa. On the contrary these results show the inability of the continuum models (both elastic and elasto-plastic) to capture the observed large and heterogeneous tunnel displacements.

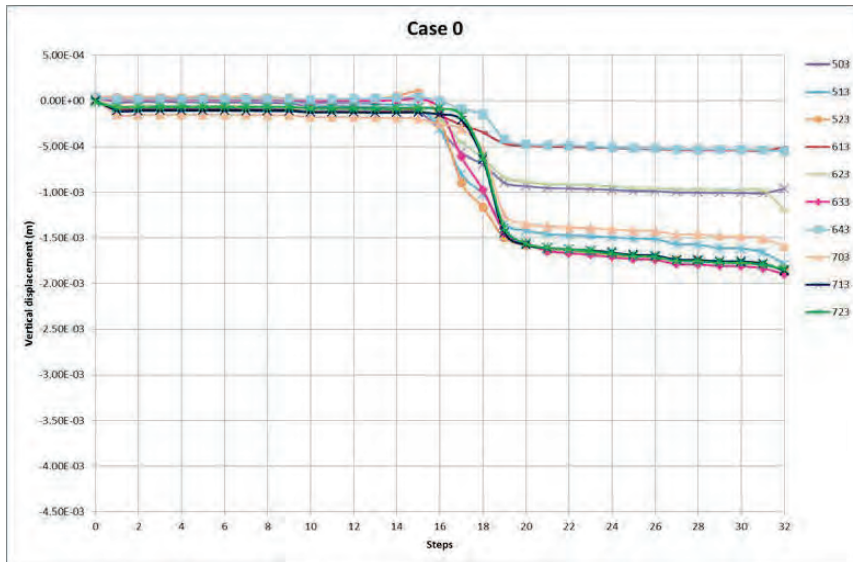


Figure 66 Simulated vertical displacements in meters at several monitoring points at the roof of the Platform tunnel vs. simulation step for stress case 0, discontinuum with fracture cohesion = 0.8 MPa.

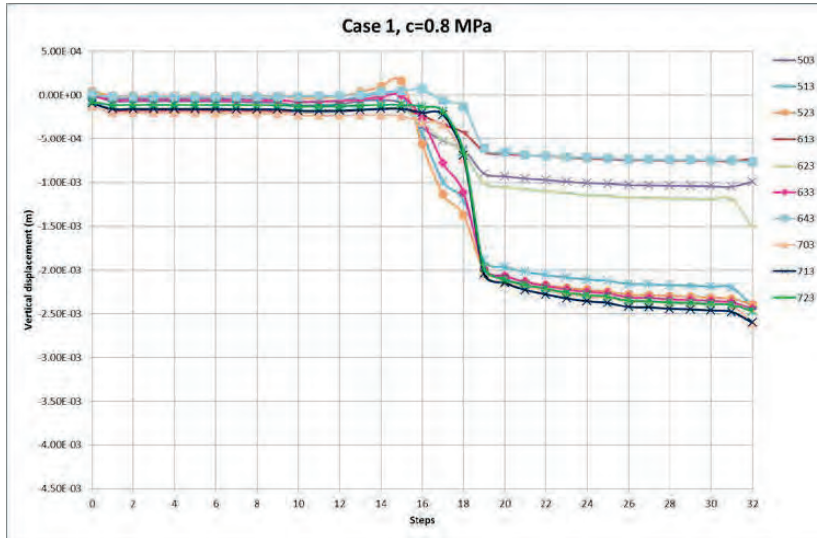


Figure 67 Simulated vertical displacements in meters at several monitoring points at the roof of the Platform tunnel vs. simulation step for stress case 1, discontinuum with fracture cohesion = 0.8 MPa.

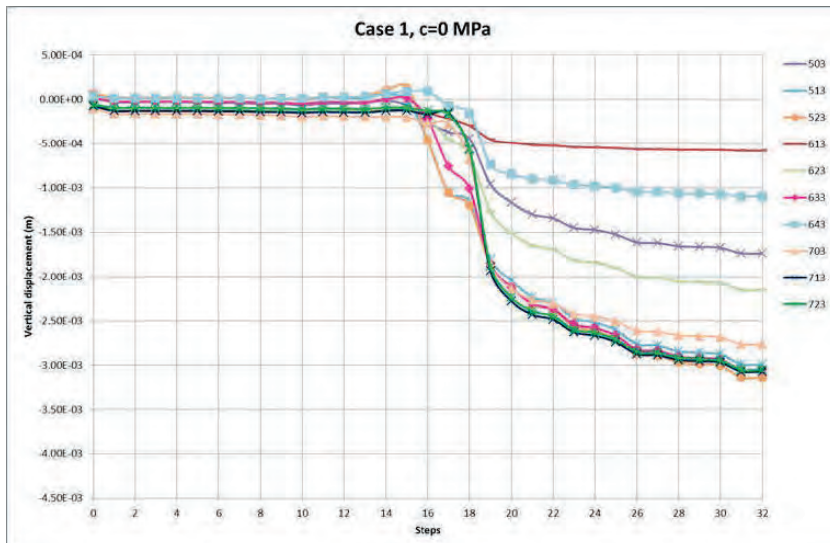


Figure 68 Simulated vertical displacements in meters at several monitoring points at the roof of the Platform tunnel vs. simulation step for stress case 1, discontinuum with fracture cohesion = 0 MPa.

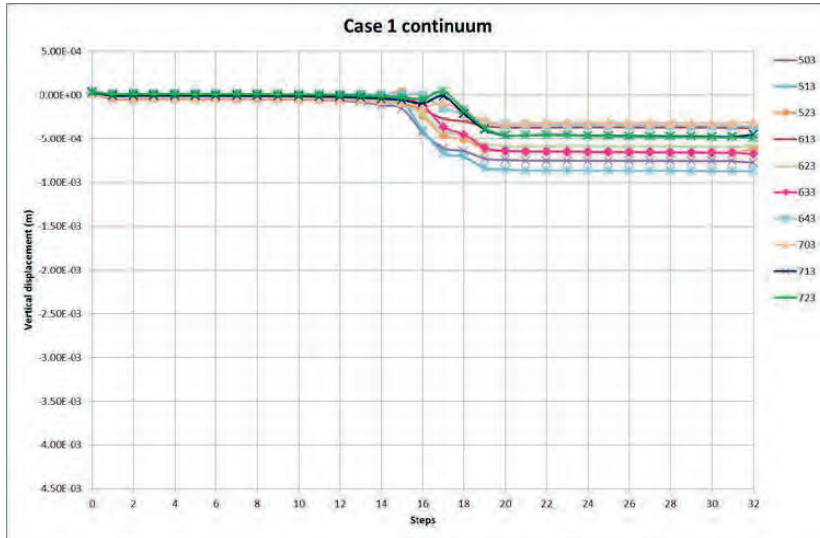


Figure 69 Simulated vertical displacements in meters at several monitoring points at the roof of the Platform tunnel vs. simulation step for stress case 1, continuum elastic.

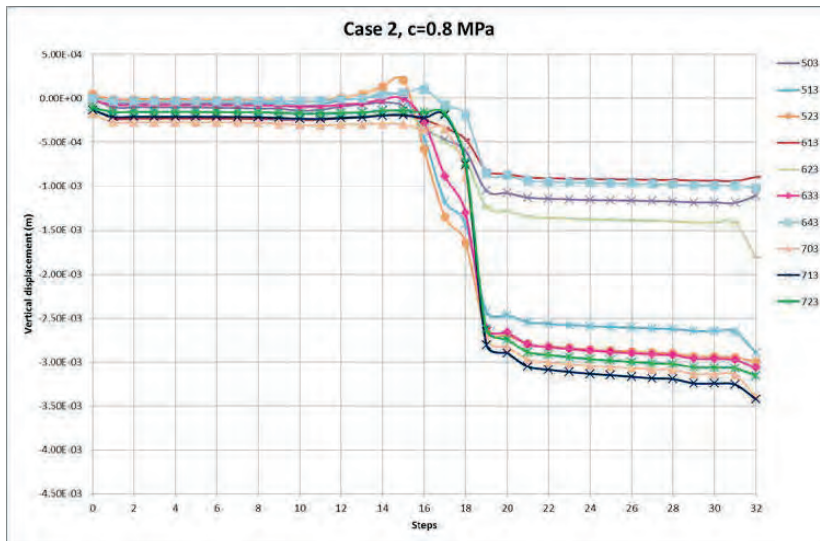


Figure 70 Simulated vertical displacements in meters at several monitoring points at the roof of the Platform tunnel vs. simulation step for stress case 2, discontinuum with fracture cohesion = 0.8 MPa.

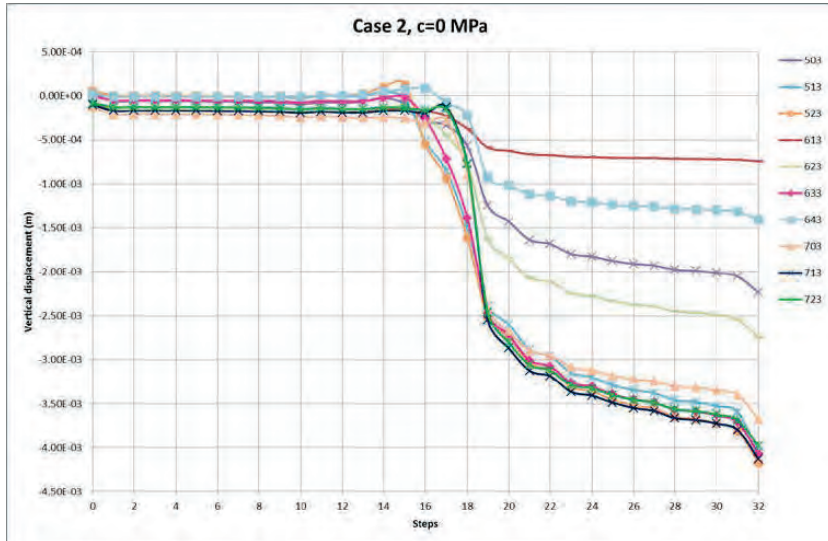


Figure 71 Simulated vertical displacements (z-displacement) in meters at several monitoring points at the roof of the Platform tunnel vs. simulation step for stress case 2, discontinuum with fracture cohesion = 0 MPa.

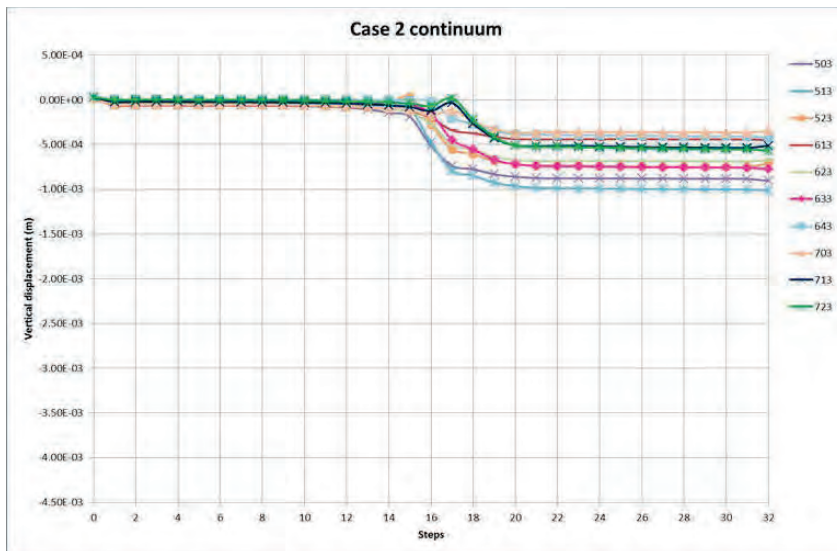


Figure 72 Simulated vertical displacements in meters at several monitoring points at the roof of the Platform tunnel vs. simulation step for stress case 2, continuum elastic.

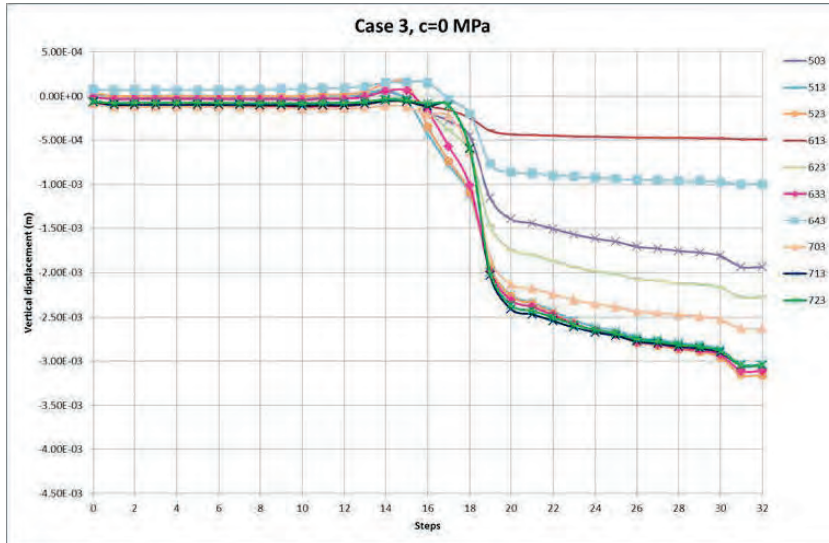


Figure 73 Simulated vertical displacements in meters at several monitoring points at the roof of the Platform tunnel vs. simulation step for stress case 3, discontinuum with fracture cohesion = 0 MPa.

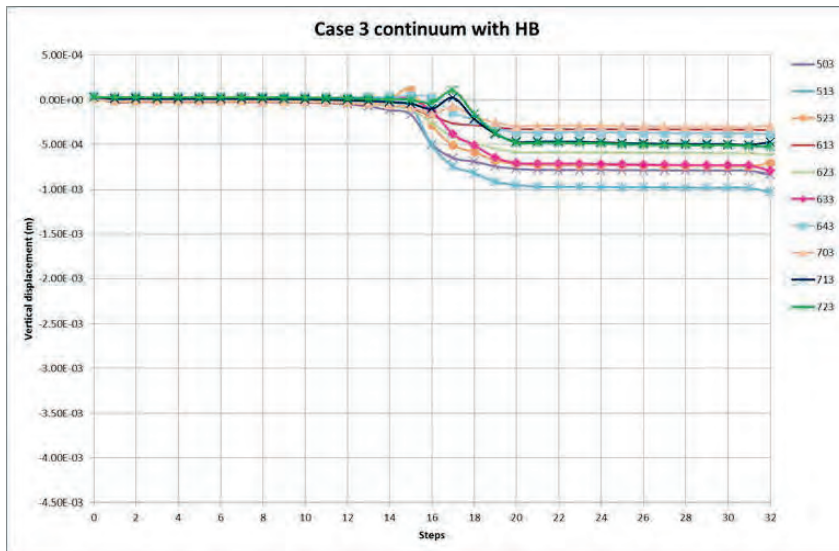


Figure 74 Simulated vertical displacements in meters at several monitoring points at the roof of the Platform tunnel vs. simulation step for stress case 3, continuum elasto-plastic (modified H-B).

6 DISCUSSION

During the excavation of the Odenplan underground station heterogeneous and relatively large rock mass dilation was measured. Previous continuum models performed in the design stage could not predict that behavior. After mapping of the tunnels it was observed that the rock mass has a blocky structure with a high persistence of the joints. Therefore, it was stipulated that rock block movements in combination with relatively high *in situ* stresses most probably caused the heterogeneous dilatational behavior. The aim of this study was to suggest a general technique for numerical back analyses under geological conditions as those present in the Stockholm area, and analyse the range of possible *in situ* stresses at Odenplan Station in the City Link project.

In order to obtain these aims, three-dimensional numerical calculations with a detailed model of the excavation of the Odenplan station has been performed with mapped fractures explicitly included in the discontinuum model. The software used was *3DEC* (Itasca, 2013). In order to analyze how well our present ability of numerical modeling could capture the true behavior of a blocky rock mass and to obtain the most suitable numerical technique for analyses of the Odenplan case, both continuum elastic and continuum elasto-plastic as well as discontinuum models were run.

Since several parameters, in addition to the *in situ* stress state, affects the observed deformations in both the continuum and the discontinuum model they should ideally be included in the back analyses. However, this would result in a considerable time for a complete back analysis of the uncertain parameters with a minimization of the least squared error against measured deformations using an optimization algorithm. Therefore, it was decided to only perform a sensitivity study of the *in situ* stress state to narrow down the range of possible values. This means that no general technique for a real back analysis was obtained in this study. However, the study gave valuable insight into which types of models that are able to properly recreate the observed ground behavior at Odenplan. Four stress cases were considered, representing minimum, typical, maximal and maximal horizontal differential stresses according to the stress profile suggested by Perman and Sjöberg (2007). The objective of the different simulation cases was to see which one of the combinations used that could better match the measurements carried out during the construction of the tunnels. In addition, two different set of discontinuum simulations were performed, one with a cohesion for the fractures equal to 0.8 MPa and one where the cohesion for the fractures was set to 0 MPa. The reason for this was to analyze the influence on the results of an over-predicted shear strength of the fractures at low normal stresses. More combinations can be

run to achieve more conclusive results but so far the results presented in this report show that:

- The minimum stress case (case 0) should be excluded as a possibility for the *in situ* stress around Odenplan station as it induces much lower values of displacement than those recorded *in situ*.
- The stress case with maximum values (case 2), as well as the stress case with maximum deviatoric values (case 3), gave the closest values to those measured *in situ*. Stress case with typical values (case 1) was not as close.
- Considering fracture cohesion to be 0 MPa caused more fracture slip and consequently higher displacement magnitudes at the roof of the railway tunnel which is more in agreement with the measured displacements *in situ*.
- The case with maximum deviatoric *in situ* stress values (case 3) showed similar displacements as the case with maximum *in situ* stress values (case 2). It is thus likely that when the horizontal stress difference is high enough to mobilize the rock mass blocks on top of the tunnel, then one of the controlling factors is the vertical stress. Even though this density could be considered high, it would be worth to run an additional simulation with case 3 *in situ* stress but with rock density of 3.2 t/m^3 to assess the validity of this statement.
- Finally, it is likely that the *in situ* stress state around Odenplan station is closer to cases 2 and 3 than to cases 0 or 1, which means that the maximum and minimum horizontal *in situ* stresses most likely lie in the range of 5.7-7.2 and 2.3-4.1 MPa respectively at a depth of 0-20 m. However, calculated deformations are in the lower region of measured ones indicating that the *in situ* stresses may be even higher. This agrees well with measured *in situ* stresses at 30 m depth, where the average value of the major and minor horizontal *in situ* stresses were 8.1 and 4.3 MPa respectively.

Overall, the results demonstrates that discontinuous modeling better capture the phenomenon of large heterogeneous displacements and rock dilation when excavating at shallow depth in blocky rock at Odenplan. In this environment, fracture slip/opening induces block movements that control the behavior of the rock mass (e.g. rock mass dilatancy). Therefore, back analysis based on a continuum elastic approach, such as classically used (for example Wiles & Kaiser 1994), might not be reliable for this kind of problems. The results also shows that even a continuum elasto-plastic approach may not be satisfying as it would not be able

to reproduce the phenomenon of block movement and thus the heterogeneous nature of the displacements controlling the rock mass dilatancy.

An aspect worth to notice when results with discontinuum models are compared with measured deformations is that large differences in movements between nearby blocks could be observed. This was clearly seen in the results at Odenplan, where the movements of the blocks where history points representing the extensometers E04, E05 and E06 were located only recorded a maximum deformation corresponding to an extension of the extensometer with 0,8 mm. However, modelled history points representing extensometers E01, E02 and E03 recorded extension of the same order of magnitude of those recorded in the field at extensometers E04, E05 and E06. At the same time, history points located on the tunnel boundary on nearby blocks recorded a vertical displacement of up to 4.2 mm (Case 2 with $c=0$ MPa) at the tunnel roof for some of the blocks (Fig. 58). This did not include the vertical heaving of some of the upper blocks, which equaled up to 1.4 mm (Fig. 27), resulting in a total dilation of the rock mass with 6 mm in the model. This value corresponds well with measured extensions in the extensometers E04, E05 and E06, which varies between 5-10 mm. This means that single history points should not be used in discontinuum models, since they will not be able to capture the general rock mass behavior around the tunnel. Instead, a larger number of points should be used covering the tunnel boundary if a proper behavior of the model should be captured.

Even though the results in this study point towards the fact that discontinuum modelling is superior in modeling rock masses with structurally controlled block movements compared to continuum modelling, it should be pointed out that the studied case only represent one example. There might exist several other possible causes to the poor fit with the continuum approach, in addition to the inability of the methods to capture relative block movements. One possible cause is that Poisson's ratio for the rock mass was set to 0.25 in the continuum model. However, as the results by Min et al. (2003) indicated, the Poisson's ratio could be higher for a blocky rock mass. Another source of uncertainty is the strength of the rock mass, which was estimated using the Hoek-Browns failure criterion. It might be possible that the unusually persistent joints in the rock mass around the tunnel resulted in a strength of the rock mass that was considerably lower than that estimated with the failure criterion, which lead to an underestimation of the plastic behavior in the continuum model. In addition, it is well known that Young's modulus of the rock mass has a considerably variation compared to the values predicted using empirical relations. It could be possible that Young's modulus of the rock mass are lower than the value used in this study, which would result in larger deformation for the continuum model. However, the good agreement between analytically

estimated modulus with the composite model and the empirical one indicate that this is probably not the case. Nevertheless, in this case study we had access to some of the best data available in an underground project and the results using discontinuum modelling were significantly closer representing the observed behavior of the rock mass.

In addition to the factors discussed above concerning modelling uncertainties, it is also questionable to use the concept with an instantaneous cohesion and friction angle to describe the peak shear strength of the rock joints, since this might overestimate their peak strength, especially at lower stresses, resulting in lower deformations in the rock mass. Instead, it is recommended to apply zero cohesion or use the curved Barton-Bandis criterion.

7 CONCLUSIONS AND SUGGESTIONS FOR FUTURE RESEARCH

The excavation of the Odenplan station for the Stockholm City Link constitutes a case study with well-documented rock mass characteristics, excavation sequences, support sequences and measured deformations. It therefore provides a unique opportunity for back analysis. Based on this case study, the main objectives of this study was to (1) suggest a general technique for numerical back analyses based on measured deformations under geological conditions as those present in the Stockholm area, and (2) analyse the range of possible *in situ* stresses at Odenplan Station in the City Link project.

Even though no general technique for a real back analysis was obtained in this study, since it would require unrealistically long computational time, the study provided valuable insight into which types of models that are able to recreate the observed ground behavior at Odenplan. The results from the study clearly showed that a continuum-elastic or continuum elasto-plastic approach does not capture the observed behavior of the blocky rock mass at Odenplan. It is therefore recommended that discontinuum approaches are used in the future where structurally controlled block movements could be expected. The peak shear strength of the joints explicitly included in the model is suggested to be modeled in such a way that the strength is not exceeded at lower normal stresses, i.e., to avoid high values of cohesion when the linear Mohr-Coulomb criterion is used or to use a curved criterion which account for the state of normal stress in the fractures.

The performed sensitivity analysis suggests that the *in situ* stresses are high. Maximum horizontal *in situ* stresses are probably in the range of 5.7-7.2 MPa at a depth of 0-20 m. Since calculated deformations are in the lower region of the measured ones, the horizontal stress might be even higher. This agrees well with the measured major and minor horizontal *in situ* stresses at a depth of 30 m, which were 8.1 and 4.3 MPa respectively. However, the uncertainties associated with the numerical modelling techniques does not make it possible to further narrow down the stress range within this project.

In this study, the same orientation of initial *in situ* stress was assumed for the four cases considered. Given that high uncertainty was associated to this data from measurements, it is recommended that the effect of stress orientation variability should also be explored in the future. Furthermore, only one fracture friction angle value has been used in all the simulations. Therefore, it is also recommended that the effect of this parameter should be further explored.

The encouraging results from this project indicate that further stress sensitivity analyses should be performed to have a better estimation of the range of *in situ* stresses in the Stockholm area by fitting displacements obtained from modeling to those measured *in situ* in different projects. These sensitivity studies are also important in order to understand our present ability to perform numerical simulations reflecting actual rock mass behavior.

8 REFERENCES

- Ask, D. 2013. E4 Förbifart Stockholm, Hydrauliska bergspänningsmätningar i borrhål 08F151K, Lovön, Bygghandling.
- Barton, N. 1976. Rock mechanics review. The shear strength of rocks and rock joints. *Int. J. Rock Mech. Min. Sci. & Geom. Abst.* 13: 255-279.
- Barton, B. and Choubey, V. 1977. The shear strength of rock joints in theory and practice. *Rock Mechanics* 10: 1-54.
- Barton, N. y Bandis, S. 1990. Review of predictive capabilities of JRC-JCS model in engineering practice. *Proc. Int. Soc. Rock Mech. Symp. On rock joints. Loen (Norway)*. pp 603-610.
- Berg, S. and Sjöberg, J. 2003. Bergspänningsmätning i borrhål KBOD3, Odenplan. Vattenfall Power Consultant AB.
- Chang, Y. 2007. PM Bergmekanik Korsning T-Blå, Bilaga 2. Dok. Nr: 0237-CT13-080-20bil02, Systemhandling.
- Cividini, A., Jurina, L., and Gioda, G. (1981, December). Some aspects of 'characterization' problems in geomechanics. In *International Journal of Rock Mechanics and Mining Sciences & Geomechanics Abstracts* (Vol. 18, No. 6, pp. 487-503). Pergamon.
- Cundall, P. A. 1971. A Computer Model for Simulating Progressive Large Scale Movements in Blocky Rock Systems. In: *Proceedings of the Symposium of the International Society for Rock Mechanics, Nancy, France, 1971, Vol. 1, Paper No. II-8.*
- Fjelberg, I., Olsson & Viksten, Söder, C-O., Söderström, C. 2009. PM Ingenjörsgelogisk prognos, Odenplan. Bygghandling. 9509-13-025-101.
- Glamheden, R., Röshoff, K., Karlsson, J., Hakami, H. and Christiansson, R. 2007. Rock Mechanics Forsmark. Site descriptive modelling Forsmark stage 2.2. SKB- R-07-31. Svensk Kärnbränslehantering AB.
- Hakami, E., Fredriksson, A., Lanaro, F. and Wrafter, J. 2008. Rock Mechanics Laxemar. Site descriptive modelling SDM-Site Laxemar. SKB- R-08-57. Svensk Kärnbränslehantering AB.
- Hoek, E., Kaiser, P. K. and Bawden, W. F. 1995. Support of underground excavations in hard rocks. Rotterdam: A. A. Balkema.

- Hoek, E. and Brown, E.T. 1997. Practical estimates of rock mass strength. *Int. J. Rock Mech. & Min. Sci.* 34:1165-1186.
- Hoek, E. and Diederichs, M.S. 2006. Empirical estimation of rock mass modulus. *Int. J. Rock Mech. & Min. Sci.* 43: 203–215.
- Itasca, 2013. 3 Dimensional Distinct Element Code (*3DEC*) Version 5.0. Itasca Consulting Group Inc., Minneapolis; 2013.
- Johansson, F. and Batres-Estrada, R. 2015. Personal communication.
- Jeon, Y. S., and Yang, H. S. 2004. Development of a back analysis algorithm using FLAC. *International Journal of Rock Mechanics and Mining Sciences*, 41, 447-453.
- Martin, C.D., Kaiser, P.K. and Christiansson, R. 2003. Stress, Instability and Design of Underground Excavations, *Int. J. Rock Mech. Min. Sci.* 40(7-8): 1027-1047 (October-December).
- McKinnon, S. D. 2001. Analysis of stress measurements using a numerical model methodology. *International Journal of Rock Mechanics and Mining Sciences*, 38(5), 699-709.
- Min, K. B., and Jing, L. (2003). Numerical determination of the equivalent elastic compliance tensor for fractured rock masses using the distinct element method. *International Journal of Rock Mechanics and Mining Sciences*, 40(6), 795-816.
- Miranda, T., Dias, D., Eclaircy-Caudron, S., Correia, A. G., and Costa, L. 2011. Back analysis of geomechanical parameters by optimisation of a 3D model of an underground structure. *Tunnelling and Underground Space Technology*, 26(6), 659-673.
- Moreira, N., Miranda, T., Pinheiro, M., Fernandes, P., Dias, D., Costa, L., and Sena-Cruz, J. 2013. Back analysis of geomechanical parameters in underground works using an Evolution Strategy algorithm. *Tunnelling and Underground Space Technology*, 33, 143-158.
- Oreste, P. 2005. Back analysis techniques for the improvement of the understanding of rock in underground constructions. *Tunnelling and Underground Space Technology*, 20(1), 7-21.
- Palmström, A. and Stille, H. 2010. *Rock Engineering*. ISBN: 978-0-7277-4083-0. Thomas Telford Limited 2010.
- Perman, F. and Sjöberg, J. 2007. Initiala bergspänningsmätningar i Stockholmsområdet underlag för projektering av Citybanan. Vattenfall Power Consultant AB, Rapport till WSP.

Rocscience, 2013. RocLab v.1033. Rocscience Inc. Toronto, Canada.

Sakurai, S., and Takeuchi, K. 1983. Back analysis of measured displacements of tunnels. *Rock mechanics and rock engineering*, 16(3), 173-180.

Söder, C-O. and Johansson, F. 2007. Bergmekaniska beräkningar. Bilaga 1. Uppskattning av bergmekaniska parametrar. Citybanan i Stockholm – del B. 18.3.5.2.2.2 Odenplan, Bygg och Anläggning, Berg. Dokumentnummer 0237-OD13-035-1.

Vardakos, S. S., Gutierrez, M. S., and Barton, N. R. 2007. Back analysis of Shimizu Tunnel No. 3 by distinct element modeling. *Tunnelling and Underground Space Technology*, 22(4), 401-413.

Wiles, T.D. and Kaiser, P.K. 1994. In situ stress determination using the under-excavation technique I. Theory. *Int. J. Rock Mech. Min. Sci. & Geom. Abst.* 31(5): 439-446.

Zhifa, Y., Lee, C. F., and Sijing, W. 2000. Three-dimensional back analysis of displacements in exploration adits—principles and application. *International Journal of Rock Mechanics and Mining Sciences*, 37(3), 525-533.

Yazdani, M., Sharifzadeh, M., Kamrani, K., and Ghorbani, M. 2012. Displacement-based numerical back analysis for estimation of rock mass parameters in Siah Bisheh powerhouse cavern using continuum and discontinuum approach. *Tunnelling and Underground Space Technology*, 28, 41-48.

Zhang, L. Q., Yue, Z. Q., Yang, Z. F., Qi, J. X., and Liu, F. C. 2006. A displacement-based back analysis method for rock mass modulus and horizontal in situ stress in tunneling— Illustrated with a case study. *Tunnelling and Underground Space Technology*, 21(6), 636-649.

APPENDIX 1: VERTICAL DISPLACEMENT MAGNITUDE AT VERTICAL CROSS-SECTIONS PARALLEL AND PERPENDICULAR TO THE PLATFORM TUNNEL CENTERED ON THE ELEVATOR SHAFT

This appendix shows vertical displacement contour plots at vertical cross-sections parallel and perpendicular to the platform tunnel and centered on the elevator shaft (Figure 37) at different simulation steps for all the studied cases.

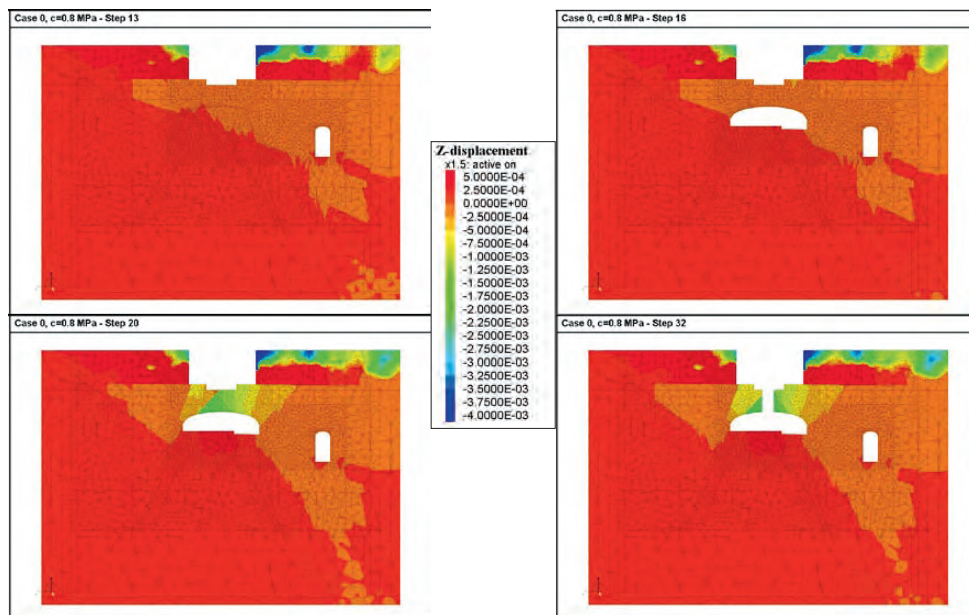


Figure 75 Vertical cross-section of the simulated z-displacement (vertical) perpendicular to the Platform tunnel at $X = 1.5$ m at different excavation steps (13, 16, 20 and 32) for stress case 0, discontinuum with fracture cohesion = 0.8 MPa.

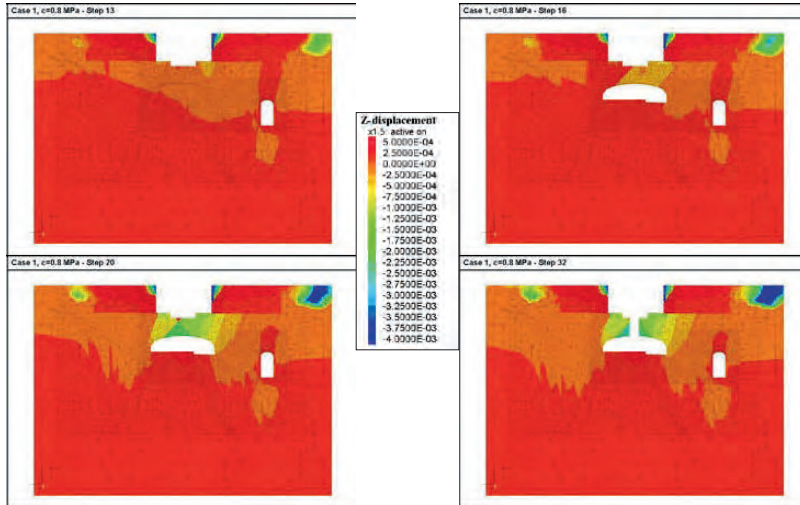


Figure 76 Vertical cross-section of the simulated z-displacement (vertical) perpendicular to the Platform tunnel at $X = 1.5$ m at different excavation steps (13, 16, 20 and 32) for stress case 1, discontinuum with fracture cohesion = 0.8 MPa.

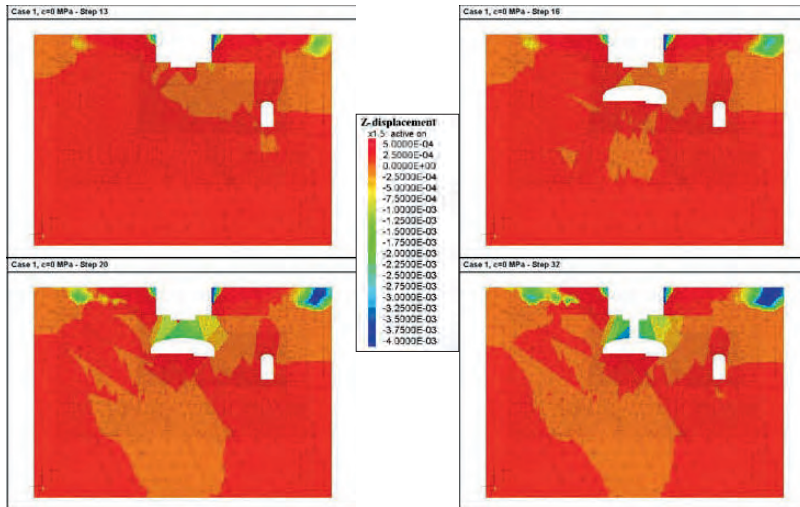


Figure 77 Vertical cross-section of the simulated z-displacement (vertical) perpendicular to the Platform tunnel at $X = 1.5$ m at different excavation steps (13, 16, 20 and 32) for stress case 1, discontinuum with fracture cohesion = 0 MPa.

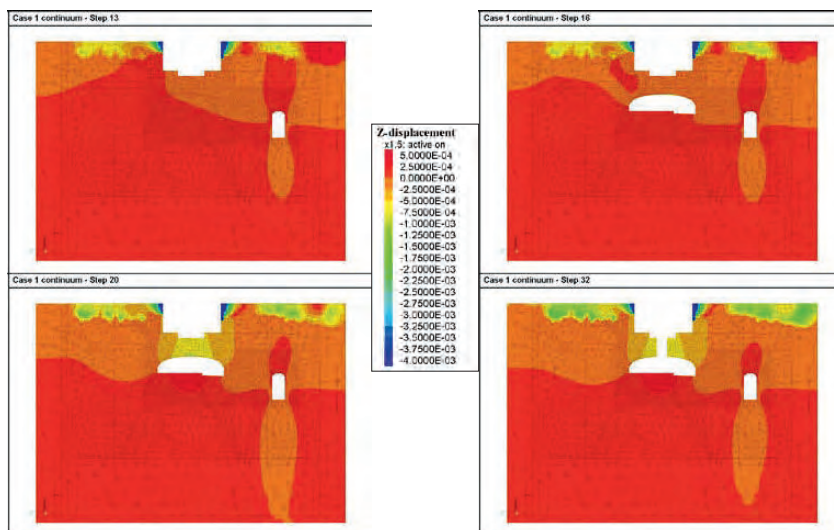


Figure 78 Vertical cross-section of the simulated z-displacement (vertical) perpendicular to the Platform tunnel at $X = 1.5$ m at different excavation steps (13, 16, 20 and 32) for stress case 1, continuum elastic.

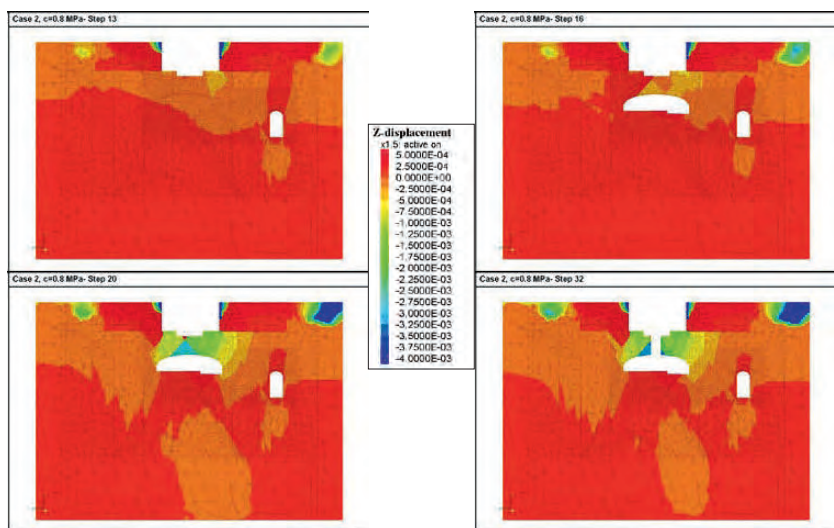


Figure 79 Vertical cross-section of the simulated z-displacement (vertical) perpendicular to the Platform tunnel at $X = 1.5$ m at different excavation steps (13, 16, 20 and 32) for stress case 2, discontinuum with fracture cohesion = 0.8 MPa.

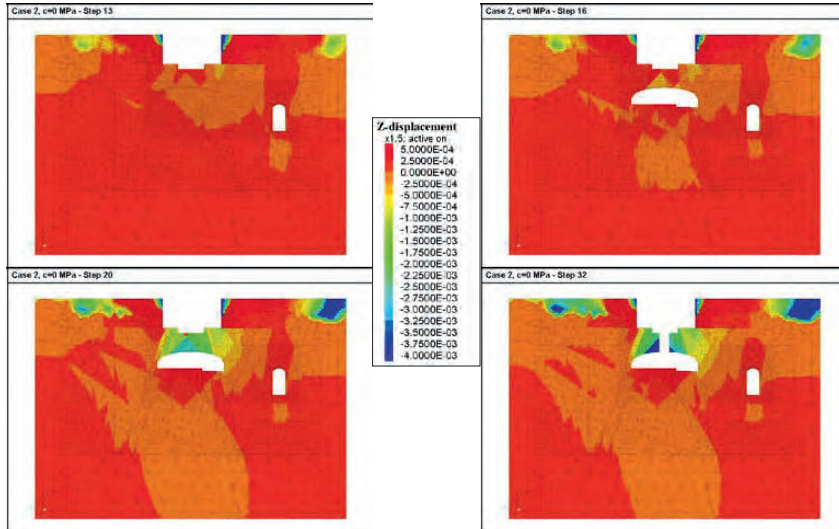


Figure 80 Vertical cross-section of the simulated z-displacement (vertical) perpendicular to the Platform tunnel at $X = 1.5$ m at different excavation steps (13, 16, 20 and 32) for stress case 2, discontinuum with fracture cohesion = 0 MPa.

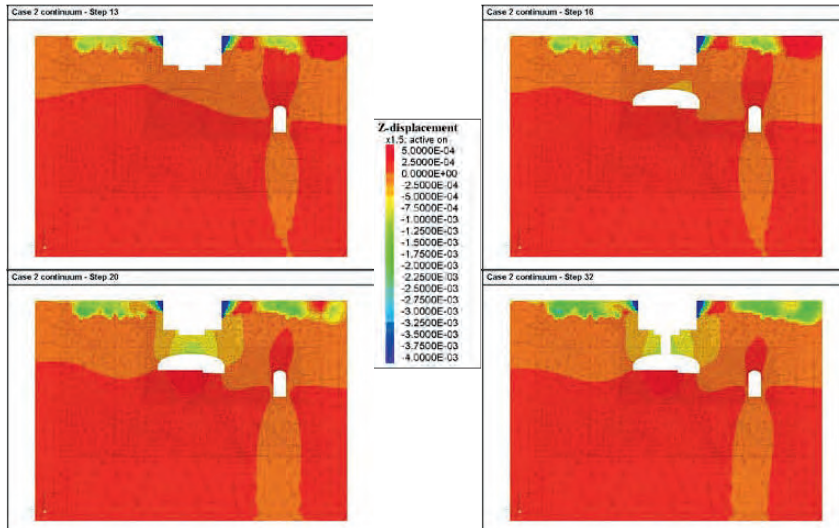


Figure 81 Vertical cross-section of the simulated z-displacement (vertical) perpendicular to the Platform tunnel at $X = 1.5$ m at different excavation steps (13, 16, 20 and 32) for stress case 2, continuum elastic.

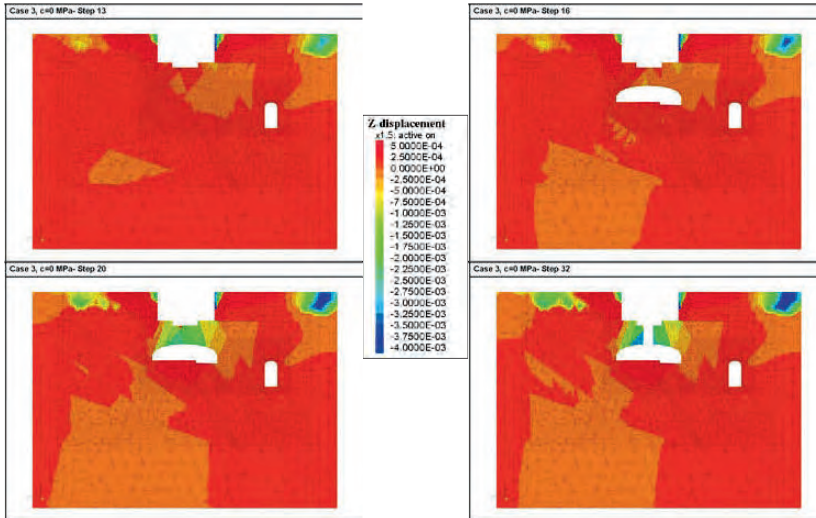


Figure 82 Vertical cross-section of the simulated z-displacement (vertical) perpendicular to the Platform tunnel at $X = 1.5$ m at different excavation steps (13, 16, 20 and 32) for stress case 3, discontinuum with fracture cohesion = 0 MPa.

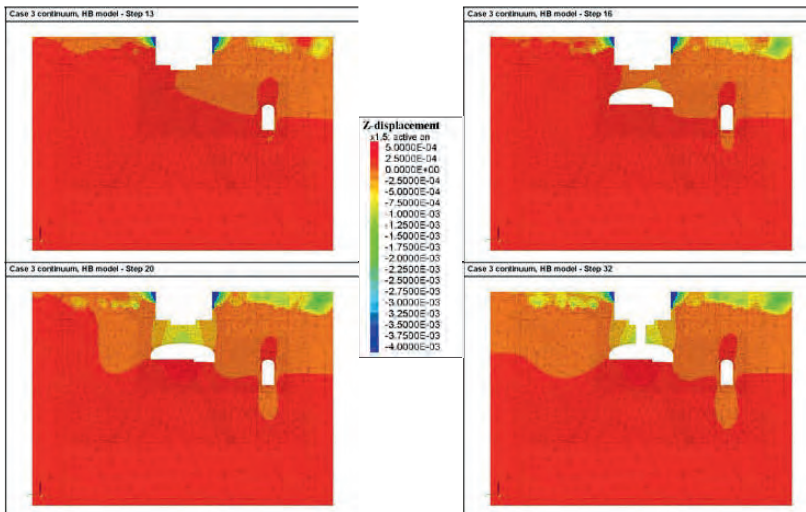


Figure 83 Vertical cross-section of the simulated z-displacement (vertical) perpendicular to the Platform tunnel at $X = 1.5$ m at different excavation steps (13, 16, 20 and 32) for stress case 3, continuum elasto-plastic (modified H-B).

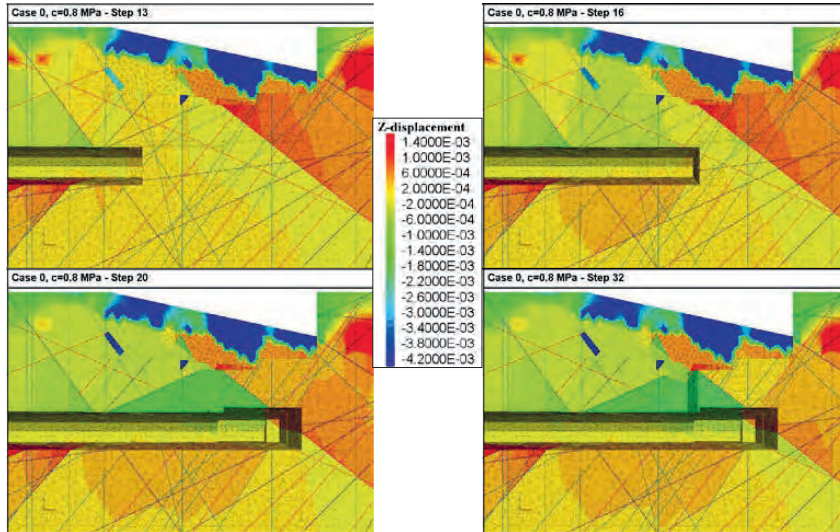


Figure 84 Vertical cross-section of the simulated z-displacement (vertical) parallel to the Platform tunnel at $Y = 3$ m at different excavation steps (13, 16, 20 and 32) for stress case 0, discontinuum with fracture cohesion = 0.8 MPa.

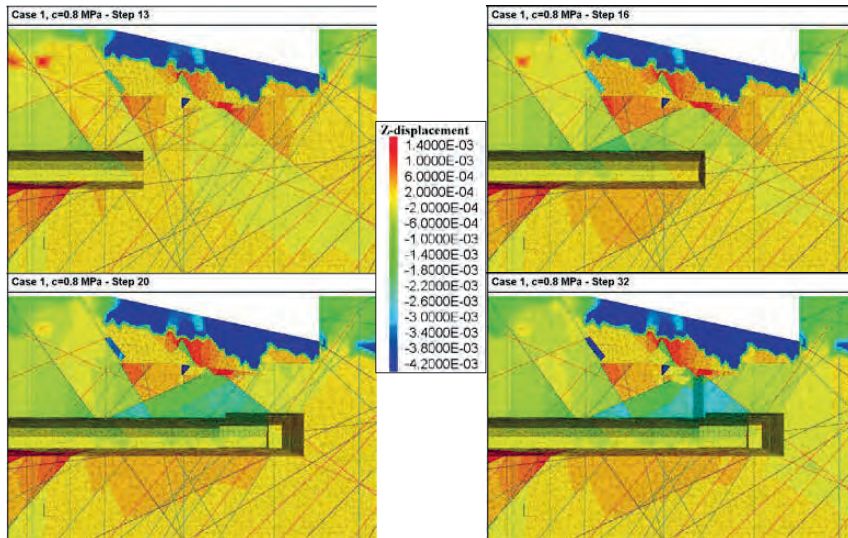


Figure 85 Vertical cross-section of the simulated z-displacement (vertical) parallel to the Platform tunnel at $Y = 3$ m at different excavation steps (13, 16, 20 and 32) for stress case 1, discontinuum with fracture cohesion = 0.8 MPa.

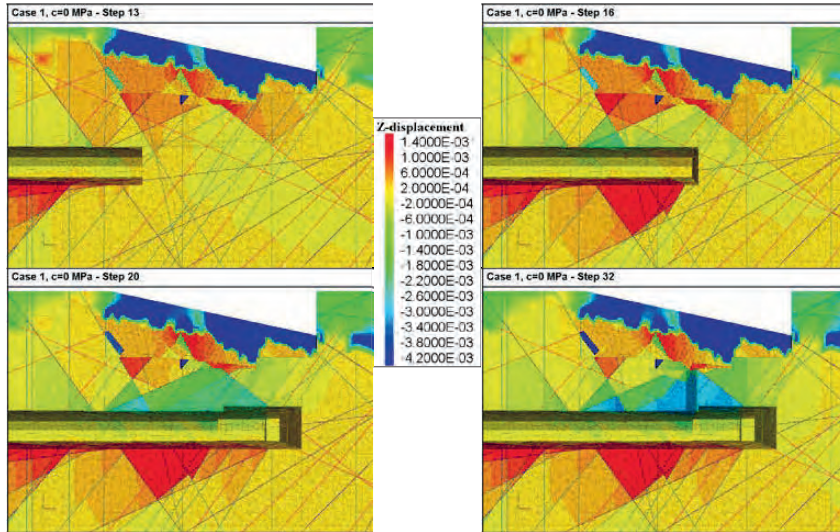


Figure 86 Vertical cross-section of the simulated z-displacement (vertical) parallel to the Platform tunnel at $Y = 3$ m at different excavation steps (13, 16, 20 and 32) for stress case 1, discontinuum with fracture cohesion = 0 MPa.

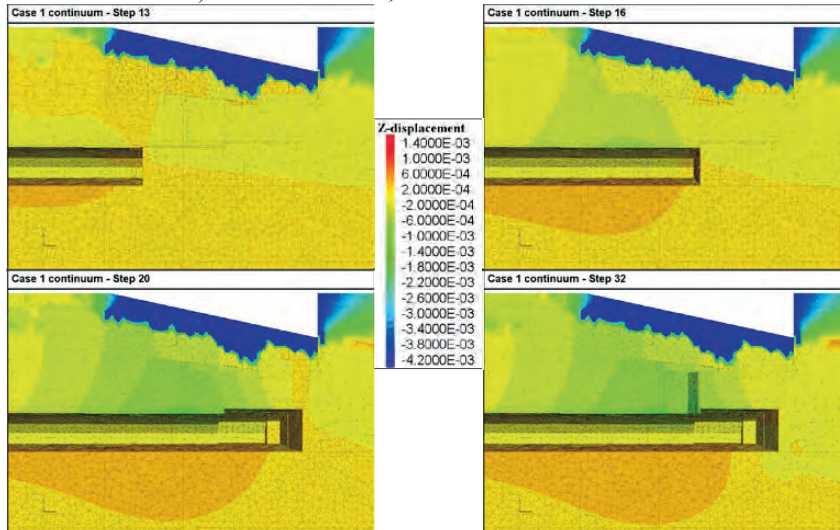


Figure 87 Vertical cross-section of the simulated z-displacement (vertical) parallel to the Platform tunnel at $Y = 3$ m at different excavation steps (13, 16, 20 and 32) for stress case 1, continuum elastic.

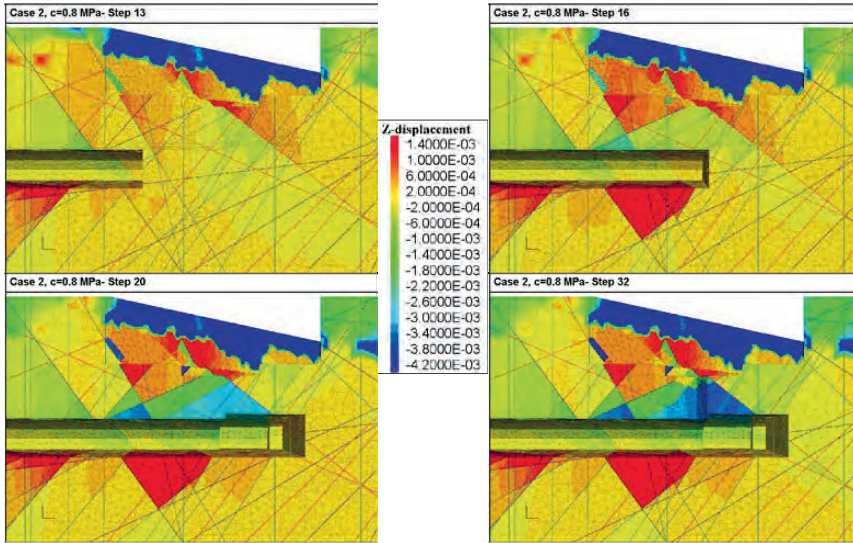


Figure 88 Vertical cross-section of the simulated z-displacement (vertical) parallel to the Platform tunnel at Y = 3 m at different excavation steps (13, 16, 20 and 32) for stress case 2, discontinuum with fracture cohesion = 0.8 MPa.

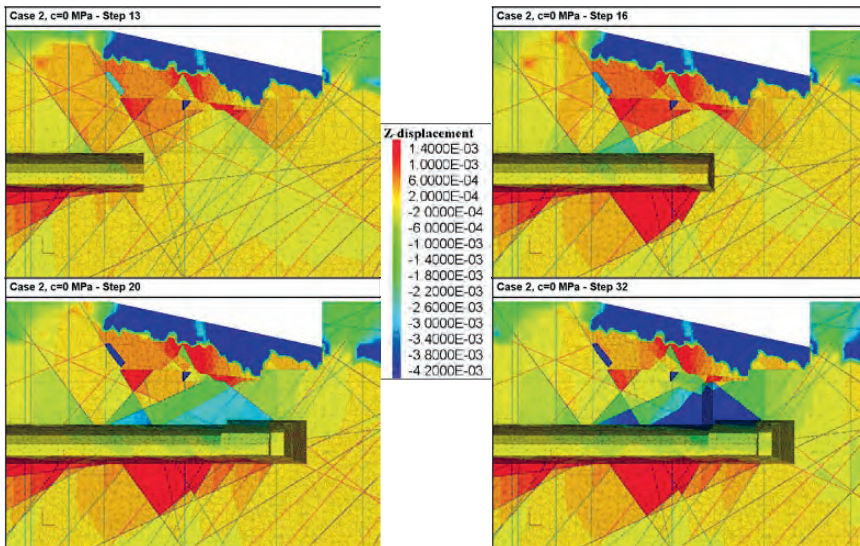


Figure 89 Vertical cross-section of the simulated z-displacement (vertical) parallel to the Platform tunnel at Y = 3 m at different excavation steps (13, 16, 20 and 32) for stress case 2, discontinuum with fracture cohesion = 0 MPa.

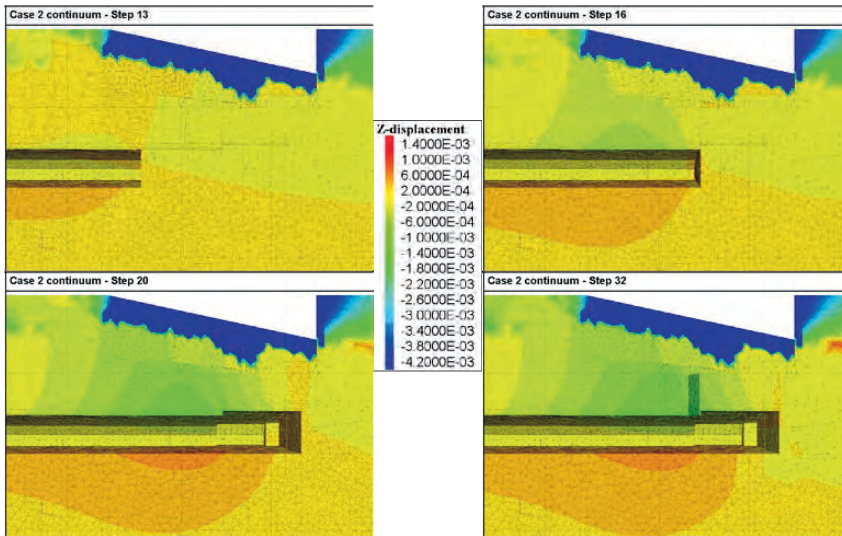


Figure 90 Vertical cross-section of the simulated z-displacement (vertical) parallel to the Platform tunnel at $Y = 3$ m at different excavation steps (13, 16, 20 and 32) for stress case 2, continuum elastic.

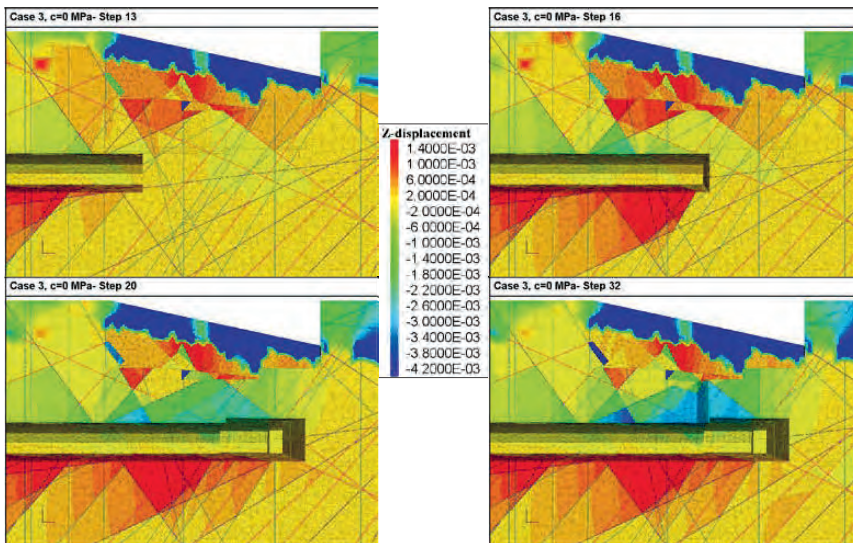


Figure 91 Vertical cross-section of the simulated z-displacement (vertical) parallel to the Platform tunnel at $Y = 3$ m at different excavation steps (13, 16, 20 and 32) for stress case 3, discontinuum with fracture cohesion = 0 MPa.

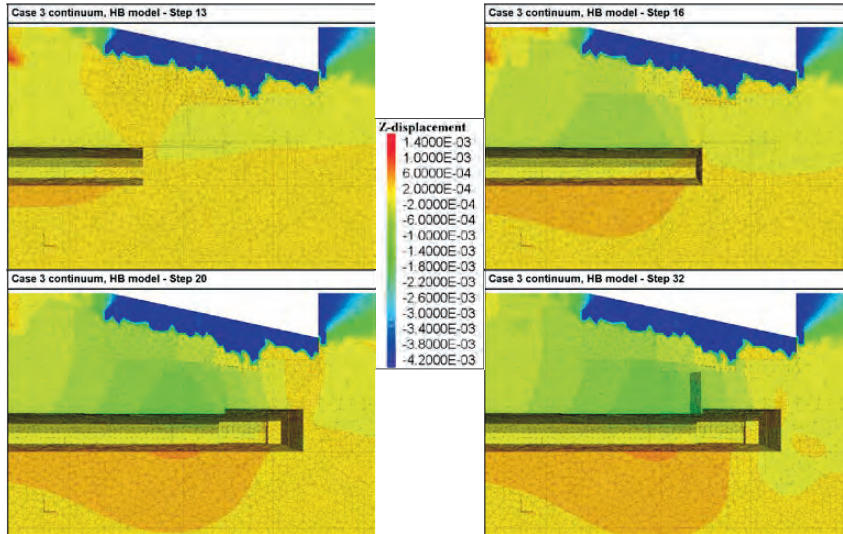


Figure 92 Vertical cross-section of the simulated z-displacement (vertical) parallel to the Platform tunnel at $Y = 3$ m at different excavation steps (13, 16, 20 and 32) for stress case 3, continuum elasto-plastic (modified H-B).

APPENDIX 2: VERTICAL DISPLACEMENT MAGNITUDE AT TOP SURFACE OF MODEL

This appendix contains plots of the simulated vertical displacement induced on the top surface at different simulation steps for all the studied cases.

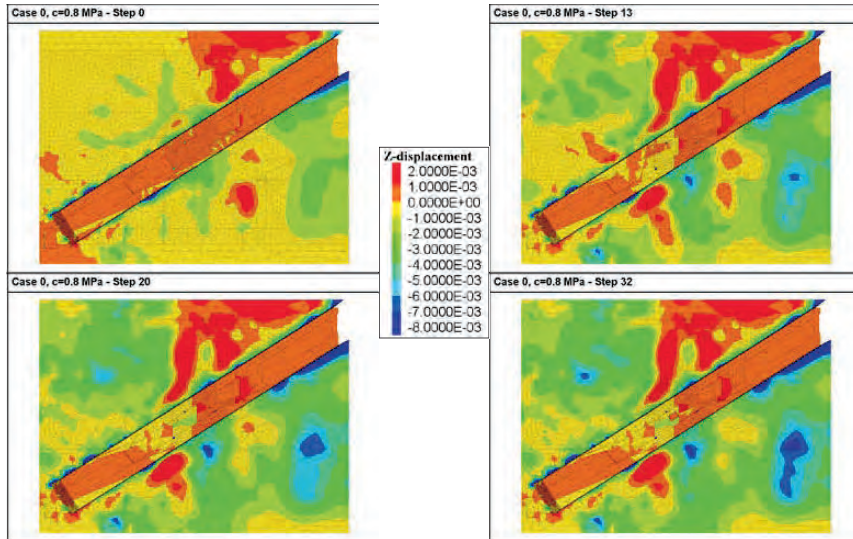


Figure 93 Simulated vertical displacement at top surface of model at different excavation steps (13, 16, 20 and 32) for stress case 0, discontinuum with fracture cohesion = 0.8 MPa.

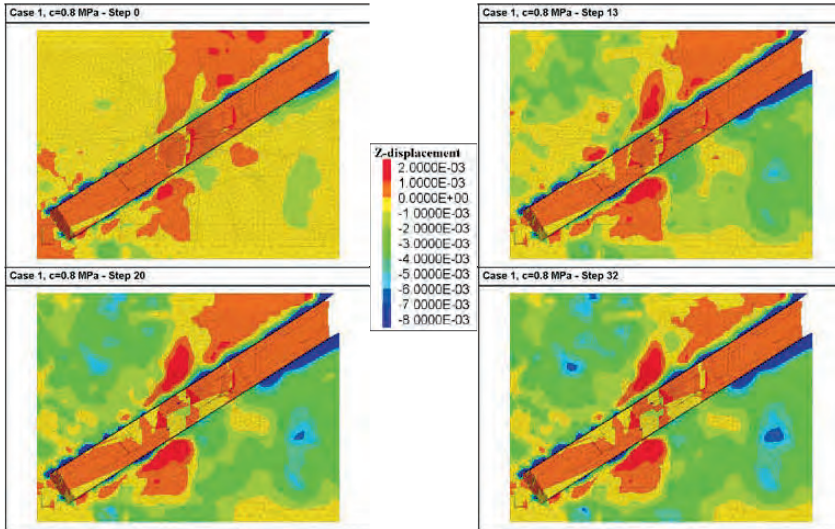


Figure 94 Simulated vertical displacement at top surface of model at different excavation steps (13, 16, 20 and 32) for stress case 1, discontinuum with fracture cohesion = 0.8 MPa.

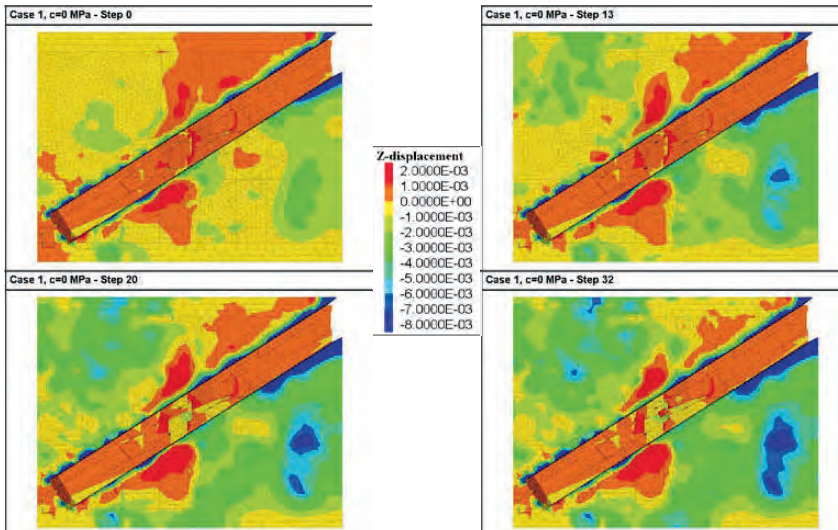


Figure 95 Simulated vertical displacement at top surface of model at different excavation steps (13, 16, 20 and 32) for stress case 1, discontinuum with fracture cohesion = 0 MPa.

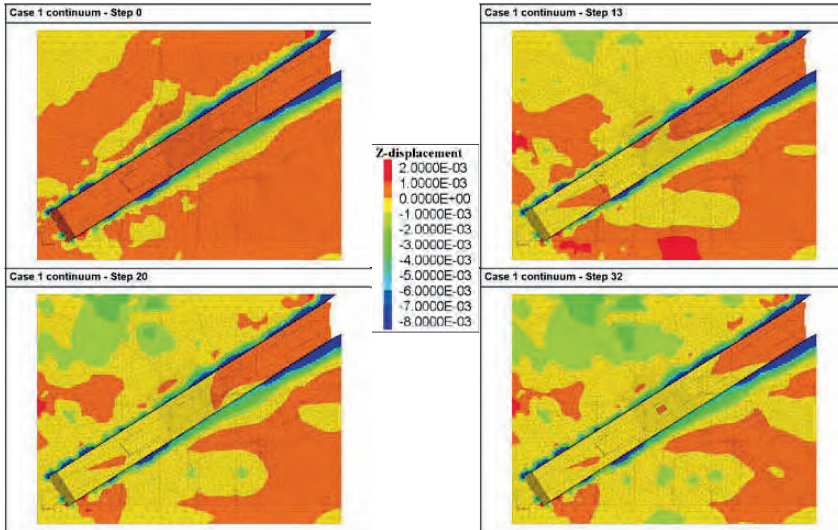


Figure 96 Simulated vertical displacement at top surface of model at different excavation steps (13, 16, 20 and 32) for stress case 1, continuum elastic.

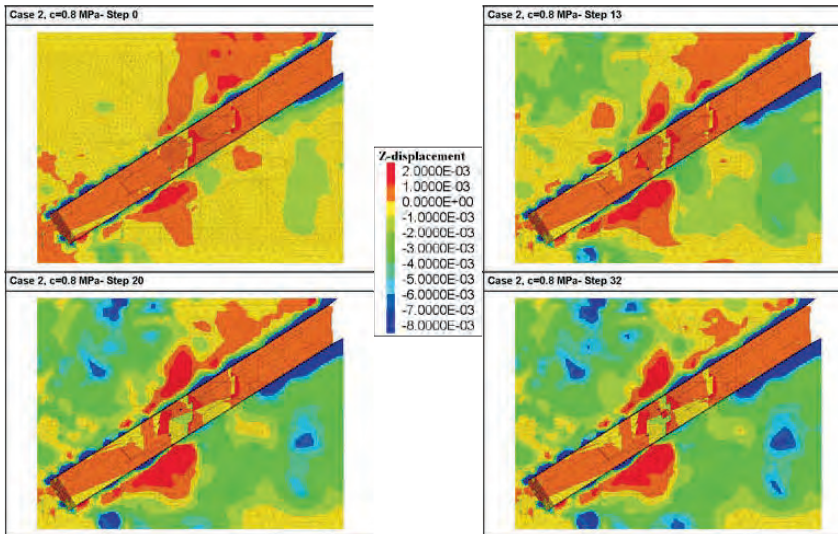


Figure 97 Simulated vertical displacement at top surface of model at different excavation steps (13, 16, 20 and 32) for stress case 2, discontinuum with fracture cohesion = 0.8 MPa.

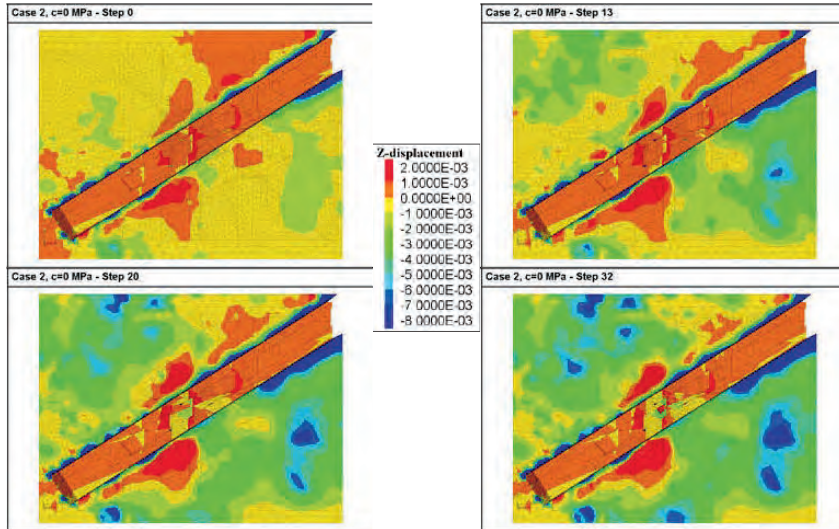


Figure 98 Simulated vertical displacement at top surface of model at different excavation steps (13, 16, 20 and 32) for stress case 2, discontinuum with fracture cohesion = 0 MPa.

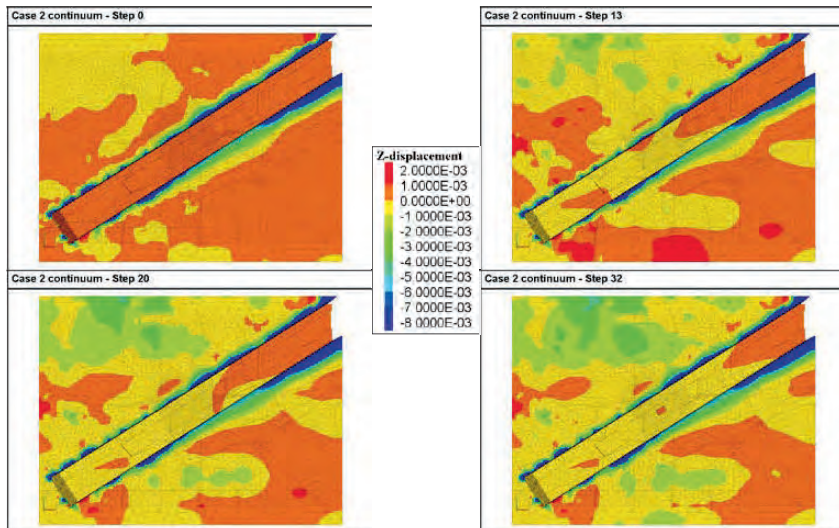


Figure 99 Simulated vertical displacement (vertical) at top surface of model at different excavation steps (13, 16, 20 and 32) for stress case 2, continuum elastic.

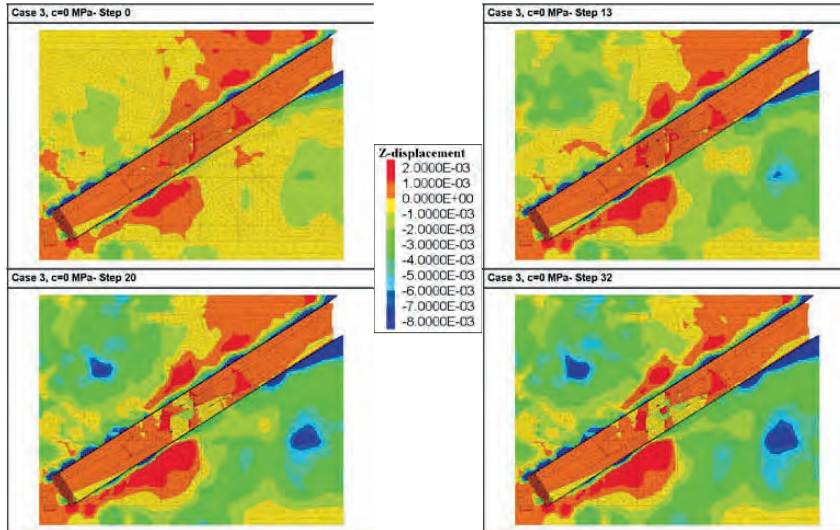


Figure 100 Simulated vertical displacement at top surface of model at different excavation steps (13, 16, 20 and 32) for stress case 3, discontinuum with fracture cohesion = 0 MPa.

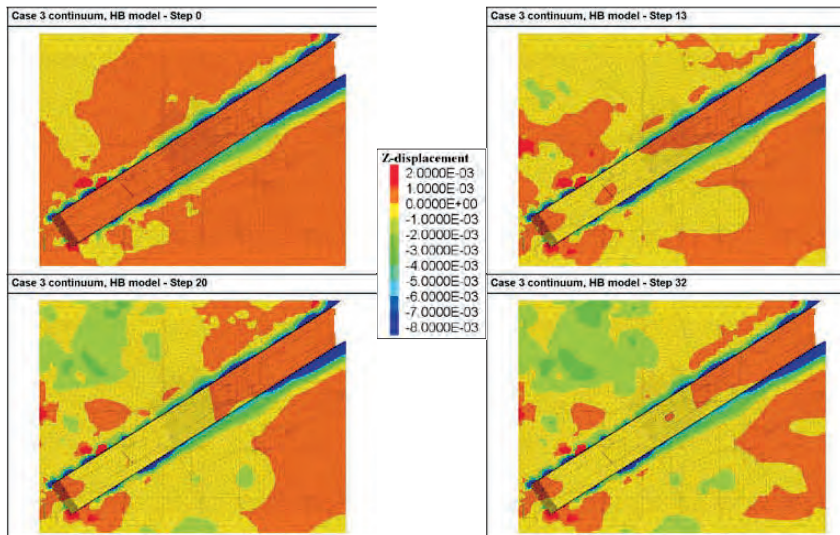


Figure 101 Simulated vertical displacement (vertical) at top surface of model at different excavation steps (13, 16, 20 and 32) for stress case 3, continuum elasto-plastic (modified H-B).



Box 5501
SE-114 85 Stockholm

info@befoonline.org • www.befoonline.org
Visiting address: Storgatan 19

ISSN 1104-1773